POST-FAILURE BEHAVIOUR IN UNIAXIAL COMPRESSION OF TWO MINE ROCKS FROM ELURA MINE, NEW SOUTH WALES.

Thesis submitted to the University of New South Wales for the degree of Master of Science in the School of Mining Engineering, Faculty of Applied Science.

Enggang Abdus Salam

B.E. (Mining), AGP, Bandung, Indonesia.
GradDip. (Mining and Mineral Engineering),UNSW.

1 9 8 5

I, the undersigned, certify that the work described in this thesis has not been submitted for a higher degree to any other University or Institution.

(Enggang Abdus Salam)

AKNOWLEGMENTS

The author wishes to thank the following persons who have, directly or indirectly, assisted in the making of this thesis.

In particular to Dr. R. L. Blackwood for his supervision, suggestion and his guidance in relation to the work carried out and the preparation of this thesis; to Assc. Prof. E. G. Thomas who was temporarily acted as author's supervisor.

To Professor F. F. Roxborough, Head of School Of Mining Engineering for the use of the school's facilities and equipment in the preparation of this thesis.

To the technical and all staff of the School of Mining Engineering, Mr. J. Haddon in particular, who assisted and helped considerably when experiments were carried out; and Mr. P. Hagan who corrected the English text.

To the Australian Development Assistance Bureau for the award of scholarship for studying in the University of New South Wales and the Indonesian Government for granting leave to undertake the study.

Finally to my wife, Ernawati, my daughter Lolyta and my son Bonni for their understanding and support.

ABSTRACT

A literature survey and a laboratory experiment have been carried out to study post-failure behaviour of mine rock under uniaxial compression.

Laboratory experiments were carried out to determine post-failure characteristics of two mine rocks i.e. siltstone and pyritic ore from the Elura Mine, near Cobar, in New South Wales, using a Schenck Trebel servo-controlled testing machine. A total of 36 specimens of 30 mm diameter with L/D ratios ranging from 1/2 to 2 have been tested under uniaxial compression. The experimental results showed that siltstone displays various post-failure modes of behaviour depending on the geometry of the specimen and the experiment conditions. Although no complete stress-strain curves for the pyritic ore specimens were obtained, this type of rock is obviously a Class II rock. To control failure of pyritic ore specimens, therefore, strain energy stored in the specimen at post peak strength region must be extracted from the specimen.

An understanding of post-failure behaviour of rock may lead to the development of better procedures for controlling violent failure of rock structures such as underground pillars and therefore its contribution to stability analysis of underground excavation and the design of mining lay outs.

TABLE OF CONTENTS

LIST OF FIGURES

LIST OF TABLES

CHAPTER ONE

I N T R O D U C T I O N

Probably the most important variants in the design of an underground, or surface excavation in rock are the strength parameter, and the load-deformation characteristics of the rock mass.

Of near equal importance to design is the structure of rock mass. This includes not only the intact rock substance, but as well structural features such as joints, faults, bedding, and other discontinuities which precence is accentuated in the post failure stages of the rock. The importance of structure varies as the depth of mining. With greater depth, the higher in-situ stress emphasizes any structural features present. In any case, the rock about an underground opening is usually fractured or in a fissured state but still remains stable. Studies by Roux et.al.(1957) have indicated that fractured rock is less prone to sudden and violent failure than is solid rock. It would therefore seem more desirable, in some instances, to work with rock which has fractured. To decrease the chances of violent failure, Roux et.al. (1957) and later Blake (1971) deliberately destressed a volume of rock in a suspected high stress or rock burst zone, by blasting (1971).

Since fracturing of the rock around excavation is generally unavoidable, an understanding of the behaviour of fractured rock

is important for devising effective methods of improving the stability of an excavation and of preventing the violent failure in a rock mass. In this context 'stability' is a condition in which sudden and violent failure does not occur, or if a rock is in the process of slow and gradual fracturing failure can be controlled or even halted. A number of other studies on the mechanism of brittle fracture, commonly associated with underground excavation, have revealed that safe and economic design of an excavation depends on the behaviour characteristics of fractured rock. One method found effective in determining failure characteristics of rock is by measuring the complete stress-strain response of rock (Bieniawski et al., 1969).

In most uniaxial or triaxial tests a 'soft' testing machine is used, that is with a machine that applies a load by means of hydraulic pressure. A characteristic of this type testing machine is that as the stiffness of the specimen is reduced through fracturing, the hydraulic pressure will still continue to drive the platens together resulting in the specimen being destroyed. This can give no information beyond the peak of the stress-strain curve.

In order to obtain information on the load-deformation characteristics of a fractured specimen it is necessary to carry out the testing in a 'stiff' machine in which the strain rather than the stress is controlled. In most modern stiff machines, the hydraulic system is servo-controlled by signals from deformation

measuring equipment on the specimen and the complete load-deformation curve can be monitored up to and beyond, the peak strength of the specimen.

1.1 A I M

The laboratory test involved the measurements of load-deformation characteristics of mine rocks under uniaxial compression using servo-controlled machine. This experimental data was then analysed with respect to variations in the post failure properties of the two types of mine rocks from Elura Mine in New South Wales.

1.2 DEFINITION

A number of terms have been used in this thesis, the precise meaning vary from author to author. The following definitions mainly by Bieniawski et al.,(1969), were adopted.

Post failure characteristics of rock are those characteristics of rocks obtained after the ultimate strength has been reached and correspond to descending part on the stress-strain curve.

Failure is a process whereby a material changes from one type of behaviour to another. Two of the more important types of failure are fracture and rupture.

Fracture occurs when new surfaces in the form of cracks are formed in a material, or when existing surfaces are extended. Various stages of fracture may be conceptualised, namely, fracture initation, fracture propagation (stable and unstable) and strength failure.

Fracture initation is the failure process by which one or more existing cracks in a material begin to extend.

Fracture propagation is the failure process which occurs when cracks in a material are extending. Hence fracture propagation always occurs subsequent to fracture initation. Two types of fracture propagation are distinguishable, stable and unstable.

Stable fracture propagation occurs when the crack extension is related to the loading and can be controlled accordingly.

Unstable fracture propagation,however, occurs when the crack extension iso governed by factors other than those directly related with loading and thus become uncontrollable.

Brittle fracture is a fracture that exhibits little or no permanent (plastic) deformation. This implies that material behaves elastically until fracture.

Rupture is the failure process by which a structure, e.g. a specimen, disintegrates into two or more pieces.

CHAPTER TWO

INFLUENCE OF TESTING MACHINE ON THE FAILURE OF ROCK IN COMPRESSION

As a brittle material, such as rock or concrete is loaded in compression and before the peak of the load-deformation curve is reached, work must be done on the combined specimen-machine system in bringing about an increment of deformation in the specimen. During the loading process, the system is considered mechanically stable till the peak of the load-deformation curve is reached. Beyond the peak, however, because potential energy is released from the machine as the load decreases, it is possible that the work needed for further deformation of the specimen can be fully provided from within the specimen-machine system. This can lead to the deformation process continuing spontaneously and uncontrollably, which can sometimes lead to violent specimen failure. This prevents the load-bearing capacity as a function of deformation of the specimen from being readily assessed. This situation commonly accompanies brittle failure of rock specimens in a conventional 'soft' testing machine especially one which is hydraulically loaded. As a results, studies of the strength and deformational behaviour of rock in the past have centered on the prefailure characteristics.

In recent years the view that such a violent failure is an

intrinstic characteristic of a rock specimen has been revised, to that it is more probably caused by the design characteristic of the system used to test the specimen. Therefore with closer monitoring and control of the test machine it should be possible, under proper test conditions, to check the development of the failure process in a rock specimen. Once this is done, the process of disintegration can be studied in greater detail (Rummel and Fairhust, 1970).
The introduction of stiff testing machines, where the release of energy in compression is controlled by regulation of the rate of deformation of the rock specimen, has shown that brittle rock can be deformed beyond failure strength. The use of stiff loading devices in laboratory tests on brittle rocks has demonstrated that these rocks do retain some strength after the ultimate strength has been applied.

2.1 MATERIAL RESISTANCE AND THE CONCEPT OF CONTROLLED FAILURE

All any materials possess a 'load-bearing ability' or 'resistance'. Its reaction on loading is shown as deformation, or failure, or both. Deformation may either be elastic or plastic; either instantaneous or time dependent, it may be manifested either in density changes or movement along cracks. Any combination of these behavioural characteristics can occur. Failure is a transition from one state of behaviour to another one, e.g. from dominantly elastic to dominantly plastic or from dominantly

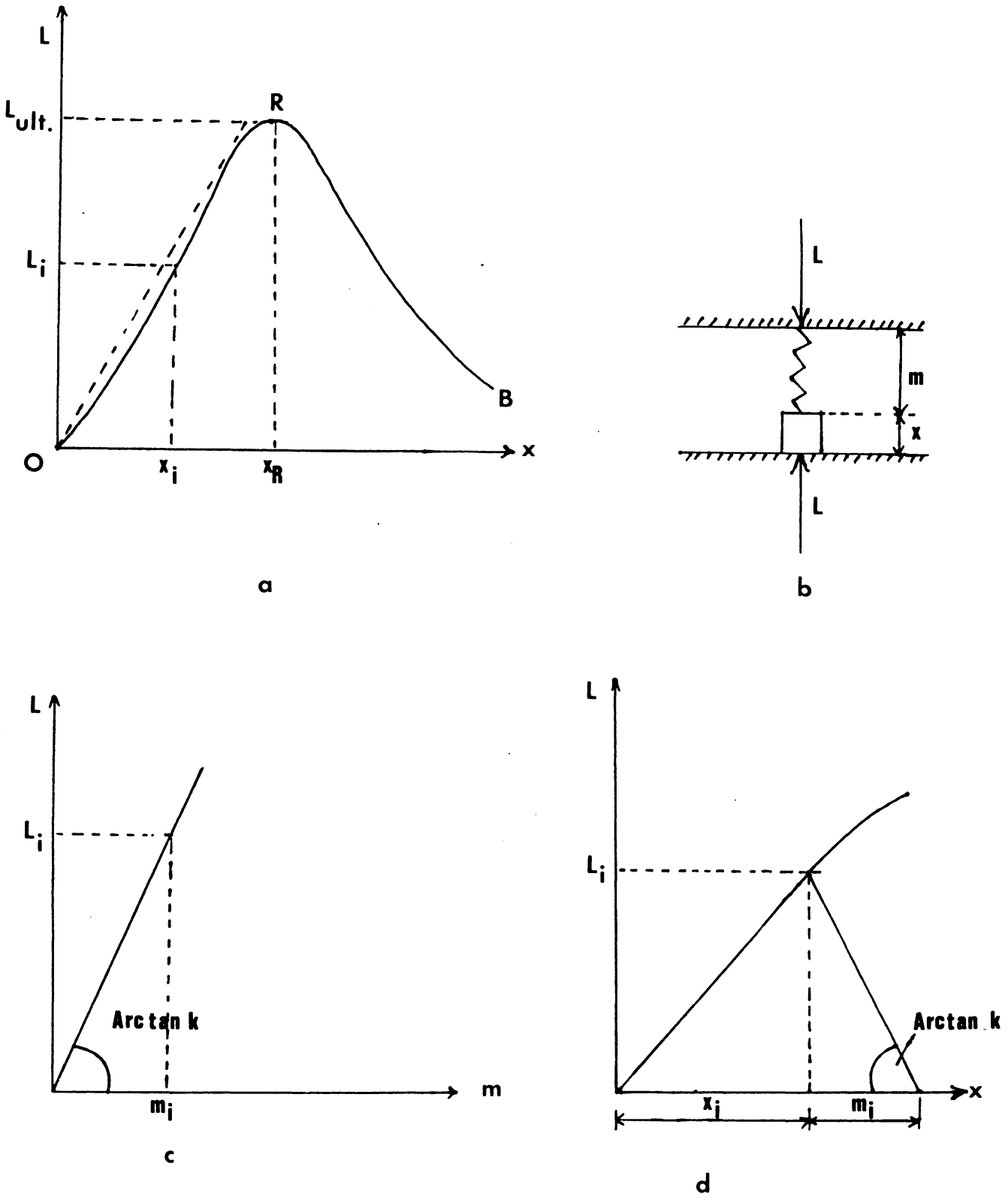

Fig. 2.1 Diagrammatical representation of specimen and testing machine deformations, under load.

density-changing deformation to dominantly movement-along-cracks deformation (Bieniawski et al., 1969). The resistance of a specimen to loading depends upon its deformation, and can be described by considering an ideal complete load-deformation curve as depicted in Fig. 2.1a. The curve ORB, which represents a complete load-deformation relationship of the specimen, consists of two distinct regions. These include an ascending region OR, where the resistance increases, and descending region RB, where the resistance decreases with increasing deformation.

In order to determine the resistance-deformation relationship in the ascending region OR, a load is applied to the specimen and then the specimen deformation is measured. For example in Fig. 2.1a the load applied to the specimen L_i resulted in a deformation x_i which in turn dictates the specimen to put up just enough resistance R_i to bear the load L_i; hence $L_i = R_i$, and any increase in load ΔL induces a change in resistance $\Delta R = \Delta L$ which results in a deformation of Δx. In other words, the specimen resistance is a function of its deformation.

The specimen-machine system, in fact, is a spring with stiffness k loaded in series with the specimen as depicted in Fig. 2.1b. This figure shows that the load applied to the system deformes both the spring (machine) and the specimen but with different magnitudes, m_i and x_i respectively. Since the machine behaves elastically the load-deformation curve can be given by

$$L = k.m \quad \ldots\ldots\ldots \quad (2\text{-}1)$$

where L = load

k = spring (machine) stiffness, and

m = machine deformation.

The machine deformation mi caused by a particular load L may, therefore, be calculated as

$$m_i = L_i/k \quad \ldots\ldots\ldots \quad (2\text{-}2)$$

or can be read off from the machine stiffness characteristic curve as presented in Fig. 2.1c. Since the machine deformation m_i is associated with the specimen deformation x_i, it can also be obtained by drawing a line at angle arctan k with the abscissa through the point L_i, x_i of the curve of Fig. 2.1a and the result as shown in Fig. 2.1d.

At point R, the specimen resistance reaches a maximum (being a function of deformation) that is the maximum of its load-bearing capacity which the specimen can support in compression; it therefore suffers strength failure. At this stage the resistance R_i is equal to $R_{maximum}$ and the corresponding its deformation is x_R. Beyond strength failure, in the descending region RB, the specimen deformation increases solely by movement along cracks, the propagation of which is self sustained because of the energy stored in the specimen itself from previous load increases being converted

into work done on creating new cracked surfaces (crack propagation) (Bieniawski, 1969).

An increase in load beyond the level L = R to a level R + ΔL is not possible since there is no reaction (in terms of a resistance increase to R + ΔR) to the attempted load increase ΔL. Any energy input intended to produce the load increase ΔL is consumed by increasing deformation and fracture propagation in the specimen but certaintly not to increase the elastic energy stored in the machine. The machine cannot store further elastic energy because the specimen has ceased to offer increasing resistance. On the contrary, the energy stored in the machine given as W being

$$W = 1/2\ R\ m \quad , \ldots\ldots\ldots (2\text{-}3)$$

This is released at an undefined rate because there is a decrease in the specimen resistance. In any event the machine deformation , m, decreases with decreasing load in the same manner as it increases with increasing load, so that

$$R - \Delta L = k(m_R - \Delta m), \ldots\ldots (2\text{-}4)$$

where R is the load at $x = x_R$, and m_R is the machine deformation corresponding to x_R, i.e. $m_R = R/k$.

In the region OR in Fig. 2.1a, increasing machine deformation, m, was in the direction opposite to that of the

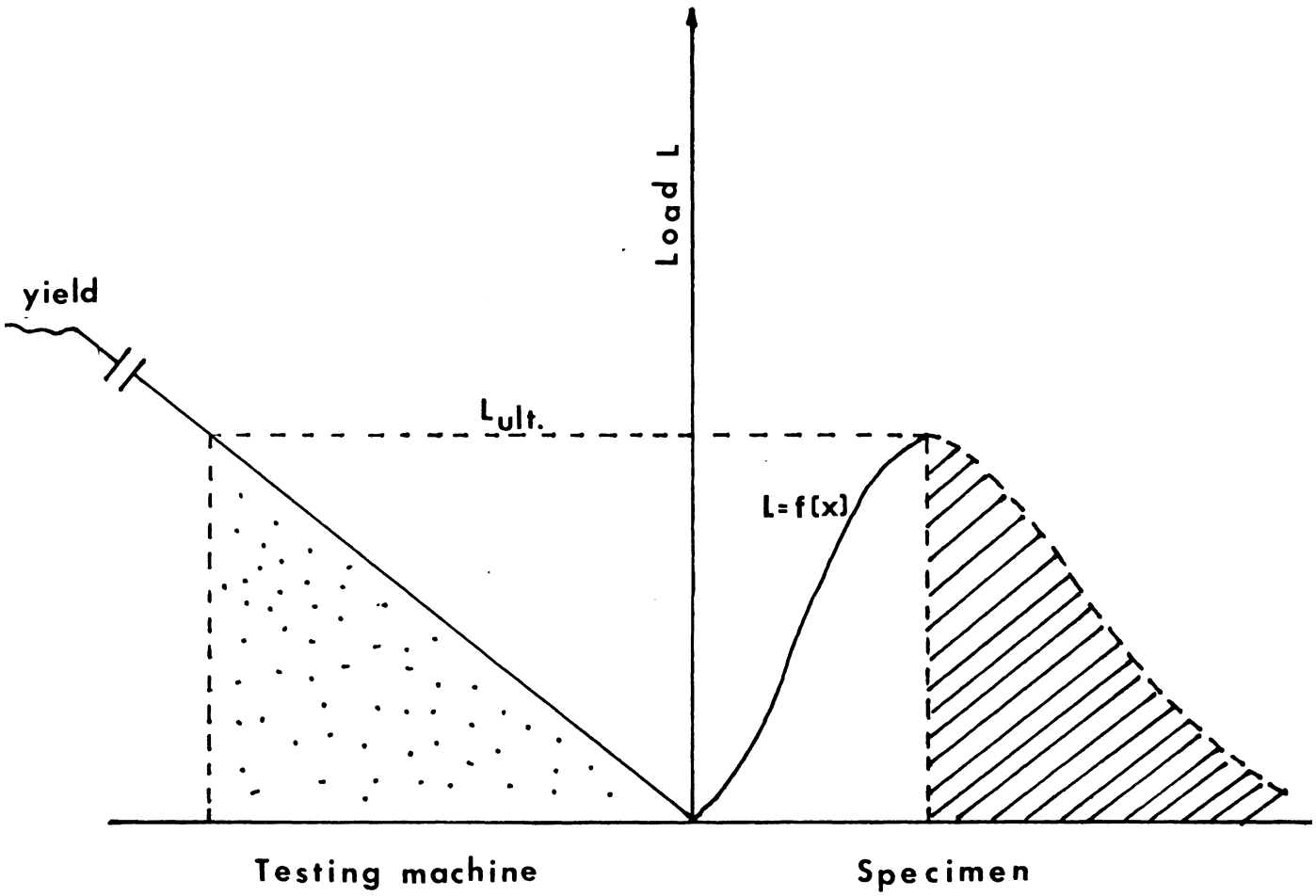

Fig. 2.2 Typical force-displacement curve for testing machine and for rock specimen.

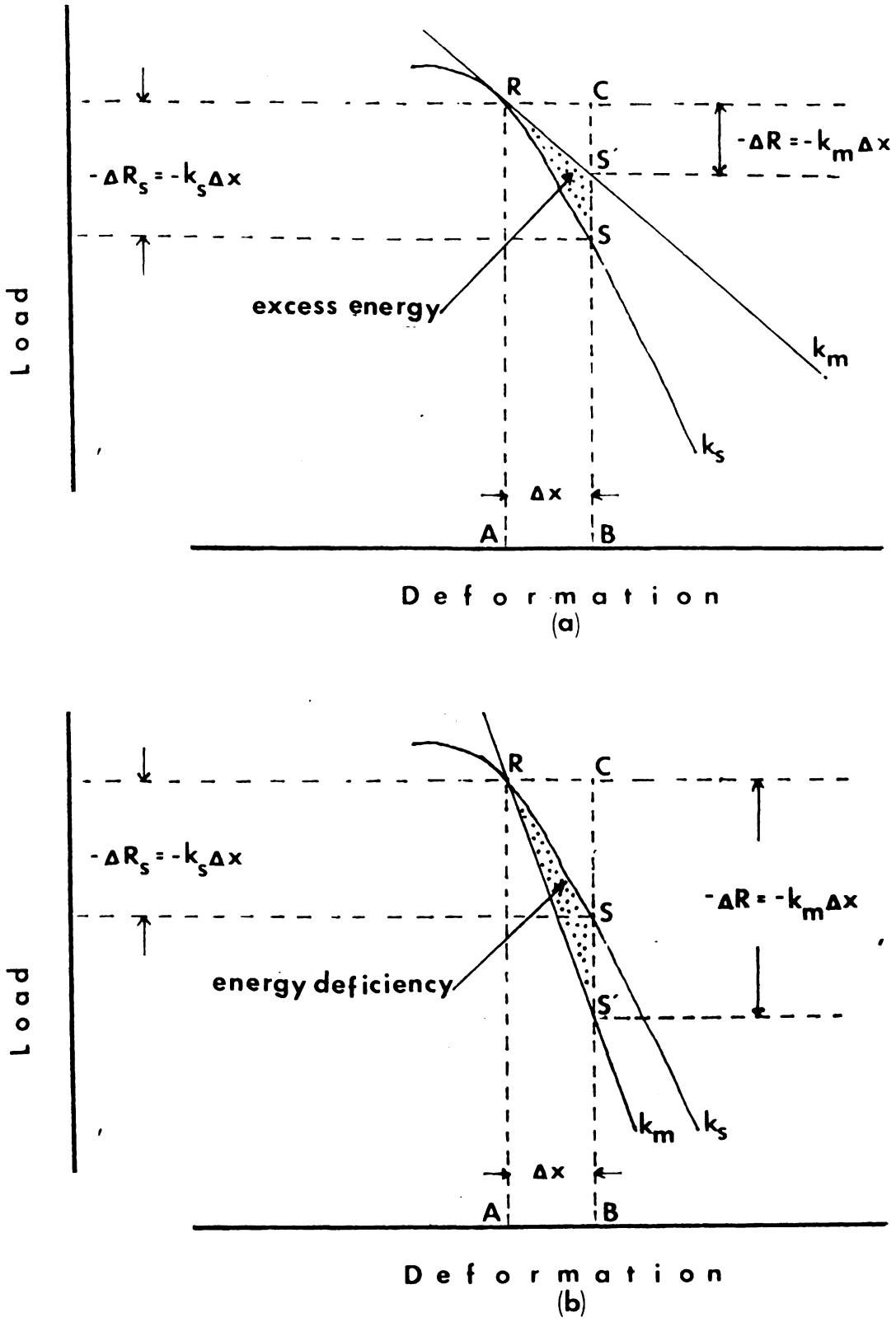

Fig. 2.3 Excess energy in (a) soft testing machine and (b) energy deficiency in stiff testing machine.

specimen, x, and did not affect the specimen as it was only associated with storing elastic energy in the machine. On the contrary a decrease in machine deformation in the region RB along the direction of the specimen deformation will affect the specimen by exerting a load onto it. The effect of this load on the post-failure behaviour of the specimen depends on the magnitude of the energy needed to deform the specimen in the post-failure region. Fig. 2.2 shows a diagrammatical representation of strain energy stored in the testing machine when ultimate strength of the specimen is reached, and energy needed to deform the specimen in post-failure region.

The effect of releasing strain energy stored in the machine to the failure behaviour of the specimen can be understood by studying the relationship between machine stiffness and the complete stress-strain curve for rock, using a load-displacement diagram depicted in Fig. 2.3. In this diagram, the stiffness of the specimen is represented by k_s, that of a soft machine is represented by a flat line k_m in Fig. 2.3a, and that of a stiff machine is represented by a steep line k_m, in Fig. 2.3b.

In general, the rock specimen under compression does not behave linearly, therefore its load-deformation curve is represented by

$$L = f(x) \quad \ldots\ldots\ldots\ldots (2\text{-}5)$$

where x is the sample compressive deformation and 'f' is some function (Fig. 2.2). Suppose that the specimen has reached its failure strength at a point R corresponding to a deformation x. Consider the effect of a small additional compression Δx; since Δx is small, the specimen load-deformation curve between x and $x + \Delta x$ is assumed as linear and corresponds to dR/dx. The compression Δx decreases the load bearing capacity of the specimen by an amount

$$\Delta R = (dR/dx)\Delta x$$

$$= k\,\Delta x \quad \ldots\ldots\ldots\ldots (2\text{-}6)$$

At this stage, the energy needed to deform the specimen is represented by the area under the load-deformation curve of the specimen that is

$$W_s = \text{Areas rectangle ABCR} - \text{triangle SCR}$$

$$= R\,\Delta x - \tfrac{1}{2}\Delta x\, k_s\, \Delta x$$

$$= R\,\Delta x - \tfrac{1}{2}\Delta x^2 k_s \quad \ldots\ldots\ldots (2\text{-}7)$$

The deformation Δx also results in a decrease of $\Delta R = k_m\, \Delta x$ in the load applied by the machine, provided energy is neither added to nor withdrawn from the system in this interval. The energy released by the machine is represented by

$$W_m = \text{Areas of rectangle ABCR - triangle SRS'}$$

$$= R\,\Delta x - \tfrac{1}{2}\Delta x\, k_m\, \Delta x$$

$$= R\,\Delta x - \tfrac{1}{2}\Delta x\, k_m \quad \ldots\ldots\ldots\ldots (2\text{-}8)$$

In the case where the stiffness of the specimen is greater than the machine stiffness as in Fig. 2.3a., that is

$$| k_s | > | k_m | \quad \ldots\ldots (2\text{-}9)$$

then by substituting (2-9) into (2-7) and (2-8) results in

$$R\,\Delta x - \tfrac{1}{2}\Delta x\, k_m > R\,\Delta x - \tfrac{1}{2}\Delta x\, k_s$$

or

$$\Delta W_m > \Delta W_s \quad \ldots\ldots (2\text{-}10)$$

This means that the strain energy released by the machine is greater than energy needed to the deform the specimen by Δx. The area of triangle SRS' represents the excess energy stored in the system. This condition is unstable and produces a violent failure of the specimen. If the stiffness of the specimen is less than the stiffness of the machine as shown in Fig. 2.3b, that is

$$| k_s | < | k_m | \quad \ldots\ldots (2\text{-}11)$$

then

$$R\,\Delta x - \tfrac{1}{2}\Delta x\ k_m < R\,\Delta x - \tfrac{1}{2}\Delta x\ k_s$$

or

$$\Delta W_m < \Delta W_s \quad \ldots\ldots \quad (2\text{-}12)$$

In this case the area of triangle SRS' represents a deficiency in energy needed to deform the specimen by Δx. Any additional deformation of the specimen always requires energy to be added to the system and the complete load-deformation curve of the specimen can be traced with such a machine.

In recent times, some technical means were made available to avoid a violent failure and to determine the load-deformation curve in the post failure range, these include

1. Increase the stiffness of the testing machine.

2. Decrease the stiffness of the rock sample:
   Consider equation (2-1) applied to the specimen tested in compression

$$L = k.\ m$$

and

$$m/l = \ /E = L/A.E$$

therefore

$$k = A.E/l$$

where L = load applied onto the specimen,

k = stiffness of the specimen,

m = deformation of the specimen,

l = length of the specimen,

= stress applied onto the specimen,

E = Young's modulus of the specimen, and

A = cross-sectional area of the specimen.

Hence it is more preferable to choose a rock sample with a small area A, over which the load is applied, and with large length l. This approach is, however, restricted because in practice the specimen tends to become unstable when using samples with a length-diameter ratio greater than 3.

3. Use a servo-controlled testing machine.

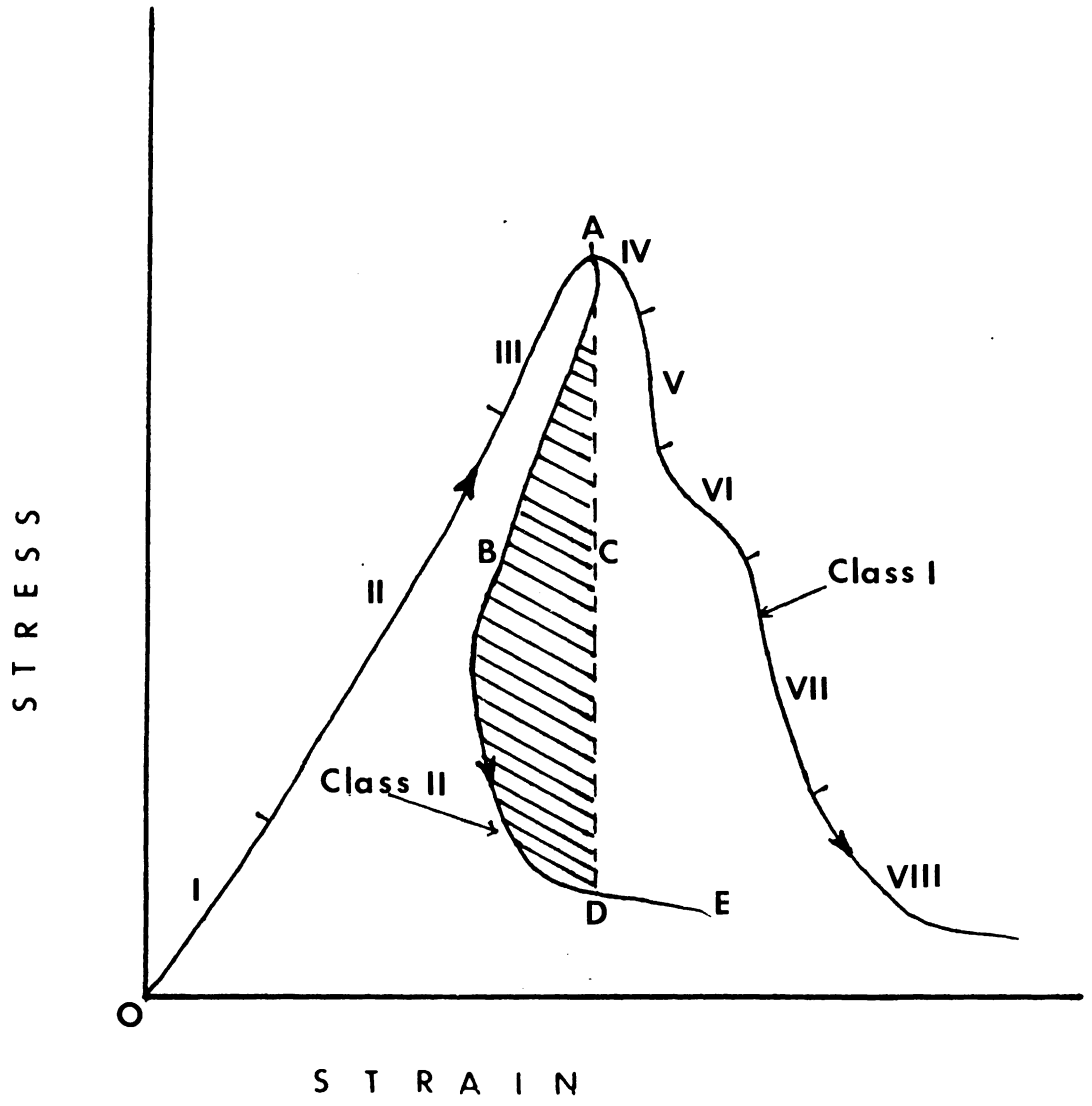

Fig.2.4 Classification of post failure behaviour of rock after Wawersik (1968).

2.2 COMPLETE COMPRESSIVE STRESS-STRAIN CURVE AND FAILURE LOCUS

Fig. 2.4 gives a typical example of a complete load-deformation curve of a specimen tested in stiff testing machine.

From the investigation of several authors (Cook, 1965; Bieniawski, 1967; Wawersik and Fairhurst, 1970) it is recognized that the stress-strain curve of intact rock specimen can be divided in several characteristic region.

In the first region refered to as region I, the behaviour of a specimen is marked by the closure of pre-existing internal and surface cracks. The degree of curvature varies between different rock types. Rock which are tightly packed have a linear path, whereas loosely packed rocks have a slight convex upward path on the stress-strain curve.

In region II the behaviour is approximately linear elastic. This region is characterized by closed cracks which can transfer frictional force.

Region III is characterized by crack growth and sliding between the existing crack interfaces; the cracks begin to extend to local micro-fractures, predominantly in the central portion of the specimen. The curve begins a gradual flattening and the behaviour is no longer elastic. At the end part of this region a rapid increase in the micro-crack density leads to the ultimate

strength of the specimen and the specimen suffers strength failure. Wawersik, 1968 (Wawersik and Fairhurst, 1970) have distinguished two classes of rock behaviour after the rock specimen experienced its strength failure. Class I rock is one in which work must be done on the rock to promote continued failure within the test specimen, resulting in a negative slope on the axial stress-strain curve. This type of rock is termed 'stable'. Alternatively 'unstable' or Class II rock, is one in which the failure process in the post failure region is partly self sustaining due to elastic strain energy stored in the specimen at strength failure is such that it is sufficient to maintain fracture propagation until the specimen has lost a greater part of its strength. To control failure of Class II rock, energy must therefore be extracted from the specimen, this produces a positive slope on the axial stress-strain curve. The dividing line between the two classes represents the case where the energy stored in the specimen is in equilibrium with the energy necessary to produce fracture (the vertical line AD in Fig. 2.4).

Region IV shows a less descending part of the curve. The formation of major crack arrays in this region can lead to sudden unstable fracture propagation.

Region V is characterized by the development of two types of major cracks, slabbing at the surface and shearing in the interior of the specimen. Slabbing usually becomes visible near the ends of

the specimen. After slabbing begins, shear cracks are generated along small segments on several sets of conjugate planes in the middle of the specimen. They are not yet connected to the surface cracks.

Region VI is characterized by the extension of the shear fractures which become interconnected in the following region VII to form a conjugate set of open shear fractures.

Region VIII is characterized by sliding along macroscopic fracture planes with increasing deterioration and crushing. The result is a loose mass of broken material.

The subdivision of the continuous progress of fracturing in a rock specimen, as presented above, should be kept general. Different rock types and geometry of the specimen can cause variation in the size of the regions. In extreme cases one or regions may not be absent at all (Hudson et al., 1972).

2.3 STIFF TESTING MACHINE

From details described in 2.1 it is possible that the complete load-deformation curve can be followed at will if the stiffness k of the machine corresponds to a slope that is steeper than the most steeply descending part of the load displacement curve of the specimen (Fig. 2.3). This approach was first explored in rock mechanics by Cook (1965).

The stiffness of a stiff testing machine is a function of the composite stiffness of machine's components which are all subjected to the same force. The stiffness k of an elastic member was given in equation (2-1) as

$$k = L/m,$$

where m is the displacement produce by load L along the direction in which it acts. The number of components contributing to the overall stiffness of a testing machine obviously depends on the machine design, and the overall machine stiffness must be computed for particular cases. The stiffness of a system k is

$$k_m = 1/(1/k_1 + 1/k_2 + \ldots 1/k_n) \ldots \quad (2\text{-}13)$$

The stiffness of an elastic member of length l, cross sectional area A, and modulus elasticity E loaded in simple compression or tension is

$$k = AE/l \ldots \quad (2\text{-}14)$$

Thus, the stiffness of such a member can be increased by increasing its cross-sectional area or modulus of elasticity, or by decreasing its length. The frame of a testing machine usually is subjected to

simple compression or tension, and its stiffness can be computed from equation (2-13).

Various stiffening devices have been used to increase the stiffness of the testing machine. Apart from the obvious step of massive construction of the machine for stiffness, these include the following

1. Load an elastic element such as a steel tube or bar in parallel with the specimen; the load is in effect, transferred to the elastic element as the load bearing capacity of the specimen diminishes (e.g., Cook, 1965; Bieniawski, Denkhaus, and Vogler, 1969; Brady, Duval, and Horino, 1971).

2. Lock the moving platen after the application of some load then raise the load to the fracture level through thermal contraction of the pre-heated columns of the machine, or by heat the specimen supports (Cook and Hojem, 1966; Wawersik and Fairhurst, 1970).

3. Use mercury as the hydraulic fluid (Hojem, Cook, and Heins, 1975).

Testing machine systems are defined as either stiff or soft depending on the specimen to be tested.

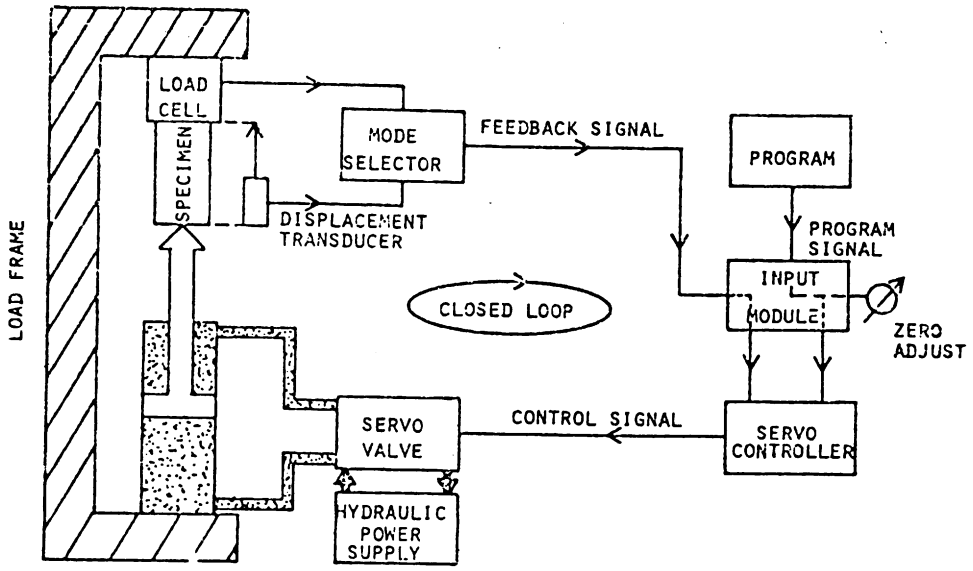

Fig. 2.5 Schematic diagram of the fast response closed-loop, servo-controlled testing system used during experimentation.

2.4 CLOSED-LOOP SERVO-CONTROLLED TESTING MACHINES

The basic principle of servo-controlled testing machines is depicted in Fig. 2.5. A feedback signal representing some experimental condition (for example the axial deformation of a sample) is generated by a transducer. The measured value is transformed into a voltage signal proportional to the loading. This electrical signal is compared with a programme signal which represents the test conditions desired. If there is any difference between the feedback and the programme signal then this is termed as an error signal which is used to activate the servo-valve. This results in the pressure on the specimen being adjusted until the desired and actual conditions coincide.

The continuous operation of such a 'closed-loop' system ensures that the experiment is automatically controlled and follows the course set by the programme.

2.4.1 The units in a servo-controlled testing machine.

Some most important units in a servo-controlled testing machine are as follows :

2.4.1.1 Feedback signal generator.

In general, any reasonable physical unit which can be

converted into an electrical signal such as displacement, force, pressure etc. is suitable as a feedback signal in the control loop. The feedback signal can be measured either directly, such as the loading rate where the signal is generated by a load cell located in the line of load action or reaction, or indirectly. If the feedback signal cannot be generated directly by a transducer, as in the case of work done on the specimen, operational amplifiers or a computer must be used to generate the feedback signal.

2.4.1.2 Programme signal generator.

The programme signal represents the required change, in the independent variable, with time. In most cases, a signal that increases at a fixed rate is sufficient to programme the experiment, such as in creep and relaxation tests where an independent variable (e.g. the confining pressure or the strain and stress levels) is held at a fixed value. This is obtained by generating a fixed voltage.

For tests in which the independent variable increases or decreases at a constant rate or according to some simple function, the programme signal is generated by an electro-mechanical or electronic function generator. For more complex tests, such as in fatique testing or simulation of in-situ conditions relating to the forces or displacements applied to a rock element during an earthquake, a computer can be used to provide the appropriate

programming signals. These signals are derived from direct measurement for example, data recorded on magnetic tape, to three actuators acting in three mutually perpendicular directions.

2.4.1.3 Feedback and program signal comparator.

Feedback and programme signals are compared in the servo-controller which supplies a control signal to the servo-valve that is proportional to the magnitude and polarity of difference between the two signals. If a difference between the two signals exists e.g. if the feedback signal indicates a higher deformation than desired, a control signal is generated to act on the servo-valve. The valve is then opened to allow high-pressure fluid into the actuator to correct the discrepancy by a rapidly reducting the effective fluid pressure acting on the hydraulic jack of the load frame.

The servo-controlled system does not, of course, respond instantaneously, a finite time in the order of milliseconds will elapse between detection and correction. It is most important that the valve is adjusted according to the polarity of the control signal so that it moves in the correct direction.

2.4.1.4 Hydraulic power supply and servo-valve.

Power for the testing system is provided by a hydraulic power

supply that can provide fluid for the servo valve at a constant high pressure. The hydraulic power supply performs a function analogous to the battery in an electrical circuit so that it is possible to run several testing systems simultaneously from the same power supply, and provided it has a sufficiently high rating.

2.4.1.5 Actuator and load frame.

Conventional actuators and load frames can usually be utilized for a servo-controlled testing system used for quasi-static or low-frequency rock mechanics tests, but in high loading, however, a stiff frame must be used. A stiff frame is preferred because it allows a certain change in load or displacement to be achieved with minimum actuator movement and hence with minimum time so that the operation of the closed-loop is optimized.

2.4.2 Factors involved in controlling rock failure in a servo-controlled testing machine.

Two important factors which govern the successful control of rock failure test in a servo-controlled testing machine are the response time of the complete closed-loop system, and the correct choice of feedback signal.

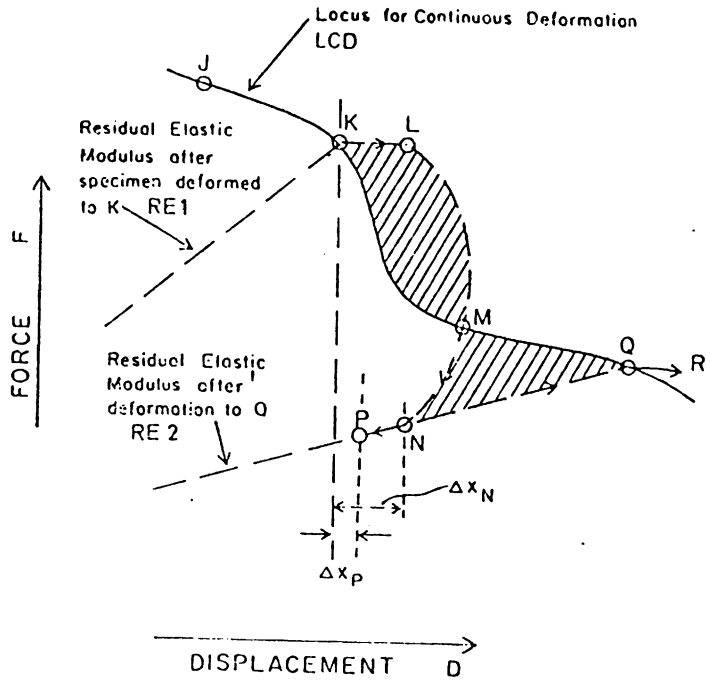

Fig. 2.6 Idealized response of the servo-system to a rapidly created condition of instability.

2.4.2.1 Response time.

The response time is the time taken by the machine to react to inhibit failure propagation in the rock specimen by generating feedback signal and adequately adjusting the closed-loop system to reduce the applied force.

Initially servo-controlled loading systems have been generally considered unsuitable for controlling rock failure because of the finite response time of all servo-systems (Jaeger and Cook, 1969). The experiments carried out by Rummel and Fairhurst (1970), have indicated, however, that this view is incorrect (at least for many rocks tested in compression) in that the response time appears to be adequate in the control of the deformation rate. Fig. 2.6 shows the sequence of events illustrating the time elapse between detection of an instability in deformation, monitored by the transducer, and adequate reduction of the applied force. Along the locus JK the specimen has been deformed at a constant rate x. At K, an instability starts to develop. Before the servo reacts, the system unloads as a fairly soft system, resulting in a rapid deformation along KL. As the servo start to act at L, the force drops following a path such as LMN. According to Berry's analysis of crack propagation, the instability has developed maximum kinetic energy at M (Berry, 1960). The specimen continues to deform but is decelerated by the kinetic energy along MN. At N instability eventually halts. If the

programmed deformation rate is x and assuming that the time lapse between K and N is t such that $xt=\Delta x_p$, then the servo-system will command further unloading, since the specimen is over-deformed to ΔxN, and this now will occur along the residual elastic curve, to point P, such that the deformation between K and P is Δx_p. Deformation will then continue at the programmed rate x, along the elastic path PNQ until the failure locus is reach at Q, and the cycle is repeated. If the programmed strain rate x is too high, the deformation during time t, i.e. xt, will exceed incremental residual elastic strain (K to Q) and place the system beyond the failure locus where failure can not be controlled. To avoid this the strain rate must be low enough so that

strain rate x response time < Δ strain (K to Q).

2.4.2.2 Choice of feedback signal.

A servo-controlled testing machine has been successfully used in the past to determine the complete force-deformation curve for specimens deformed in compression until totally disintegrated (Rummel and Fairhurst, 1971). This was obtained by programming a linear increase in axial-deformation with time; the system linearly increases the deformation with time even though the specimen fails and suffers a progressive reduction in load-bearing capability during the process. This situation occurs with the specimen of

Class I behaviour. If the complete force-deformation curve does not monotonically increase in deformation, however, such as in Class II behaviour, the linear increase can only be achieved along the curve OABCE shown in Fig. 2.4. Since the material behaviour is represented by the curve OABDE, there is excess energy (proportional to the shaded area) supplied to the specimen which causes uncontrolled failure of the specimen. Special technique must be used to test specimens that exhibit Class II behaviour.

In a stiff testing machine one method of withdrawal of the excess energy from a system is by cycling the deformation in the post failure region manually (Wawersik and Brace, 1971). A similar approach can be applied in servo-controlled machines but the programme signal must be changed. The programme signal, however, cannot be satisfactorily altered since it is difficult to construct a meaningful programme involving a non-linear or non-monotonic function (Hudson et al., 1972). Therefore, controlled failure under these circumstances can not be achieved automatically under this circumstance. When rock failure is studied in a servo-controlled testing machine, control of failure and recording of the required experimental output are two separate considerations (Hudson et al., 1971), therefore there is much more flexibility associated in choosing an independent variable and hence the feedback signal. The control of rock failure is optimized when the transducer is choosen for maximum sensitivity in detecting any tendency towards failure.

In general, since specimens tend to develop cracks

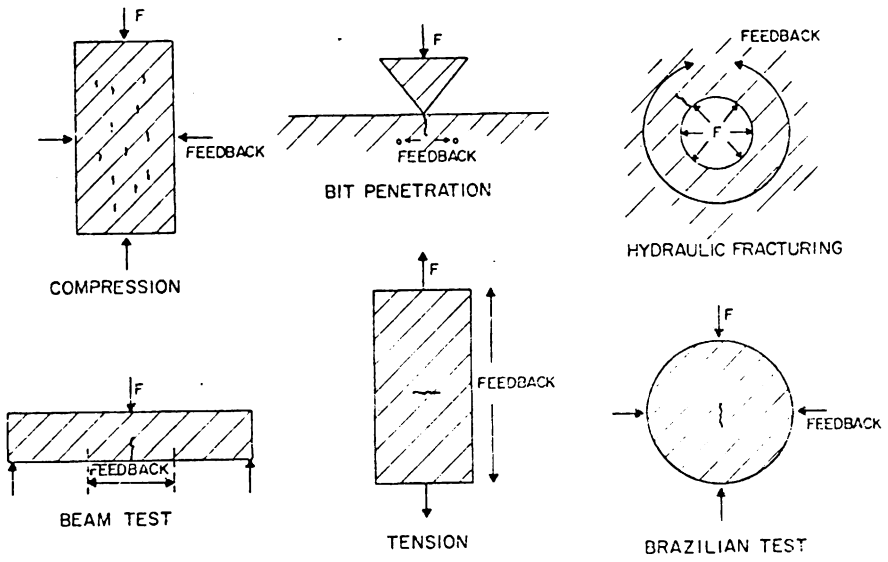

Fig. 2.7 Response requirements for optimum displacement control in various situations.

perpendicular to the least principal stress, a displacement transducer used to generate the feedback signal should be mounted in the direction of the least principal stress. Fig. 2.7 shows the direction in which the displacement should be measured for optimal control in a variety of situations.

CHAPTER THREE

SAMPLE PREPARATION AND EXPERIMENTAL PROCEDURE

This chapter contains a brief description of the test sample origin, specimen preparation, apparatus, and experimental procedure used in the experiment. Information is tabulated in the relevant sections.

3.1 SAMPLE HISTORY

Two rock types were used in the experiment, they were : siltstone and pyritic ore, both from the Elura Mine, near Cobar, in New South Wales.

The siltstone is fine grained with distinct graded bedding. It contains minor cross-bedding and very minor pyrite (<1%). It has been detached from its parent rock for a period of over a year. The pyritic ore is a coarse grained, with pyrite grain size greater than 1 mm. The ore was from a part of the Elura orebody located in the vicinity of the siltstone sample. The samples were located some 160 metres below the surface and both rock types can normally be subjected to wet and dry conditions.

3.2 SPECIMEN PREPARATION

All rock samples were drilled out of selectively, oriented blocks so as to ensure the greatest possible sample homogenity. A Hercus No.4A coring machine with impregnated diamond bit was used to core the specimen from roughly cubical blocks of approximately 30 cm size. The drilling rate used was 0.127 mm/rev. with a rotational speed of 162 rev./min. Cores were trimmed to approximate length with a diamond saw and the ends ground on a diamond impregnated disc. Wet drilling, cutting and end finishing were used throughout.

The 30.50 cm (1.25 inch) specimen diameter was chosen so as to avoid causing macro-cracks in the sample. This diameter satisfies the requirement that the ratio of diameter to size of the largest grain must be at least 10:1. Other dimensional tolerances included (1) ends of the specimen were ground flat to within 0.02 mm and perpendicular to the axis of the specimen to within 0.05 in 50 mm, and (2) the sides of the specimen were smooth, free of abrupt irregularities and straight to within 0.3 mm over the full length of the specimen.

The specimen dimensions and descriptions for the two rock types are listed in Table 3.1 and Table 3.2 respectively.

TABLE 3.1

SILTSTONE SPECIMEN DIMENSION AND DESCRIPTION

Specimen code number	Mean length (mm)	Mean diameter (mm)	Mean area ($m^2 \times 10^{-4}$)	Length to diam. ratio	Density (T/m^3)	Description
S1.1	61.36	30.45	7.282	2.02	2.736	Top and bottom surfaces are good. Minor spall at the mid height
S1.2	62.35	30.47	7.299	2.05	2.725	Good top and bottom. Minor hair cracks on the side surface.
S1.3	59.84	30.33	7.225	1.97	2.704	Good surfaces. Quartz band at the mid plane.
S1.4	67.21	30.35	7.234	2.21	2.698	Good surfaces. Quartz band at the mid plane.
S1.5	58.58	30.43	7.273	2.10	2.714	Good surfaces.
S2.1	62.24	30.35	7.234	2.05	2.710	Good surfaces.
S2.2	64.11	30.40	7.258	2.11	2.726	Good surfaces.
S2.3	63.80	30.43	7.273	2.10	2.714	Good surfaces. Massive appearance with coarser sand grains.
S2.4	64.80	30.41	7.263	2.13	2.744	Good surfaces. Massive appearance with coarser sand grains.
S2.5	63.26	30.38	7.249	2.08	2.718	Minor hair cracks at the bottom.
S2.6	64.11	30.40	7.258	2.11	2.732	Hairy cracks on the surfaces.
S2.7	66.58	30.41	7.263	2.19	2.736	Good surfaces. Massive appearance.
S2.8	61.16	30.40	7.258	2.01	2.734	Good surfaces. Massive appearance.
S2.9	62.40	30.39	7.254	2.05	2.726	Good surfaces.
S2.10	62.31	30.43	7.273	2.05	2.742	Good surfaces. Quartz band at the mid plane.
S3.1	30.78	30.45	7.282	1.01	2.736	Good surfaces. Massive appearance.
S3.2	31.12	30.35	7.234	1.03	2.710	Good surfaces.
S3.3	31.90	30.38	7.249	1.05	2.732	Good surfaces.
S3.4	30.54	30.40	7.258	1.00	2.734	Good surfaces.
S3.5	30.62	30.38	7.249	1.01	2.704	Minor spall at the top.
S4.1	15.80	30.39	7.282	0.52	2.724	Massive appearance.
S4.2	16.77	30.45	7.282	0.55	2.710	Hair cracks on the top.
S4.3	16.68	30.51	7.311	0.55	2.712	Hair cracks on the top.
S4.4	15.18	30.51	7.311	0.50	2.732	Massive appearance. Good surfaces.
S4.5	16.01	30.41	7.326	0.53	2.736	Good surfaces.
S4.6	15.63	30.51	7.311	0.51	2.732	Good surfaces.

TABLE 3.2

PYRITIC ORE SPECIMEN DIMENSION AND DESRIPTION

Specimen code number	Mean length (mm)	Mean diameter (mm)	Mean area ($m^2 \times 10^{-4}$)	Length to diam. ratio	Density (T/m^3)	Description
P1.1	64.05	30.43	7.273	2.10	3.865	Hair cracks at the top and bottom. Galena cavity filled at the mid height.
P1.2	63.73	30.48	7.297	2.09	4.130	Hair cracks at the top and bottom. Minor spall at the top side
P1.3	63.84	30.58	7.345	2.09	3.839	Good surfaces.
P1.4	61.79	30.47	7.292	2.02	4.290	Good surfaces.
P1.5	62.31	30.45	7.282	2.05	3.888	Hair cracks at the top.
P2.1	30.46	30.25	7.187	1.01	4.451	Micro cracks at the mid height. Good top and bottom.
P2.2	30.42	30.25	7.187	1.01	3.943	Hair cracks at the top.
P2.3	30.54	30.42	7.268	1.00	3.980	Hair cracks at the top and side surfaces.
P2.4	31.04	30.44	7.277	1.02	3.878	Good surfaces.
P2.5	30.62	30.38	7.249	1.01	3.654	Good surfaces.

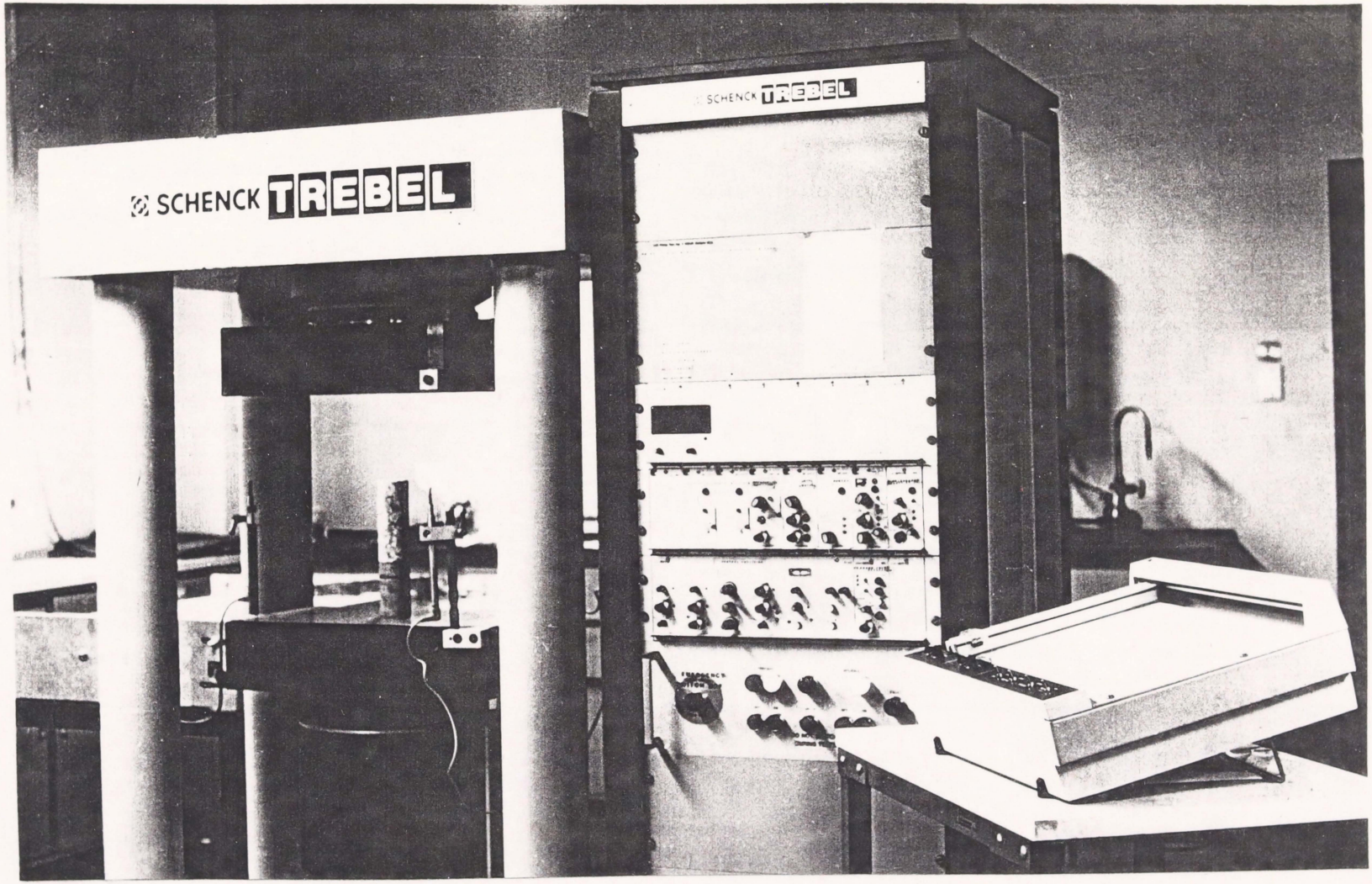

Fig. 3.1 Schenck Trebel servo-controlled testing machine.

3.3 APPARATUS

The apparatus used in the experiment was a Schenk-Trebel Hydropuls servo-controlled, stiff-framed compression testing machine. The loading frame consists of four steel columns and two steel cross-heads, rectangularly shaped. The loading frame has a rated composite stiffness of 1660 kN/mm. The capacity of the machine is 500 kN. The applied load was measured internally by a load cell and displayed digitally.

The deformation of the specimen was measured axially with three inductive extensometers placed on holders on the lower cross-head and rested on magnetic blocks mounted on the upper cross-head. The three extensometers were positioned around the specimen at 120° angles, with their signals summed to diminish the effect of possible non-uniform deformation. The deformation displayed, represented the arithmetic mean of the three extensometers. Each extensometer had a nominal displacement of 10 mm, a spring constant of 10 g/mm and the linearity error of the system was less than 0.5%.

Load, displacement and deformation can be read through an internal digital display. The readouts had a time basis error of 0.01% and linearity error of 0.01%. A Hewlett-Packard 7040A x-y Recorder connected to the servo-controlled mechanism was used to record the load and deformation of the machine-specimen system during a test. The x and y axis scales were determined from the

machine control panel. Fig. 3.1 shows the testing machine and the x-y recorder.

4.4 LOADING CONDITION

Specimens were subjected to a monotonically increasing axial strain of constant rate up to strength failure point. This condition renders as an independent variable. In the region beyond strength failure, for most of the specimens cyclic loading was applied to prevent uncontrolled failure. During unload and reload along post failure region, again strain rate was used as an independent variable.

A rubber jacket was used to enclose each sample so as to keep it intact during the failure process and to minimise specimen disintegration due to side spall. It was assumed that the rubber was not of sufficient strength to provide a lateral stress to the sample but merely prevented the specimen from spalling during failure, to enable test to be continued beyond strength failure.

A preliminary series of tests was performed on both the pyritic ore and siltstone specimens with mean length to diameter ratio of 2:1. The strain rates applied were 40,20 and 5 millimicrometre/minute which correspond to 1.11×10^{-5}; 5.56×10^{-6} and 1.39×10^{-6}/second respectively. Based on the these early tests and limitations on test duration, strain rates of 1.39×10^{-6} /second, 2.78×10^{-6}/second and 3.08×10^{-6}/second were adopted for

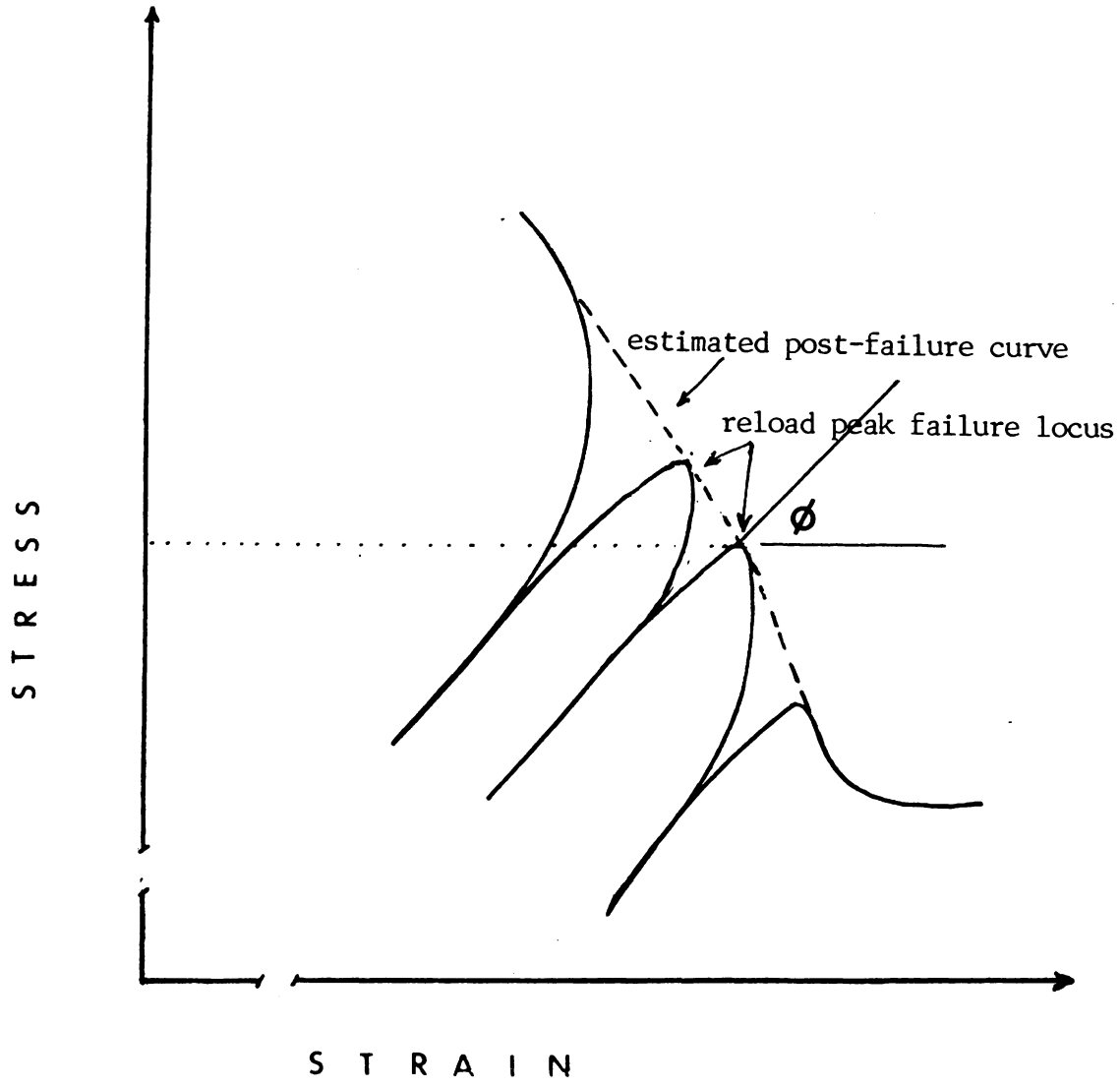

Fig..Method of approach to determine the post-failure curve.

testing the specimens with mean L/D ratios of 2 : 1, 1 : 1 and 0.5 : 1 respectively. Table 3.3 shows a list of strain rates used by several authors in their experiments.

From the preliminary tests it was also found that even at a ver low strain rates, constant monotonical loading on specimen of certain sample geometry resulted in violent failure after strength failure was reached. To overcome this, cyclic loading in post failure region, developed by Wawersik and Fairhurst (1970), was applied. By closely watching an X-Y plot of load versus deformation, the load was quickly removed when the strength began to drop. This means that deformation was reversed to the negative direction. Because post-failure curve is a limited curve for material stability (i.e. a positive displacement from any point to the left of the post-failure curve can be affected only by a force increase), this negative displacement resulted in a decrease of the sample force below the local strength. Failure was halted as soon as all the remaining energy associated with fracture propagation (inertia effects) was attenuated or converted into effective surface energy. When failure stopped, the sample was reloaded until the failure curve was reached again and fracture propagation commenced. By repeatedly unloading and reloading the specimen within the post-failure region, an approximation to the actual complete stress-strain curve of the specimen can be obtained by extrapolating the peaks of reload curves as shown in (Fig. 3.2).

TABLE 3.3

LOADING CONDITION REFERENCES

Reference	Strain Rate per second	Specimen Geometry	
		Diameter	L/D ratio
Wawersik & Fairhurst (1969)	10^{-5}	25 to 50 mm (1 to 2 inch)	2 : 1
Wawersik & Brace(1970)	10^{-5}	25 mm (1 inch)	2 : 1
Rummel & Fairhurst (1970)	2.5×10^{-5} to 2.5×10^{-7}	50 mm (2 inch.)	2 : 1
Hudson et.al.(1971)	1.5×10^{-6}	19 to 100 mm (3/4 to 4 inch)	1/3 : 1 to 3 : 1
Peng & Podnieks (1972)	10^{-2} to 10^{-7}	32 mm (1.25 inch)	2 : 1
Sarkka (1979)	1.35×10^{-5}	32 mm	0.3 : 1 to 3 : 1
Houpert (1979)	2.5×10^{-4} to 2.5×10^{-7}	-	-
White M.J. et.al.(1984)	2×10^{-6}	50 mm	2 : 1

CHAPTER FOUR

EXPERIMENTAL RESULTS AND DISCUSSION

To control failure of the specimen in the post failure region, the axial strain rate was set as low possible, taking into account the machine capability, the specimen geometry and the time duration for each test. In addition, consideration was given to the type of loading to be applied (see Section 3.4).

Table 4.1 shows the number of the specimens tested and loading condition applied.

TABLE 4.1

NUMBER OF SPECIMENS TESTED AND LOADING CONDITION APPLIED

No.	Type of rock	Number of specimens tested	Mean L/D ratio	Loading Condition	
				Strain rate 10	Type of loading in post failure region
1.	Siltstone	5 (S1.1-S1.5)	2	1.39	monotonic
2.	Siltstone	10 (S2.1-S2.10)	2	1.39	cyclic
3.	Siltstone	5 (S3.1-S3.5)	1	2.78	cyclic
4.	Siltstone	6 (S4.1-S4.6)	0.5	3.08	monotonic
5.	Pyritic ore	5 (P1.1-P1.5)	2	1.39	attempted cyclic
6.	Pyritic ore	5 (P2.1-P2.5)	1	2.78	attempted cyclic

The load-deformation curves recorded for the individual specimens obtained from the x-y plotter have been reduced to stress-strain curves as shown in Appendix 1 (Fig. 4.7 to Fig. 4.38). From these curves, the shape of the stress-strain curves, types of failure and failure parameters were observed.

4.1 SHAPE OF STRESS STRAIN CURVES AND FAILURE BEHAVIOUR

Shape of the complete stress-strain curve of rock and the type of failure of a specimen under compression are not just an intrinsic property of the rock but dependent on many other factors. Generally, stress-strain relationships in the pre-failure region for rocks under uniaxial compression are qualitatively identical. The same cannot, however, be said of the post-failure region especially when the fracture has been servo-controlled. The curve obtained will depend on both the intrinsic property of the material and the conditions underwhich the test was carried out.

4.1.1 Siltstone specimen behaviour.

Various types of behaviour shown by siltstone specimens are related to their geometry and the loading type applied. From observations during and after the tests and from analysis of stress-strain curves obtained, four basic types of failure are

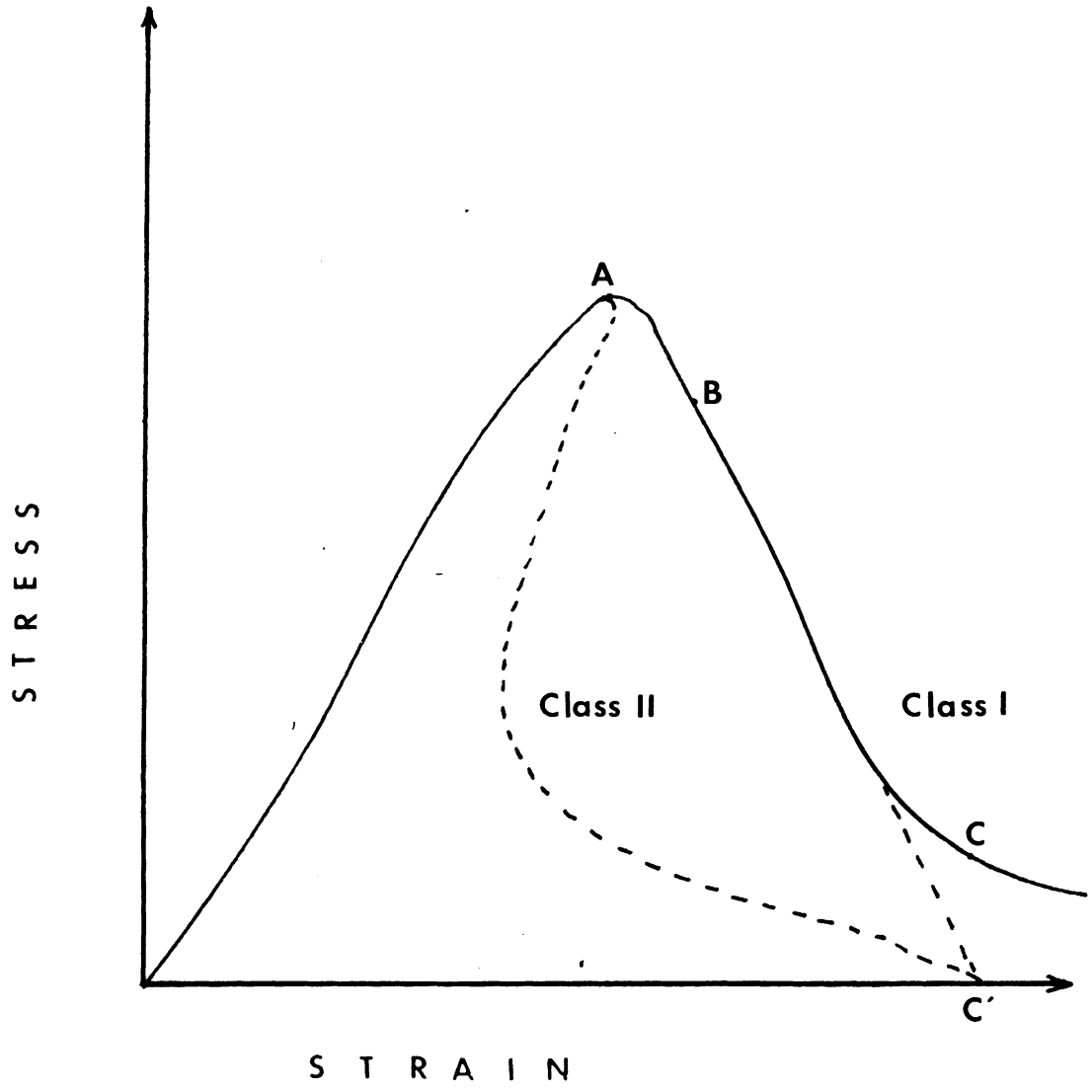

Fig. 4.2 Generalized stress-strain curve for siltstone specimens.

recognizable as illustrated in Fig. 4.1, these are :

1. Instantaneous failure, where a specimen failed at or just after the peak load-bearing capability of the specimen (point A).

2. Partly-controlled failure, a specimen can no longer sustain the maximum load required for safety or stability in a given situation (e.g. point B).

3. Fully-controlled failure, the specimen failure can be controlled until the residual strength level is reached (point C).

4. A variation of types 1 and 2 above where the unloading curve does not drop to zero stress but it regain its unloading stability at residual strength level.

Inspection of the failed specimens after a test was completed indicated that the specimens failure mode generally occured as local fracturing, and predominantly parallel to applied stress.

4.1.1.1 Specimen with L/D of 2:1 (Fig. 4.7 to Fig 4. 12 in Appendix 1).

In the post failure region all the specimens with L/D of 2:1 were tested at a strain rate of 1.38×10^{-6} per second. Five specimens were tested under monotonic loading, and ten under cyclic loading.

Under monotonic loading four of the five specimens tested, i.e. S1.1, S1.2, S1.3 and S1.5, failed instantaneously just after the peak strength was reached. The specimens S1.1 and S1.2 regained their residual strength level at about 30% of the peak strength, while S1.3 and S1.5 had no residual strength. The failure of S1.4 specimen could partly be controlled before rupture at about 65% of its peak strength and then regained the unloading stability at residual strength level.

From 10 specimens tested under cyclic loading, specimens S2.3, S2.7 and S2.9 failed instantaneously just after the strength failure was reached. None of them had any residual strength. The failure of specimens S2.1, S2.2 and S2.10 can be partly controlled. Specimen S2.1 ruptured after the second recycling at about 50% of the peak strength, and regained its residual strength. Specimens S2.2 and S2.10 ruptured just after the peak point of the first reloading cycle; both had no residual strength. The failure of specimens S2.4, S2.5 and S2.6 can be fully controlled down to the residual strength level.

4.1.1.2 Specimen with L/D of 1:1 (Fig. 4.21 to Fig. 4.24 in Appendix 1).

All the five specimens of L/D of 1:1 were tested at a strain rate of 2.78 x 10^{-6} per second under cyclic loading in the post failure region. The failure of specimen S3.1 was partly controlled until the second reloading cycle, and then the specimen ruptured at about 30% of the peak strength. It had no residual strength. Specimens S3.2, S3.3 and S3.4 were fully controlled and they regained their residual strength.

4.1.1.3 Specimen with L/D of 1/2:1 (Fig. 4.25 to Fig. 4.28 in Appendix 1)

Six specimens of this geometry were tested at a strain rate of 3.08 x 10-6 per second under monotonic loading. Two of them (S4.2 and S4.3) produced unreliable results. The failure of specimens S4.1, S4.4, S4.5 and S4.6 were fully controlled until reached the residual strength level.

4.1.2 Pyritic ore specimen behaviour.

Unlike siltstone all the pyritic ore specimens with an L/D ratio of either 1 or 2 failed instantaneosly at or just after the peak strength was reached. In these cases, the machine

unloading path dropped instantly to zero stress level. Specimen numbers P1.2, P1.5, P2.1 and P2.2 failed quite violently which produced shock wave that was felt extensively throughout the laboratory. Only a few remnant were left on the platen. These consisted mostly of small and fine fragments. Most of the specimen was laid about the testing machine. The other specimens failed less violently though some vibration was produced. Fractured specimens were characterized by vertical fracturing failure in the direction parallel to the major compressive stress.

The stress-strain curves of the pyritic ore specimens are shown in Fig. 4.29 to Fig. 4.38 (Appendix 1). They generally do not indicate that local fracturing have occured at pre-peak load. It may be concluded that in these specimens, fracture initation and propagation occurred at the peak of the stress-strain curve. Therefore if violent failure is to be prevented, large amounts of energy must be extracted from the specimen very quickly. Although this has not been done in this experiment an attempt was made to reverse the loading just at the point when the peak strength was reached (see Section 3.4). Eventhough no complete stress-strain curves for these pyritic ore specimens were obtained, they are obviously very much of Class II rock.

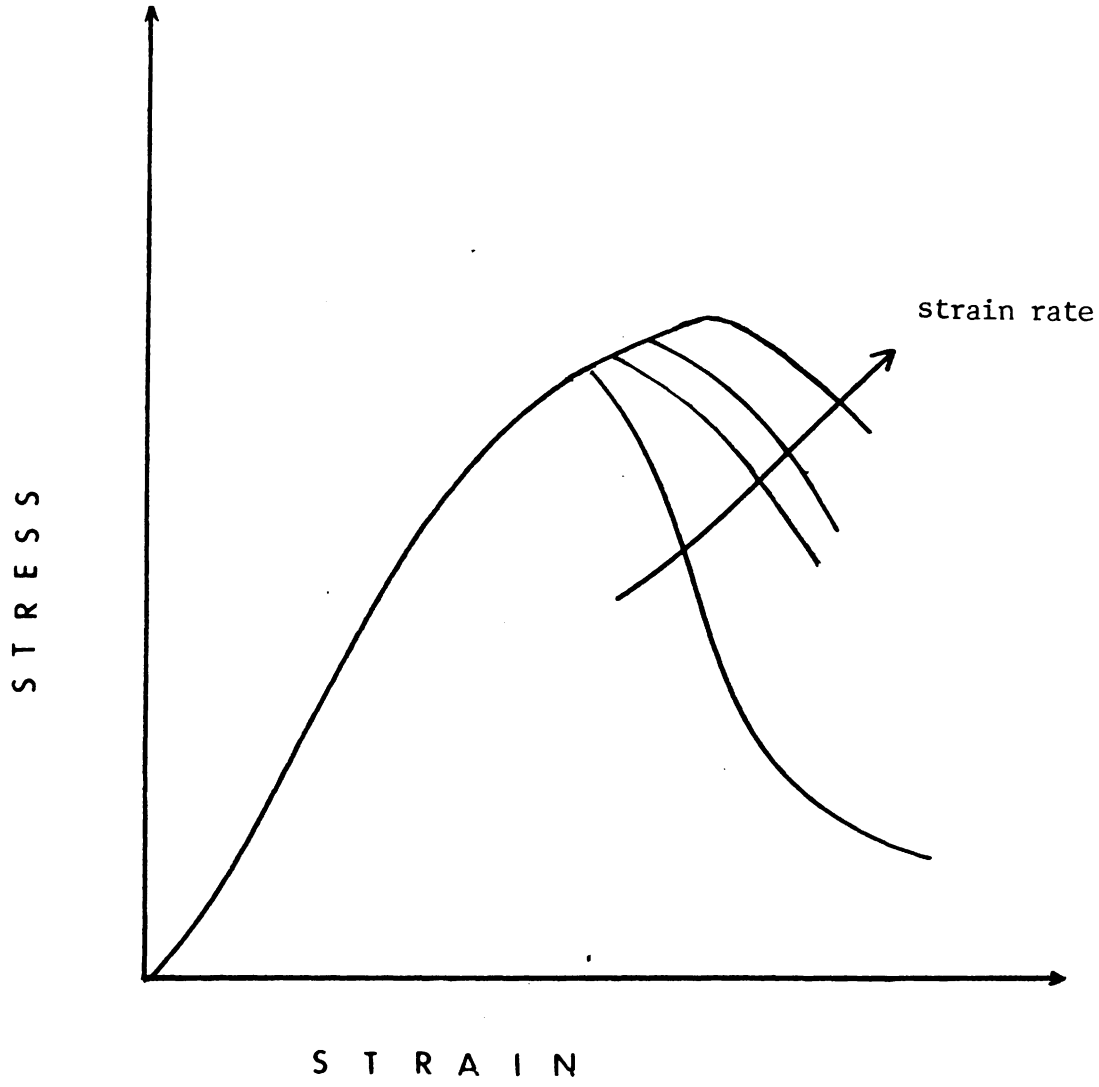

Fig. Idealized schematic stress-strain curve with varying rate of strain.

4.1.3 Factors influencing the shape of stress-strain curve and failure behaviour.

Factors which influence the shape of stress-strain curve when rock specimens are tested under uniaxial compression in stiff or servo-control testing machine, have been recognized by previous investigators; these include strain rate, micro structure and specimen geometry.

4.1.3.1 Strain rate.

It is generally agreed that for most types of brittle rock, fracture control is easier at lower strain rates rather than at higher ones. Fig. 4.2 is a schematical representation of a stress-strain curve as a function of strain rate.

As described in Section 3.4, preliminary tests carried out in this experiment showed a finding that the form of the complete stress-strain curve depended on the value of the applied strain rate, and that controlled failure is most likely to be obtained at a slower strain rate. Therefore in order to measure under controlled failure, the strain rate applied in this experiment was selected to be as low as possible to take account of machine capability, specimen geometry and time duration availability.

Houpert (1979) has found, however, that over certain Class I materials such as marbles, coarse-pored limestones and sandstones, and rocks with a high degree of cracking, failure can be fully controlled irrespective of the value of strain rate applied. His tests involved strain rates between 2.5×10^{-4} to 2.9×10^{-7} per second).

4.1.3.2 Micro structure.

Brown and Hudson (1971) investigated the influence of a rock's microstructure rock on the shape of stress-strain curves and found three distinctive types of behaviour which may be recognized :

1. In highly porous, clastic, sedimentary rocks (e.g. some sandstones) and in weathered rocks having similar porous, granular texture (e.g. weathered granite), the only observable 'fracture' feature in the region about the peak along the stress-strain curve is a collapse of the pore structure. Macro fracture surfaces appear near the specimen ends only after the load-bearing capability has been reduced to 50-80% of its peak value. As the porosity decreases, microscopic materials are characterized by low deformation moduli in the loading range and unloading curves. Failure can be controlled in any reasonably stiff testing system, and in

many cases in a conventional hydraulic testing machine.

2. In crystalline rocks other than those with ultra-fine grains (e.g. in the majority of igneous and metamorphic rocks), the structural break down process is a gradual one in which the formation of a number of inter- and intra-granular sub-axial cracks is the predominant feature. Load-deformation curves may be of either Class I or II, depending on the nature of the rock. Limited evidence available suggests that as average grain size decreases, the unloading portion of the load-deformation curve steepens and in some cases becomes Class II.

3. In dense, ultra-fine grained rocks (e.g. Solenhofen limestone), attempts to control failure, so far, have not been successful. Apparently this is because the structural break-down process is an almost instantaneous rather than a gradual or progressive one. Most likely all such rocks are Class II.

Generally each of the samples of the siltstone and pyritic ore specimens had a visually uniform appearance. The siltstone was well bedded fine grained. Whilst the pyritic ore, although it has a coarse grains with average diameter of 1 mm, was homogeneous, massive and free from macro cracks. According to

the classification above, the observations on on failure behaviour and the shape of the stress-strain curve of the samples tested as described in Sections 4.1.1 and 4.1.2, the siltsone specimens can be grouped as type 2 and pyritic ore specimens as type 3.

4.1.3.3 Specimen geometry.

Hudson et al.(1971) studied the variations of the shape of stress-strain curve related to specimen geometry. He was concluded that the axial cracks were generally concentrated in the central portion of the specimen's length because lateral restraint at the specimen ends inhibits their growth near the specimen-platen interface. In longer specimens, the central region failed whilst the ends were elastically loaded and then unloaded. For specimen with lower L/D ratio , however, the cracks appear to be uniformly distributed throughout the length of the specimen. If the failure is uniformly distributed throughout the specimen then failure progresses in a gradual manner to result in controlled failure. Such was the case with specimens of small L/D ratio.

The results also tended to show that the failure of sltstone specimens of smaller L/D ratio, are more controllable then the longer specimens. In the case of pyritic ore specimens, however, where the L/D ratio ranged between 2 : 1 and 1 : 1,

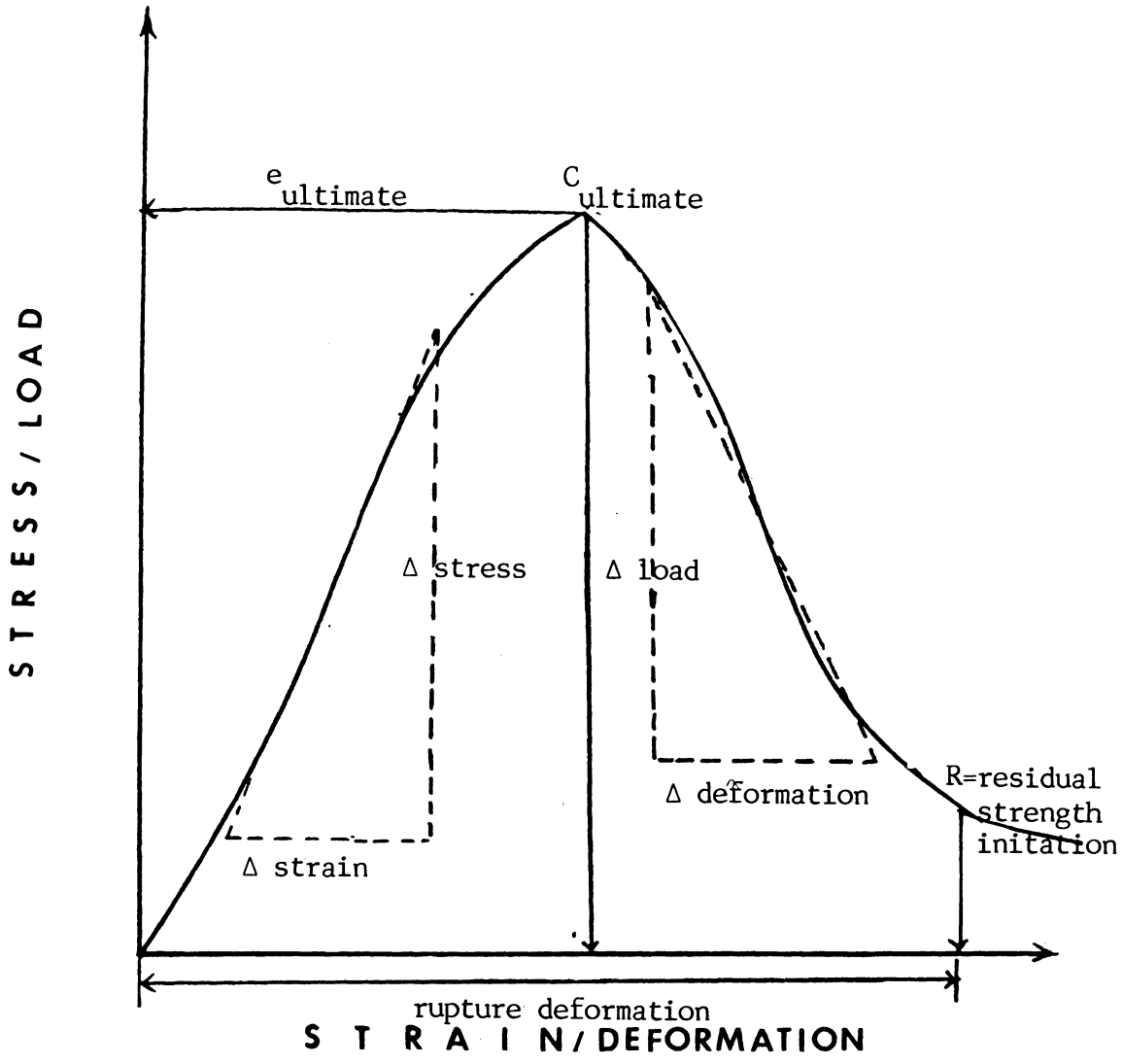

Young's modulus E = Δstress/Δstrain

Post failure stiffness k = -Δload/Δdéformation.

Fig. 4.3 Method of approach to determine the post-failure parameters.

geometry did not seem to have any effect on the failure mode since all the specimes failed in an uncontrolled manner.

4.3 FAILURE PARAMETER

In the absence of recognized standards to define the post failure properties of a rock, the following parameters were calculated; Young's modulus, compressive strength, deformation and post failure stiffness. These were measured from the graphical records using methods as outlined in Fig. 4.3. The measured values are presented in Table 4.2 and 4.3. Mean values and standard deviation for each measurement were calculated where possible.

4.3.1 Young's modulus.

Since lateral strain did not observed, only Young's elastic moduli was measured in this experiment. According to Hooke's law for an ideally elastic material, the relationship between normal stress and resulting normal strain is given by

$$E = \sigma/\varepsilon \quad \ldots\ldots\ldots (4\text{-}1)$$

where, E = Young's modulus of elasticity

σ = normal stress calculated as force or load, F,

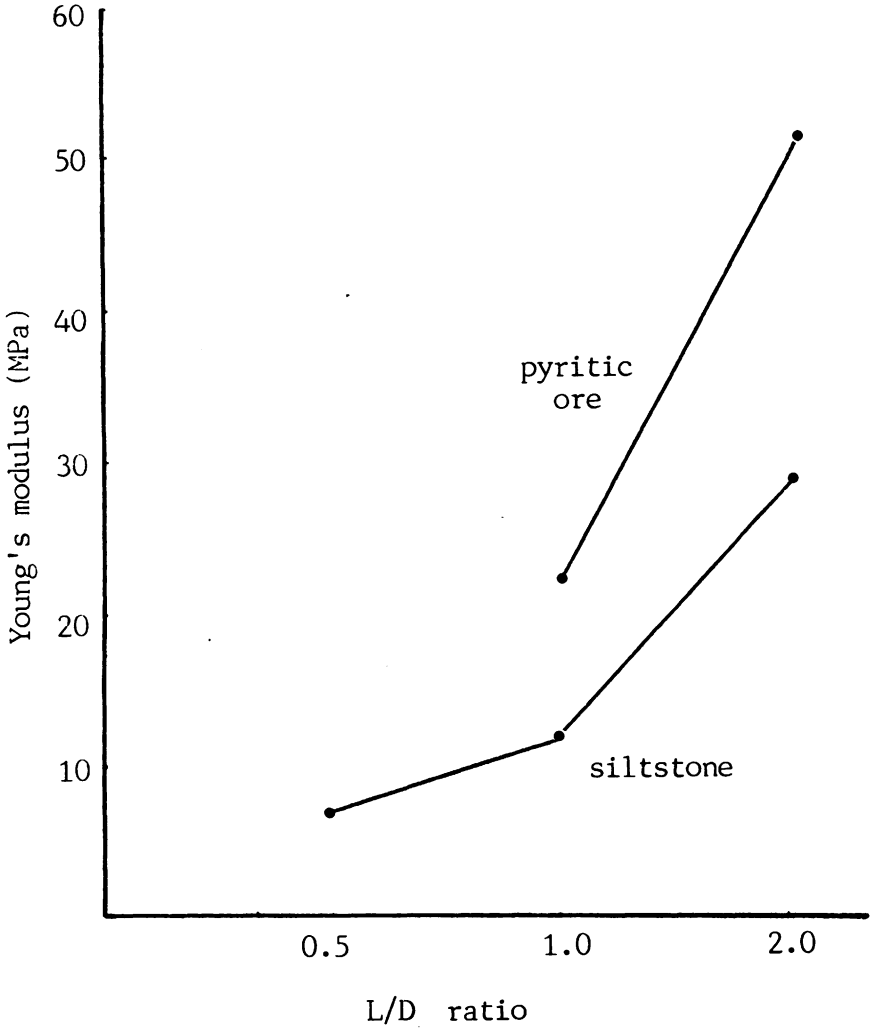

Fig. 4.4 Effect of L/D ratio on Young's modulus.

exerted over a unit area, A, of the specimen, i.e., $\sigma = F/A$

ε = normal strain calculated from the deformation, Δl, of a material due to an applied normal stress, compared to the original length of the specimen, l, in the direction of the stress i.e., $\varepsilon = \Delta l/l$.

Average slope of apparent linear portion of each curve was used to define elastic modulus of each specimen tested. These results are tabulated in Tables 4.2 and 4.3. Both the pyritic ore and siltstone specimens indicated that Young's modulus decrease as the values of L/D ratio of the specimen decreases, as illustrated in Fig. 4.4.

4.3.2 Strength.

The strength of a rock can be specified for different conditions. The strength of rock at any point along the failure locus is determined by dividing the load at that point by the original cross-sectional area of the specimen. In this experiment compressive strength and residual strength initation were observed as follows:

4.3.2.1 Compressive strength.

Compressive strength or ultimate strength which is commonly regarded as the strength of a rock, was obtained from the equation :

$$C = F/A \quad \ldots\ldots\ldots\ldots\ldots \quad (4\text{-}2).$$

where, C = uniaxial compressive strength,

F = load at failure, and

A = cross-sectional area of the specimen.

For the specimens with L/D ratio less than 2, strength was calculated using the
equation suggested by ASTM standard (1979):

$$C = Ca/(0.88+(0.24b/h)) \quad \ldots\ldots\ldots \quad (4\text{-}3).$$

where, C = computed strength of an equivalent L/D = 2 specimen,

Ca= measured compressive strength of the specimen tested,

b = test core diameter, and

h = test core height.

Mean strength of both types of specimens were plotted in

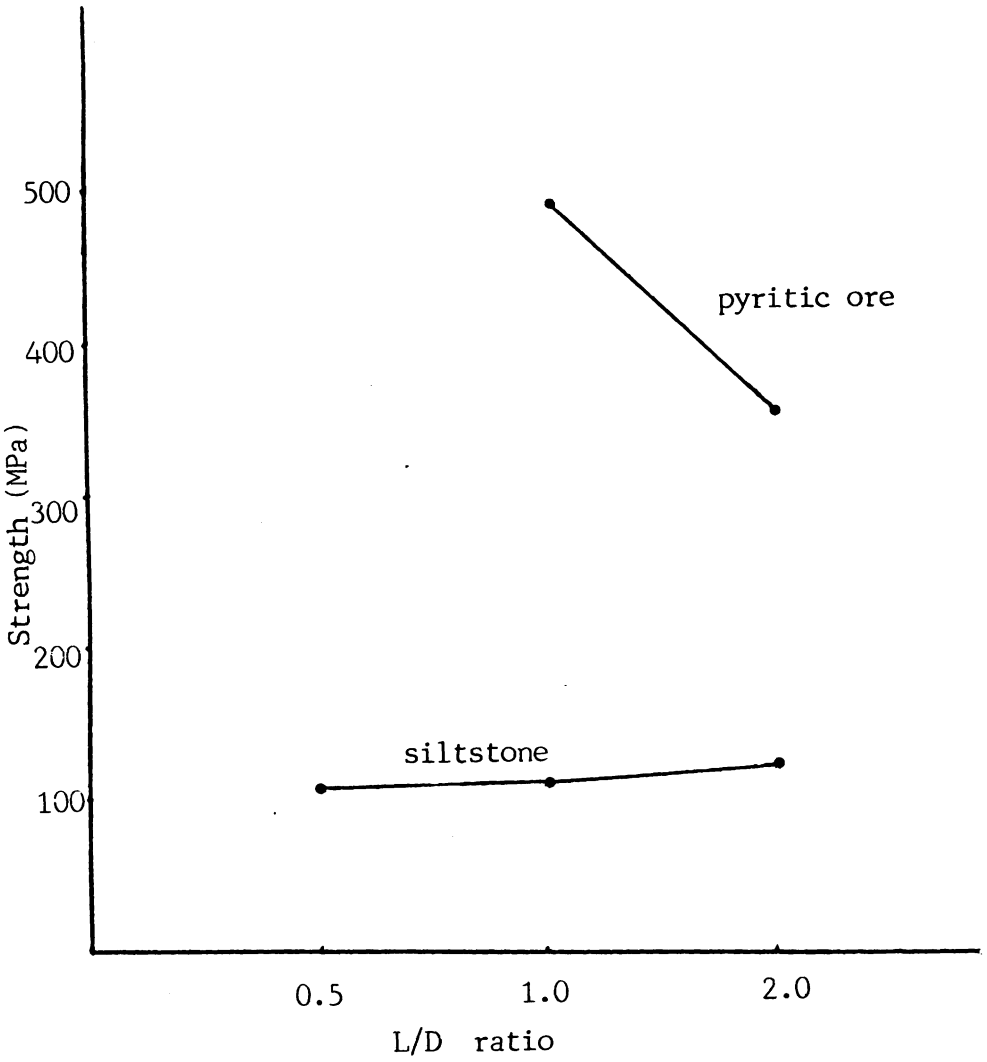

Fig. 4.5 Effect of L/D ratio on Ultimate strength.

Fig. 4.5. For pyritic ore specimens, the compressive strength increases remarkably as the L/D ratio decreases. The specimens with an L/D ratio of 1:1 were found to possess a compressive strength of about 40% higher than those specimens with a ratio of 2:1. For the siltstone specimens, however, the compressive strength increased slightly as the L/D ratio increased. Previous researchers concluded that for high modulus rocks without major discontinuities, with a diameter in the range of 25 to 150 mm, small changes in specimen size have no appreciable effect on their strength. However, if the specimen size changes are large, say up to 1 m in diameter and over, there is a definite decrease in the uniaxial compressive strength by up to a factor of ten (Sarkha, 1978).

4.3.2.2 Residual strength initation.

Residual strength initation is defined as the point afterwhich further fracturing does not significantly alter the strength parameter. Increasing deformation beyond this point had little effect on the variation in strengthn compared with deformation before reaching this point.

For siltstone specimens residual strength were retained by some specimens of any specimen geometry. Their values are presented in Table 4.2.

Since all the pyritic specimens failed violently and

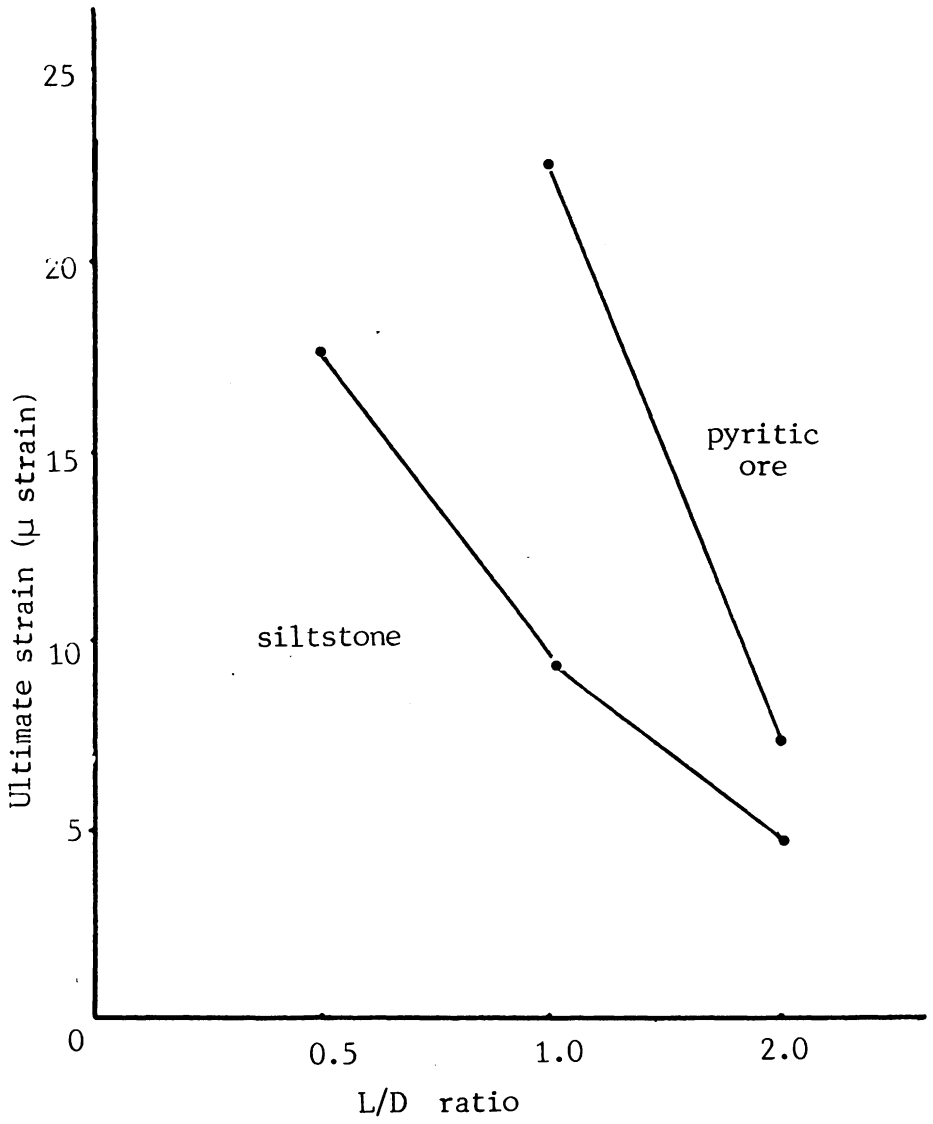

Fig. 4.6 Effect of L/D ratio on Ultimate strain.

completely ruptured after they reached the peak strength, they did not regain their load bearing capability after unloading path dropped to zero stress. Obviously they have no residual strength at all.

4.3.3 Deformation.

Deformation is determined in the same way as the strength. The ultimate deformation and rupture deformation which was observed in this experiment are described in the following sections.

4.3.3.1 Ultimate deformation or ultimate strain.

Ultimate deformation or ultimate strain is deformation corresponding to the ultimate strength of the specimen. The ultimate strain values for both siltstone and pyritic ore specimens can be seen in Tables 4.2 and 4.3. The ultimate strain as a function of the L/D ratio is illustrated in Fig. 4.6. For both rock types, the ultimate strain decreased as the L/D ratio decreased.

4.3.3.2 Rupture deformation.

Rupture deformation is defined as the maximum deformation

at which progressive stable failure in the post failure region can be controlled. For specimens which retain their residual strength, rupture deformation is measured at the residual strength initation. Since siltstone specimens failed variously, even for the same specimen with same L/D ratio and the same type of loading, it could be said that the rupture deformation depended on its mode of failure. As a consequence, the specimens which failed partly controlled have lower relative rupture deformation compared with the specimens which failed completely controlled. For pyritic ore specimens, no rupture deformation was observed, and it is because the specimens could no longer sustain any stress after the ultimate strength was reached.

4.3.4 Stiffness.

It was stated in Chapter 2 that the failure of a specimen beyond its strength failure depends on the relationship of the stiffness of the loading system to the stiffness of the specimen. Apart from the stiffness of the loading system, the stiffness of the specimen is, therefore, the most important parameter which determined the failure characteristics of a specimen. The post failure stiffness of the specimen can be determined from the load-deformation by drawing a tangential line in post-failure region of the curve. As shown in Fig. 4.3. the post failure stiffness is related to Δl and Δd by

$$k = -\Delta l/\Delta d \quad \ldots\ldots\ldots\ldots \quad (4\text{-}4)$$

where, Δl = decremental load, and

Δd = incremental deformation.

This relationship is applicable only as far as post-failure curve can be produced. The post failure stiffness values define a negative slope curve and have a negative sign.

The specimens which failed uncontrollably, such as all pyritic ore and some of siltstone specimens, no post-failure stiffness can be observed. As shown in the results, the post-failure stiffness can be produced better from the siltstone specimens with smaller L/D ratio. This result is in agreement with Hudson, et al.(1971) who studied the influence of specimen geometry on the shape of the complete stress-strain curve of the specimen tested in uniaxial compression. From this study it was found that the axial cracks are generally concentrated in the central portion of the specimen's length because lateral restraint at the specimen ends inhibits their growth near the specimen-platen interface. In the longer specimens, the central region is failed whilst the ends are elastically loaded and unloaded. For the specimen with lower L/D ratio, however, the cracks appear to be uniformly distributed throughout the length of the specimen. If the failure uniformly distributed within the specimen, it progresses in gradual manner result in controlled failure.

TABLE 4.2

EXPERIMENTAL RESULTS OF SILTSTONE SPECIMEN

Specimen number	L/D ratio	Loading Condition		Ultimate strength MPa	Ultimate strain millist.	Young's modulus GPa	Slope after strength failure MN/m	Residual strength initation MPa	Rupture strain millist.	Failure mode
		Strain rate $x10^{-6}$/sec.	Loading type							
S1.1	2	1.39	monotonic	82.24	4.01	22.03	-	27.30	4.80	instantaneously
S1.2	2	1.39	monotonic	87.88	4.97	22.73	-	30.22	5.30	instantaneously
S1.3	2	1.39	monotonic	128.17	5.35	31.25	-	-	-	instantaneously
S1.4	2	1.39	monotonic	92.91	3.27	31.25	400	11.20	4.60	partly controlled
S1.5	2	1.39	monotonic	116.98	4.36	28.90	-	-	-	instantaneously
S2.1	2	1.39	cyclic	128.55	4.98	26.80	400	13.82	5.70	partly controlled
S2.2	2	1.39	cyclic	135.71	4.29	36.23	-	-	-	uncontrolled
S2.3	2	1.39	cyclic	73.11	5.12	17.42	-	-	-	instantaneously
S2.4	2	1.39	cyclic	73.66	3.42	26.74	1400	27.54	4.24	fully controlled
S2.5	2	1.39	cyclic	108.63	3.48	37.51	300	13.80	5.53	fully controlled
S2.6	2	1.39	cyclic	112.98	4.29	32.68	1000	39.64	6.26	fully controlled
S2.7	2	1.39	cyclic	243.06	6.46	40.00	-	-	-	instantaneously
S2.8	2	1.39	cyclic	destructed at the beginning of the test						
S2.9	2	1.39	cyclic	246.76	7.61	34.48	-	-	-	instantaneously
S2.10	2	1.39	cyclic	103.12	5.12	23.47	400	-	-	partly controlled
Mean		:		123.84	4.77	29.39	-	-	-	
Standard deviation		:		55.05	1.19	6.56	-	-	-	

continued . . . . .

TABLE 4.2 (continued)

EXPERIMENTAL RESULTS OF SILTSTONE SPECIMEN

Specimen number	L/D ratio	Loading Condition		Ultimate strength MPa	Ultimate strain millist.	Young's modulus GPa	Slope after strength failure MN/m	Residual strength initation MPa	Rupture strain millist.	Failure mode
		Strain rate $x10^{-6}$/sec.	Loading type							
S3.1	1	2.78	cyclic	126.29	11.05	12.5	2000	-	12.50	partly controlled
S3.2	1	2.78	cyclic	127.00	10.44	11.76	800	43.00	15.00	fully controlled
S3.3	1	2.78	cyclic	104.70	9.40	12.12	1100	35.00	11.00	fully controlled
S3.4	1	2.78	cyclic	86.12	6.55	12.50	133	45.00	16.00	fully controlled
S3.5	1	2.78	cyclic	unreliable result						
Mean :				111.03	9.36	12.22	1008.25	-	-	
St.dev.:				19.57	1.99	0.34	774.90	-	-	
S4.1	0.5	3.08	monotonic	112.73	18.99	5.88	750	18.34	24.98	fully controlled
S4.2	0.5	3.08	monotonic	unreliable result						
S4.3	0.5	3.08	monotonic	unreliable result						
S4.4	0.5	3.08	monotonic	94.54	16.47	6.25	540	20.12	31.12	fully controlled
S4.5	0.5	3.08	monotonic	99.83	13.12	9.09	667	18.34	24.98	fully controlled
S4.6	0.5	3.08	monotonic	143.87	21.75	7.41	1400	43.12	30.39	fully controlled
Mean :				112.74	17.58	7.16	839.25	24.98	27.87	
St.dev.:				22.11	3.67	1.44	383.68	12.12	3.34	

TABLE 4.3

EXPERIMENTAL RESULTS OF PYRITIC ORE SPECIMEN

Specimen number	L/D ratio	Loading Condition		Ultimate strength MPa	Ultimate strain millist.	Young's modulus GPa	Slope after strength failure MN/m	Residual strength initation MPa	Rupture strain millist.	Failure mode
		Strain rate $x10^{-6}$/sec.	Loading type							
P1.1	2	1.39	(attempted) cyclic	356.11	7.18	52.63	-	-	-	failed violently
P1.2	2	1.39	"	376.88	7.85	50.00	-	-	-	"
P1.3	2	1.39	"	328.11	7.52	42.86	-	-	-	"
P1.4	2	1.39	"	342.84	7.12	56.60	-	-	-	"
P1.5	2	1.39	"	343.31	6.90	55.56	-	-	-	"
Mean				349.45	7.31	51.53	-	-	-	
St.dev.				18.26	0.37	5.49	-	-	-	
P2.1	1	2.78	(attempted) cyclic	552.13	23.20	27.27	-	-	-	failed violently
P2.2	1	2.78	"	506.22	26.13	23.08	-	-	-	"
P2.3	1	2.78	"	444.71	20.63	23.68	-	-	-	"
P2.4	1	2.78	"	488.83	19.97	26.48	-	-	-	"
P2.5	1	2.78	"	455.73	21.23	25.00	-	-	-	"
Mean				489.52	22.23	25.10	-	-	-	
St.dev.				42.86	2.49	1.78	-	-	-	

CHAPTER FIVE

POST-FAILURE BEHAVIOUR AND PILLAR STABILITY

On any rock mass at depth there are both gravitational and tectonic stress fields acting which result in strain energy being stored in the rock. When an underground opening is mined, both stress and strain energy on a unit volume basis are concentrated in the rock surrounding the opening.

As the underground excavation deepens, the concentration of stress around these excavations can be sufficient to deform the surrounding rock past the peak of its stress-strain curve into the region of post-failure behaviour. The way the structure surrounding an excavation such as a pillar, fails depends on the relation between the deformation characteristics of the structure subjected to the stress and the deformation characteristics of the mine loading system.

Pillars are used in various forms for a great variety of purposes in underground mining. It can be stated that no mineral extraction by subterranean methods can do without employing pillars either as main support elements or in some secondary role.

Instances of sudden failure of pillar workings are well accounted in mining literature. An approach to stability problems of underground pillars taking account of the contribution of post-failure mechanics is described in the following sections :

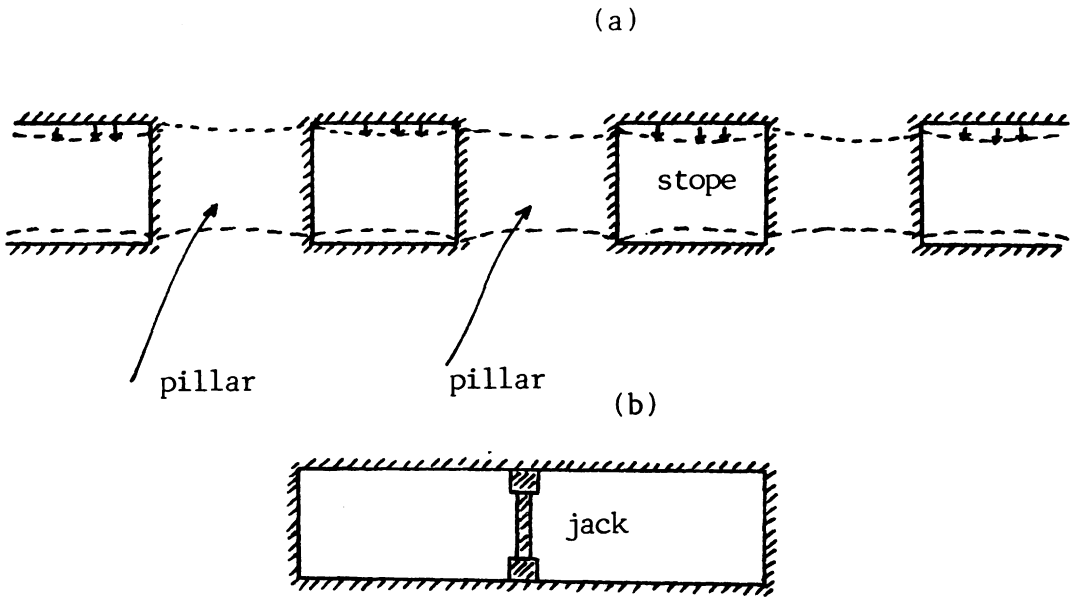

Fig. 5.1 (a) Wall and pillar deformation.
(b) Hydraulic jack representation of support pillar.

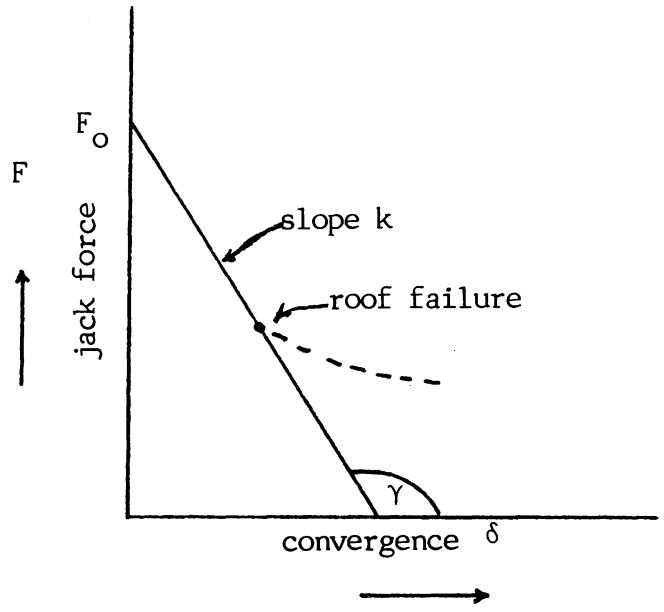

Fig. 5.2 Load-deformation graph showing local mine stiffness curve.

5.1 LOCAL MINE STIFFNESS.

The conventional pillar design is based on the dimensioning of a pillar to resist the complete load concentrated on them. The load or stress imposed on a pillar should not exceed the strength of that pillar. The application of this concept, together with some safety factor is a safe method but especially in the case with a single, or few pillars, this lead to over-estimation of the pillar size (Hoek and Brown, 1980).

Salamon (1967, 1970) and Starfield and Fairhurst (1968) put forwarded an approach to the problem by introducing the concept of stiffness of rock, concerning both pillar and the surroundings. Excavating an opening in rock removes the pressure holding the remaining rock in place. This removal of pressure is equivalent around the boundary of an opening to an increment of inward stress equal to that formerly acting outward so that it results in zero stress on the boundary. However, it is this increment of stress acting inward that causes the boundary to deform as shown in Fig. 5.1a.

To determine the deformation characteristics of roof and floor of the opening a jack is placed in the opening, as shown in Fig. 5.1b. The initial load on the jack is designated as Fo. As the jack is slowly retracted, to simulate a pillar collapse, the load will drop because more load is shifted away to the rock

surroundings (it could be either pillars or abutments or both). The roof will sag and some floor uplift can occur. Provided the roof remains intact, the curve relating force on the jack (F) to convergence (δ) between the roof and floor should resemble that shown in Fig. 5.2. If the roof fails at some stage of convergence, then the jack would be supporting a dead load, so that the Force-Convergence curve may follow the dot line in Fig. 5.2. The negative slope of the F-δ curve will depend on the geometry of the opening, the sizes of adjacent pillars and abutments, and the location of the jack. This slope is called the 'local-mine stiffness' or k. The local-mine stiffness equals the negative tangent of γ, where γ is the angle between the loading line and the positive direction of the δ-axis in Fig. 5.2. Since $90° < \gamma < 180°$, parameter k is always positive. If the jack is replaced by a pillar this situation is analogous to the situation where a rock specimen is being compressed under a testing machine as described in Section 2.1. The experiment described in Section 2.1, can then be interpreted in mining terms. The specimen corresponds to the pillar and the loading machine represents the rock mass surrounding the mine working, and so the behavioural relationship of an underground pillar and the surrounding rock mass can be explained in similar way.

5.2 STABILITY ANALYSIS AND METHODS TO PREVENT VIOLENT FAILURE OF A PILLAR.

The concept of stability analysis of a pillar is based on the fact that deformations and stresses around an opening in rock can be calculated quite reliably using different element techniques, at least in elastic-brittle conditions of rock mass. Stiffness of rock mass around the opening can then be obtained from the relationship between load and deformation. By this method, various stiffness of a rock mass, which corresponds to local mine stiffness, can be simulated depending on geometry of pillar under consideration. On the otherhand the pillar stiffness is not so easy computed, especially concerning post-failure region characteristics of the pillar. The pillar stiffness, however, can be obtained from small-scale tests in the laboratory or from in-situ tests performed with the same rock material of a given width-to-height relation. Once these two stiffness are available it is possible to determine whether the relation between the two result in stable or unstable conditions.

In practice, therefore, a stability analysis of pillar requires:

1. The computation of the local mine stiffness.
2. The Experimental determination of the deformation curve of a pillar of a given width-to-height relation.
3. The Analysis of the relation between local mine stiffness

and deformation characteristic of the pillar.

From Section 2.1, it can be concluded that violent failure of a rock specimen under compression occurs when the following two conditions are satisfied :

1. stress on the specimen exceeds strength of the specimen, i.e.

$$\sigma_s > C_s$$

2. stiffness of the specimen exceeds the stiffness of loading system:

$$| k_s | > | k_m |.$$

In actual mining terms, the specimen represents the pillar, and loading system represents the rock mass surrounding the mine working. If only one of these conditions is satisfied, no instability can arise in such condition. Hence violent failure of the pillar can be prevented, (in theory) either by

1. ensuring that the stress in the pillar is below the value of its strength, or
2. ensuring that the stiffness of the loading system is greater than the stiffness of the pillar.

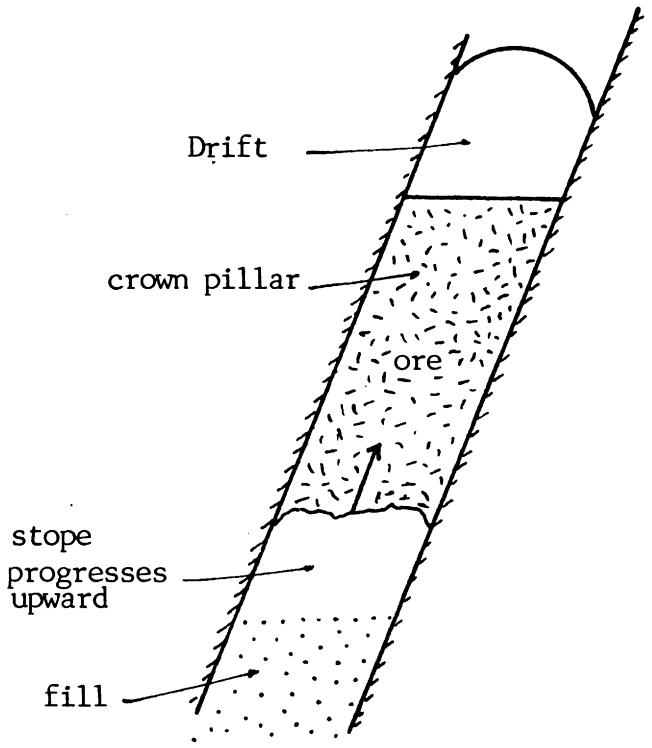

Fig. 5.3 Schematical diagram of a crown pilar.

In underground metal mining where a 'crown pillar' has to be made, due to mining method employed, problems concerning violent failure of the pillar are frequently encountered. Fig. 5.3 shows a typical crown pillar created in an underground excavation using cut and fill mining method. The stope is worked upward to the next level. A horizontal pillar is usually left below adjacent drive to stop them collapsing. When the pillar is being made or mined out, as the openings approach each other, the pillar size is reduced and the stress in the pillar increases approaching the strength of the pillar. It is at this stage violent failure of the pillar can be expected to occur. Measures should, therefore, be taken to prevent the pillar fails in uncontrolled manner.

In the following sections briefly described the examples of methods to create a 'stable' pillar, taking post-failure mechanics into account.

5.2.1 Interactive pillar dimensioning.

Sarkha (1980) reported on a study to determine the optimum size of crown pillar at Rautuvaara iron ore mine in Finland. In this mine crown pillars are made between stopes above and under the +200 level in the NE district where the sublevel caving method is used. Calculation showed that the pillar contained 20000 tonnes per

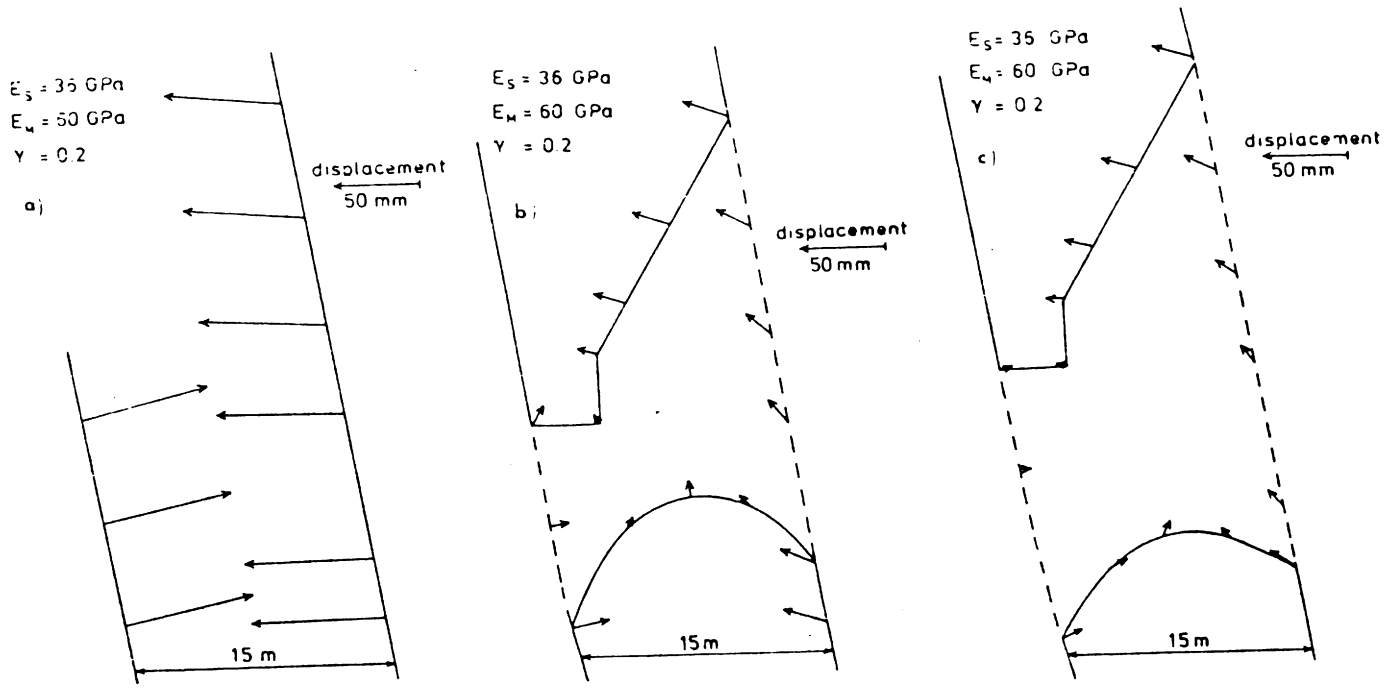

Fig. 5.4 The displacement of ore-country rock contacts with different pillar thicknesses. E_{ore}=60 MPa, $E_{country\ rock}$= 36 MPa. a) no pillar b) pillar thickness =6 m, c) pillar thickness = 11.5 m (Sarkha, 1980).

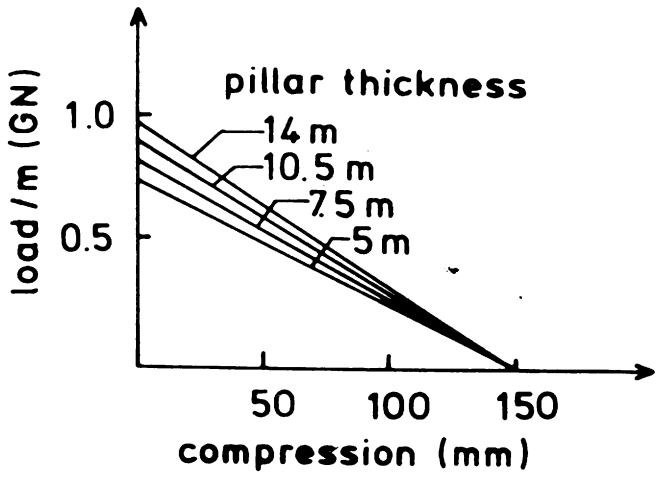

Fig. 5.5 Loading curve on a pillar of different thickness due to mass of surrounding country rock.

metre of thickness i.e. totally about 250000 tonnes of ore. The pillar could possibly, be stoped at later. It was therefore very important to optimize the thickness of it.

Computer simulation was carried out to evaluate the displacement of the pillar and country rock using the finite element method at various configurations. Fig. 5.4 shows the results of finite element method simulation concerning diplacements of pillar and country rock for some pillar thicknesses at a horizontal stress of 10 MPa and vertical stress of 6 MPa. The state of stress in the pillar was then calculated by numerically integrating the stress of single elements at the thinnest point of the pillar. From the data obtained the loading-compression curves caused by the country rock for different pillar thicknesses were created as shown in Fig. 5.5. These curves represent the local mine stiffness.

From the small-scale test carried out in a servo-controlled testing machine, with L/D ratio of specimens correspond to L/D ratio of a real pillar, the behaviour characteristics were obtained and the results matched with the local-mine stiffness as shown in Fig. 5.6. The shadowed area represents the variations between the curves. From this it can be seen that for pillars with thicknesses of 5 and 7.5 m, the pillars would cave with a probability of 70% and 20%. With thickness of 10.5 m the pillar would stay 100% up provided there is no crushed zone in the pillar. At a thickness of 13 m even with existing minor crushed zones the pillar would not

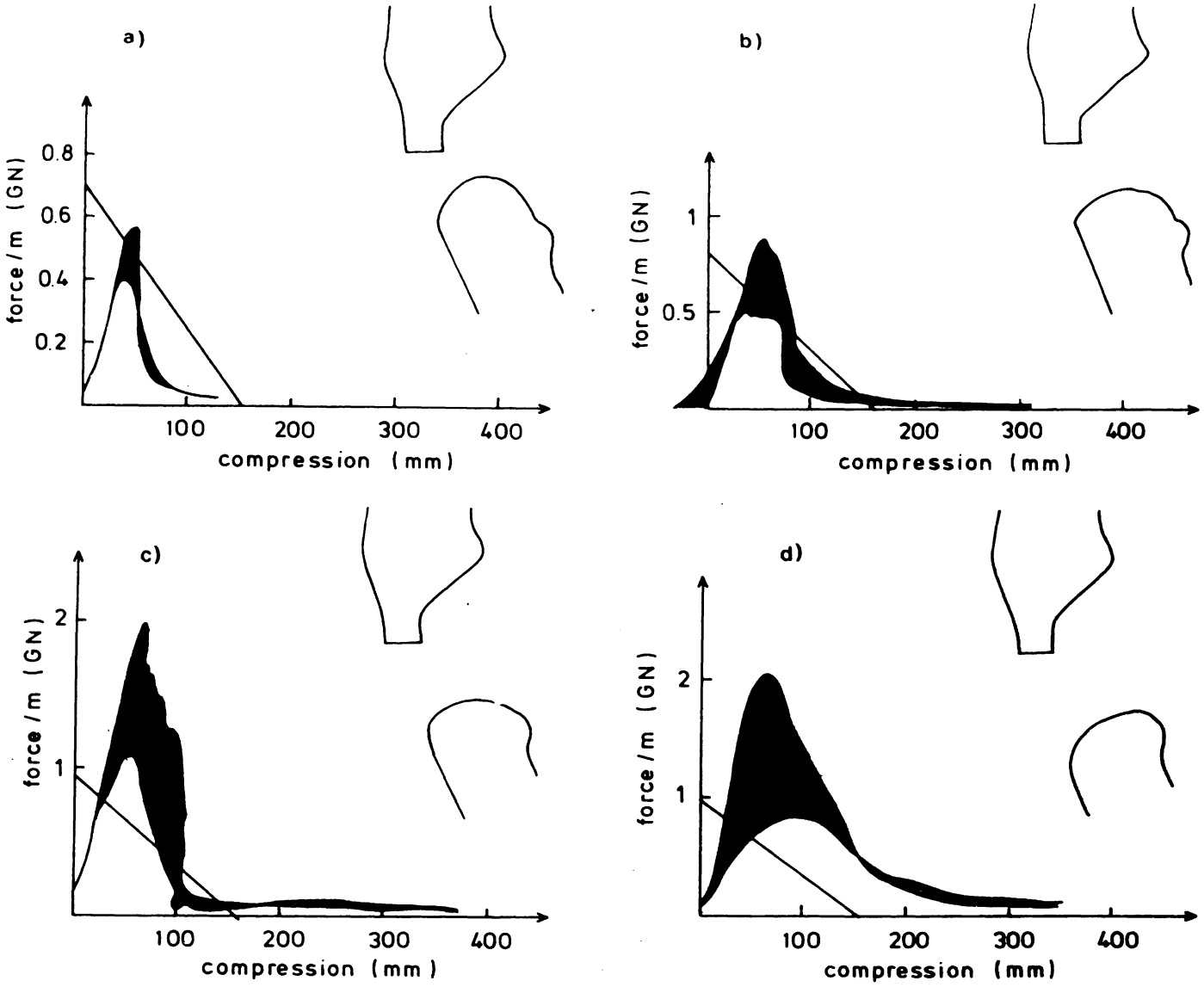

Fig. 5.6 Loading compression curves of the pillar-country rock system with different pillar thicknesses.
a) pillar thickness= 5 m. b) pillar thickness= 7.5 m
c) pillar thickness= 10.5 m. d) pillar thickness= 13 m.

fail.

From these results it was decided that the minimum thickness for a stable pillar should be about 14 m which would also take account of any the broken zones.

5.2.2 Destressing to prevent violent failure.

An application of stability and failure control concept has been briefly described in Section 5.2.1. To obtain the optimum size of a pillar, the mining geometry should be modified in a way to prevent violent failure in the pillar. In the previous example, the pillar was assumed to be left before its size approached a critical geometry. In that case it was neccessary to optimize the pillar size. If a stope pillar is to be mined out, however, as the mining sequence continued the pillar size is continually reduced and the stress and strain energy are further concentrated in the pillar. When the pillar reaches a critical geometry the stress in the pillar exceeds the strength of the pillar, and the pillar fails. For hard and brittle rock material where its stiffness is greater then the stiffness of the mine loading system, the pillar can fail violently and in some cases rock bursts occur which can cause a severe operational hazard.

If mining methods can not be changed, or modified economically, violent failure or bursting in burst-prone pillar can be controlled by destressing the pillar.

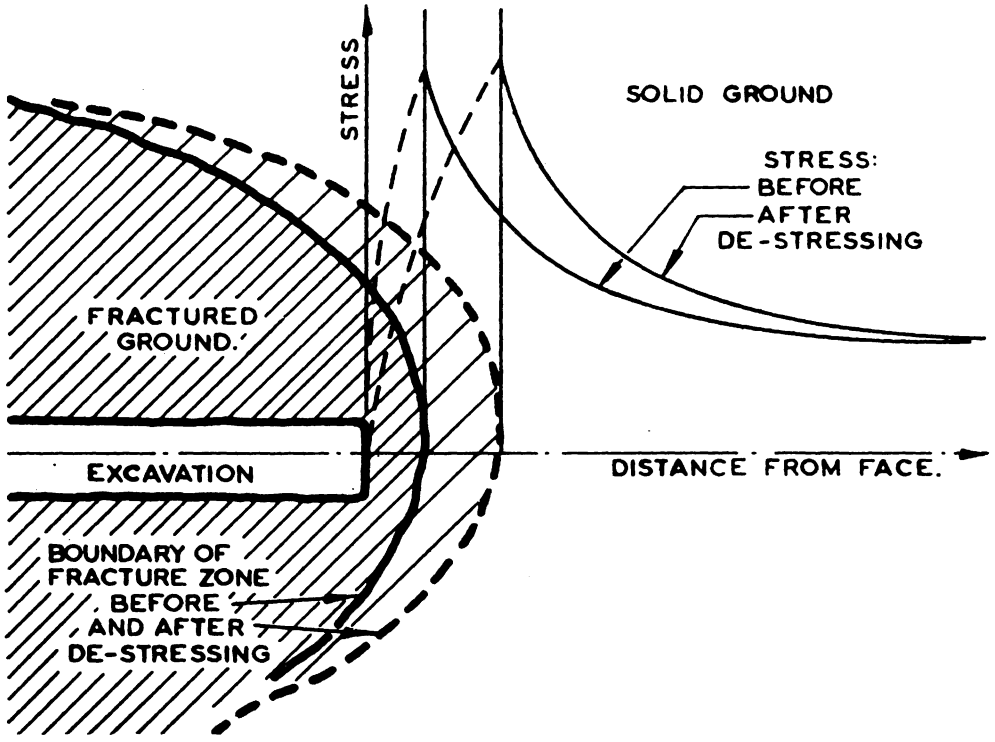

Fig. 5.7 Concept of destressing (Roux, et al., 1957).

5.2.2.1 Background.

Destressing was conceived as a blast fracturing technique to stress-relieve potential rock burst zones. The concept of destressing resulted from the observation that the zone of rock which is hard and solid in appearance immediately surrounding underground openings is more likely to burst than one which has a fractured appearance. The zone of highly fractured rock seemed to offer some shielding to both the occurence and damage from rock bursting. It was then postulated that if this naturally fractured zone could be extended by blast fracturing ahead of the face, both the occurence and effect of rock bursting should reduce (Roux et al., 1957). Fig. 5.7 shows a sketch of the original concept of destressing. After destressing, the boundary of fractured ground is transferred or shifted from one area to another and so the stress concentration is shifted to the adjacent solid rock. The purpose of destress blasting, therefore, is to fracture a volume of rock in a suspected high stress or potential rock-burst zone. This fracturing reduces the load-carrying ability of the rock which results in a stress decrease in the fractured zone. In other words fracturing reduces the effective elastic modulus of rock; since strain energy stored in the rock is proportional to the square of the stress divided by elastic modulus, i.e.

$$W = \sigma^2/2E \quad \ldots\ldots (5\text{-}1),$$

the stored energy in the rock will also be reduced. If the strain energy stored in the fractured rock was reduced to well below that is in the loading system (the surrounding solid rock), the failure process of fractured rock, due to continued loading, will progress in a stable manner (see Section 2.1).

5.2.2.2 Pillar destressing.

Blake (1971) carried out a comprehensive study on the application of destressing to control pillar rock burst at Galena Mine, Wallace, Idaho. The following account briefly describes this investigation.

1) Mining method and rock burst geometry.

The mining method at Galena Mine is an overhand horizontal cut and fill system. Stoping progress upward from one level to another by a series of horizontal cuts. A pillar is created as a stope is and mined upwards. This mining method results in mined out areas above an unmined stope. As the pillar size is reduced, the stress in the pillar is increased until the strength of the pillar is reached and the pillar bursts. This characteristic is analogous to the characteristic of the specimens of the same rock material tested in soft testing machine (No data available for specimen tested in stiff testing machine).

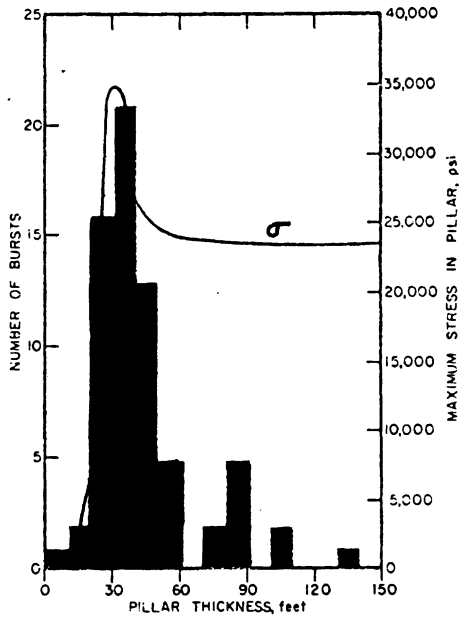

Fig. 5.8 Maximum principal stress in the pillar and incidence of damaging rock bursts at Galena Mine, Idaho (Blake,1971).

From rock pillar burst history at Galena Mine it had been recognized that the critical geometry of the pillar should be as shown in Fig. 5.8. It is apparent that initial burst geometry is reached when the pillar size is reduced below 18.3 m (60 feet) a critical burst geometry is reached when the pillar size is reduced below 12.2 m (40 feet).

2) Microseismic field monitoring.

To detect instability in the underground mine, microseismic method were used. This method relies on the fact that as rock is stressed, strain energy is stored in the rock. The build-up of strain energy is accompanied by small-scale displacement adjustments that release small amounts of seismic and sometimes, acoustic energy. These small scale disturbances, micro cracking, shearing, sliding and crushing of crystal grains, are termed microseism or rock noises and can be detected with the aid of special geophysical equipment. Using this method, the rock noise source locations and thus the area of inferred high stress which are potential rock-burst zones can be determined. Besides locating potential rock-burst zones, microseismic methods are used to study the sequence of events leading up to bursting in burst-prone mine structure.

The behaviour of a pillar in 40-135E stope has been monitored to study the definite sequence of events prior to a

pillar burst at Galena Mine. From this it was found that when the pillar is greater than 22.9 m (75 feet) in thickness, little rock noise is generated by blasting and the locatable events are scattered around the stope area. As the pillar is further reduced to approach the critical burst geometry, of less than 12.2 m (40 feet), the number and magnitude of rock noise generated by blasting increased. At a critical burst geometry of some 10.7 m (35 feet), most of the rock noises are now generated from the immediate pillar area. This findings suggest that the average stress in the pillar increases gradually according to the reduction in its geometry. This pattern is consistent with the observations on damaging rock bursts with respect to pillar size, as shown in Fig. 5.8.

3) Computer simulation.

Based on data obtained from rock burst observation and microseismic monitoring, the mining of 40-135E stope pillar was simulated on the computer. There were 3 stages involved in the simulation.

i) Model idealization.

ii) Prior to destressing simulation.

iii) Destressing simulation.

Before destressing the maximum principal stress for the 9.2 m (30 feet) pillar is 245 MPa (35,000 psi). In Fig. 5.8 it

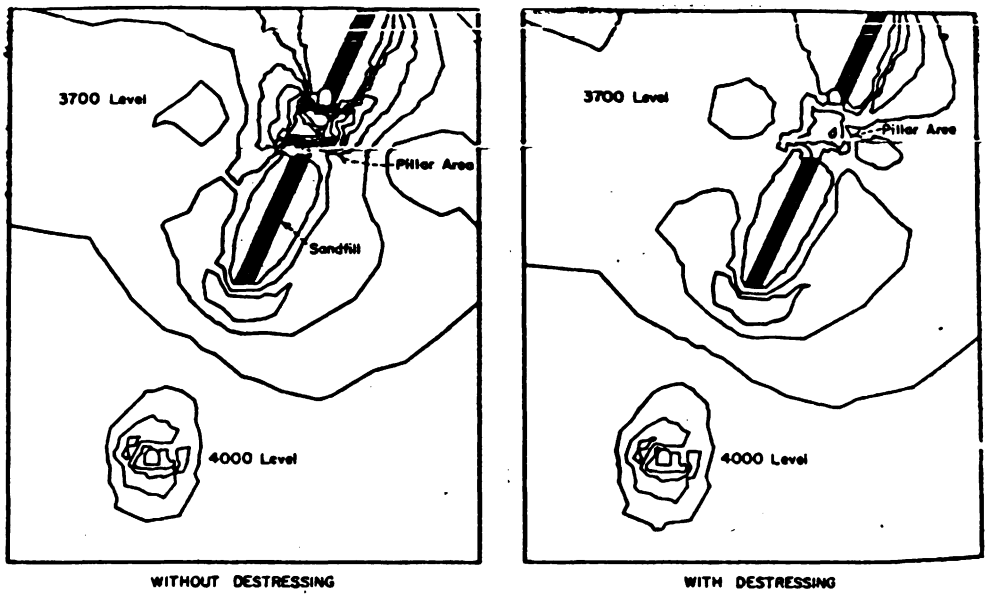

Fig. 5.9 Maximum shear stress contour plots for a 9.2 m (30 ft. pillar).

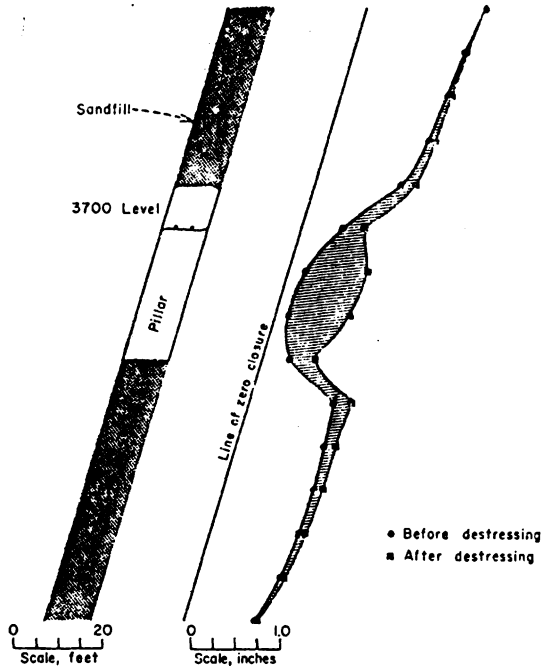

Fig. 5.10 Compression of pillar and stope wall closure resulting from destressing.

can be seen that maximum principal stress with respect to pillar size is consistent with incidence of damaging rock burst obtained from rock burst obsevations as mentioned in a.

In the computer model destressing was simulated by reducing the elastic modulus of the vein from 39.6 to 6.9 GPa (5.75×10^6 psi to 1.0×10^6 psi) (determined by seismic velocities in fractured rock). For the critical 9.2 m (30 ft) pillar this simulation results in a large reduction of the stress in the pillar as shown in Fig. 5.9. The maximum principal stress in the pillar was reduced from 245 to 68 MPa (35,500 psi to 9,900 psi). Placing these values into equation (5-1), this softening of elastic modulus and reduction stress in the pillar would results in a two-fold the reduction in the stored elastic strain energy within the pillar. Fig. 5.10 shows the compression of the pillar and the closure of the stope walls before and after destressing. Since these displacements involve a large volume of rock, large amounts of both stored strain energy and potential energy have been released.

Prior to destressing the pillar stiffness was 5.5×10^6 t/m per metre (7.8×10^6 lb/in per inch) of stope length, and the loading system stiffness was 2.3×10^6 t/m per metre (3.4×10^6 lb/in. per inch) of stope length which indicated the pillar was burst prone. After destressing the pillar stiffness was reduced to 2.0×10^6 t/m per metre (2.8×10^6 lb/in. per inch) of stope length, which means that the pillar-loading system

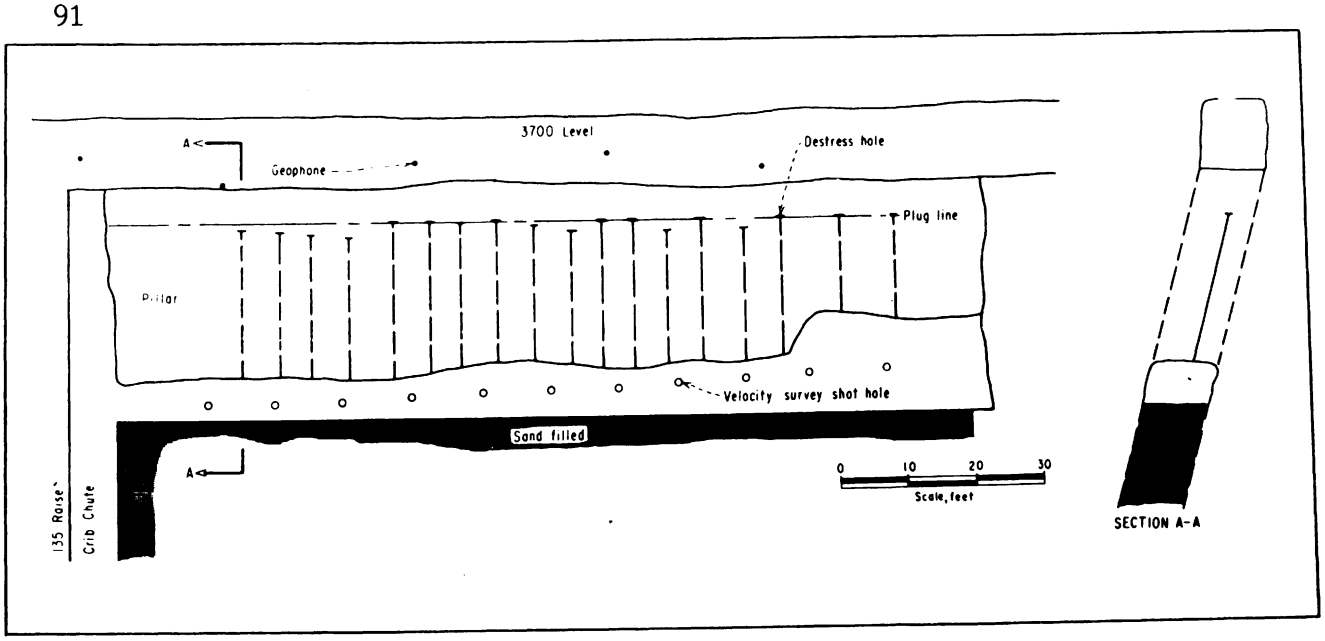

Fig. 5.11 Destressing pattern, at 40-135E stope.
(Blake, 1971).

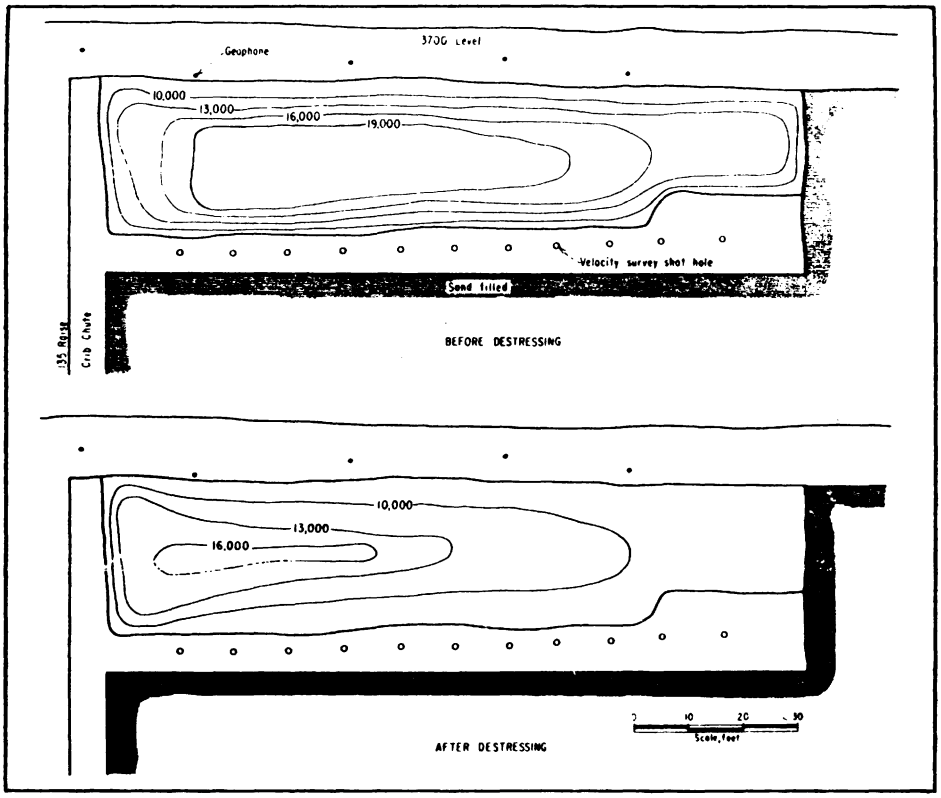

Fig. 5.12 Contour plots of seismic velocities at 40-135 stope
(Blake, 1971).

stiffness relationship was a in stable condition and the pillar was no longer burst prone.

4) Destressing operation.

Based on the data obtained from computer simulation, destressing 40-135E pillar was undertaken using a pattern as shown in Fig. 5.11. The pillar was destressed by blasting a series of longholes, 4.8 cm (1-7/8 in.) in diameter, drilled in the footwall of the vein on 1.5-m (5-foots) centers. These holes were loaded with AN-Prill to 1.5 m (5 feet) of the sill and 0.9 m (3 feet) from the collar, and fired with millisecond delays.

To determine the effectiveness of the destressing test, microseismic monitoring and seismic velocity surveys of the pillar were carried out. The microseismic monitoring indicated that the rock noise sources generated by blasting in this stope pillar were located out in the solid rock surrounding the pillar. This means that the stress had shifted to the solid country rock. Seismic velocity survey indicated a reduction in seismic velocity after destressing as can be seen in Fig. 5-12. Since seismic velocity is related to the elastic modulus of the rock, this means that the pillar has been fractured or softened and the effective modulus of the pillar has been lowered. It was reported that the destressed pillar was later completely extracted without any difficulty.

CHAPTER SIX

CONCLUSIONS AND RECOMENDATION

The main purpose of this investigation was to study post failure behaviour of mine rocks under uniaxial compression, through a literature survey and a laboratory experiment.

A Schenck-Trebel servo-controlled testing machine has been used to test a total of 36 samples which consisted of 26 silstone and 10 pyritic ore specimens from Elura Mine, in New South Wales. Monotonic and cyclic loading with constant axial strain rate was used to control failure of the specimens in the post-failure region.

Within the limits of the experimental programme undertaken, the following major conclusions and recommendation may be drawn.

1. Failure of rock structure.

a. Rocks will fail violently in any rock structure when the following conditions are satisfied:
   - stress in the rock structure exceeds the strength of the structure.
   - post-failure stiffness of the rock structure exceeds post-failure stiffness of the loading system.

b. In the laboratory tests a constant strain rate in a stiff or servo-controlled testing machine eliminates the violent nature of failure of rock specimens. The use of such a system, however, does not ensure stable failure; violent failure of specimen can still occur due to the natural characteristics and geometry of specimen and the test conditions applied.

2. Siltstone specimen behaviour.

Various modes post-failure behaviour for siltstone specimens were monitored, these include.

a. By applying monotonic axial loading beyond strength failure the specimens with L/D ratio of 2 generally failed instantaneously at or just after strength failure was reached. By applying cyclic loading, however, the failure could be controlled only up to about 50% of strength failure.

b. For specimens with an L/D ratio of 1, fully controlled failure was produced by applying cyclic loading.

c. Specimens with L/D ratio of 1:2, even with monotonic loading, the failure of the specimens could be fully controlled.

d. The siltstone specimens with smaller L/D ratio have a higher

Young's modulus compared to that of specimens with higher L/D ratio, while ultimate strength indicates no significant differences.

3. Pyritic ore specimens behaviour.

a. Using constant axial strain rate, even at very low rates, all pyritic ore specimens failed violenty at or just after maximum bearing capability was reached. The failure process in the post peak strength region is self-sustaining due to elastic strain energy stored in the specimen at strength failure is sufficient to maintain fracture propagation until the specimen has totally lost all of its strength. Although no complete stress-strain curves have been obtained the pyritic ore specimens is obviously a Class II rock. To control failure of this type of rock, strain energy stored in the specimen in post peak strength region must be extracted from the specimen.

b. Similar to siltstone, the pyritic ore specimens with small L/D ratios indicated having higher Young's modulus than specimens with greater L/D ratio but that the ultimate strength decreased as the L/D ratio increased.

4. Post failure behaviour and pillar stability.

An understanding of post failure behaviour of rock may lead

to the development of better procedures for controlling violent failure of rock structure such as underground pillar and therefore it contributes in determining stability analysis of underground excavation and the design of mining lay out. Once the post failure characteristics of rock and response to deformation of a rock surroundings have been recognized, an underground structure (such as a crown pillar) can be optimized such that the pillar while it is dimensioned safely its geometry is not over estimated.

In some instances, stress accumulated in a potential rock burst zone can be relieved by destressing methods such as blasting which deliberately fracture the rock. By this a solid massive zone is converted to a post-failure state zone which less prone to violent failure. This means that the rock structure is allowed to fail in controlled manner and not endanger the workings. Thus mining extraction is maximised and commensurate with adequate mining safety.

5. Recommendation.

a. In the absence of recognized standards to define the post-failure characteristics of rock under uniaxial compression, efforts should be made to establish a standardized test procedure for post-failure compression tests of both Class I and Class II rocks. This will allow direct comparison of results from different rock.

b. While it is recognized that the concept of the post-failure behaviour of rock which has emerged from laboratory investigations is most valuable for practical applications, it necessitates, however, in-situ determination of post failure-behaviour of rock. The complete load-deformation data of large rock specimens tested in underground conditions would give first insight into the behaviour of actual pillars after failure.

REFERENCES

1. A.S.T.M., 1979. Standard test method for unconfined compressive strength of intact rock core specimens, Designation : D 2939 - 79.

2. A.S.T.M., 1980. Standard test method for elastic moduli of intact rock core specimens in uniaxial compression, Designation : D 3148 - 80.

3. Berry, J. P., (1960), Some kinetic considerations of the Griffith criterion for fracture-I. Equations of motion at constant force., J. Mech. Phys. Solids 8, pp. 194-206.

4. Bieniawski, Z. T., 1967a. Mechanism of brittle fracture of rock, Int. J. Rock Mech. Min. Sci., Vol. 4(4), pp. 395-430.

5. Bieniawski, Z. T., 1967b. Stability concept of brittle fracture propagation in rock, Engineering Geology, Vol. 2(3), pp. 149-162.

6. Bieniawski, Z. T., Denkhaus, H. G. and , Vogler, V. W., 1969. Failure of fractured rock, Int. J. Rock Mech. Min. Sci., Vol. 6, pp. 323-341.

7. Bieniawski, Z. T. and , Vogler, U. W., Load-deformation behaviour of coal after failure, Proceedings 2nd Congress, ISRM, pp. 345-351.

8. Blake, W., 1971. Destressing test at the Galena Mine, Wallace, Idaho., Society of Mining Engineers of AIME, 71-AM-103.

9. Blake, W., 1972. Rock Burst Mechanics, Quarterly of The Colorado

School of Mines, Vol. 67, No. 1, pp. 1-64.

10. Bock, H., ed. 1978. An Intoduction to Rock Mechanics, Dept. of Civil and Systems Eng., James Cook University of North Queensland.

11. Brady, B. T., Duvall, W. I. and , Horino, F. G., 1973. An experimental determination of the true uniaxial stress-strain behavior of brittle rock, Rock Mech., Vol.6 pp. 107-120.

12. Brown, E. T. and Hudson, J. A., 1971. The influence of micro-structure on rock fracture on the laboratory scale, Symp. I. S. R. M., Nancy., pp. 11-20.

13. Chang, K. J. and Yang, T. W. , 1982. A constitutive model for the mechanical properties of rock, Int. J. Rock Mech. Min.Sci., Vol. 19, pp. 123-133.

14. Coates, D. F., 1981. Rock Mechanics Principles, Monograph 874 (Revised 1981), Canmet Energy, Mines and Resources Canada.

15. Cook, N. G. W., 1965. The failure of rock, Int. J. Rock Mech. Min. Sci., Vol. 2, pp. 389-403.

16. Hojem, J. P. M., Cook, N. G. W. and Heins, C., 1975. A stiff, two meganewton testing machine for measuring the work-softening behaviour of brittle materials, The South Af. Mech. Engineer, Vol. 25, pp. 250-270.

17. Houpert, R., 1979. The fracture behaviour of rocks, I. S. R. M. Proceeding, Vo. 3, Montreux (Suisse), pp. 107-104.

18. Hudson, J. A., Brown, E. T. and Fairhurst, C., 1971a. Shape of the complete stress-strain curve for rock, Rock Mech. Vol. 3, pp. 773-795.

19. Hudson, J. A., Brown, E. T. and Fairhurst, C., 1971b. Optimizing the control of rock failure in servo controlled laboratory tests, Rock Mech., Vol. 3, pp. 217-224.

20. Hudson, J. A., Crouch, S. L. and Fairhurst, C., 1972, Soft, stiff and servo controlled testing machines: a review with reference to rock failure, Engineering Geology., Vol. 6(3), pp. 155-189.

21. I. S. R. M., 1972. Suggested Method for Deteriming the Uniaxial Compressive Strength of Rock Materials and the Point Load Strength Index.

22. Jaeger, J. C. and Cook N. G. W., 1979. Fundamental of Rock Mechanics, 3rd Edition (Chapman and Hall London).

23. Kovari, K., 1977. Micromechanics model of progressive failure in rock and rock-like materials, The Geotechnics of Structurally Complex Formations, Associazione Geotecnica Italiana, Capri.

24. Pethukov, I. M. Linkov, A. M., 1979. The theory of post-failure deformations and the problem of stability in rock mechanics.,Int.J.Rock Mech.Min.Sci.Vol.16(2), pp. 57-76.

25. Roux, A. J. A., Leeman E. R. and Denkhaus H. G., 1957. De-stressing: A means of ameliorating rockburst conditions, Journal of the South African Institute of Mining and

Metallurgy, Vol. 58, pp. 104-146.

26. Rummel, F. and Fairhurst, C., 1970. Determination of the post failure behaviour of brittle rock, Rock Mech. Vol. 2(4).

27. Salamon, M. D. G., 1970, Stability, instability and design of pillar workings, Int. J. Rock Mech. Min. Sci., Vol. 7(6), pp. 613-631.

28. Salamon, M. D. G., 1983. The role of pillar in mining, Rock Mechanics in Mining Practice, Edited by S. Budavari, The South African Institute of Mining and Metallurgy, Monograph series No. 5.

29. Salamon, M. D. G. and Oravecz, K. I., 1976. Rock Mechanics in Coal Mines, (The Chamber of Mines of South Africa).

30. Sarkha, P., 1978. The failure behaviour of some Finnish Mine Rocks in Uniaxial Compression,Helsinki University of Technology, Laboratory of Excavation Engineering Otaniemi, Finland.

31. Sarkha, P., 1980. The interactive dimensioning of a crown pillar in the Rautuvaara Mine, Proceedings, I. S. R. M., pp. D 101 - D 106.

32. Simmons, J. V., 1984. Preliminary studies of class II brittle rock behaviour,Fourth Australia-New Zealand Conference on Geomechanics, pp. 58-61.

33. Starfield, A. M. and Fairhurst, C., 1968. How high-speed com computers advance design of practical mine pillar systems, Eng. Min. J., Vol. 169, pp. 78-84.

34. Sture, S. and Hon Yim Ko, Inst. J. Num. An. Meth. in Geomech. Vol. 2, pp. 237-253.

33. Wawersik, W. R. and Brace, W. F.,1971. Post failure behaviour of granite and diabase, Rock Mech. Vol. 3(2).

34. Wawersik, W. R. and Fairhurst, C., 1970. A study of brittle rock fracture in laboratory compression experiments, Int. J. Rock Mech. Min. Sci., Vol. 7, pp. 561-575.

APPENDIX 1

———————— recorded stres-strain curve.

– – – – – – – – extrapolated post-failure locus

–.–.–.–.–.–. test machine recovery curve

SPECIMEN NUMBER			FIGURE		
S1.1	to	S1.5	Fig. 4.7	to	Fig. 4.11
S2.1	to	S2.10	Fig. 4.12	to	Fig. 4.20
S3.1	to	S3.4	Fig. 4.21	to	Fig. 4.24
S4.1	to	S4.6	Fig. 4.25	to	Fig. 4.28
P1.1	to	P1.5	Fig. 4.29	to	Fig. 4.33
P2.1	to	P2.5	Fig. 4.34	to	Fig. 4.38

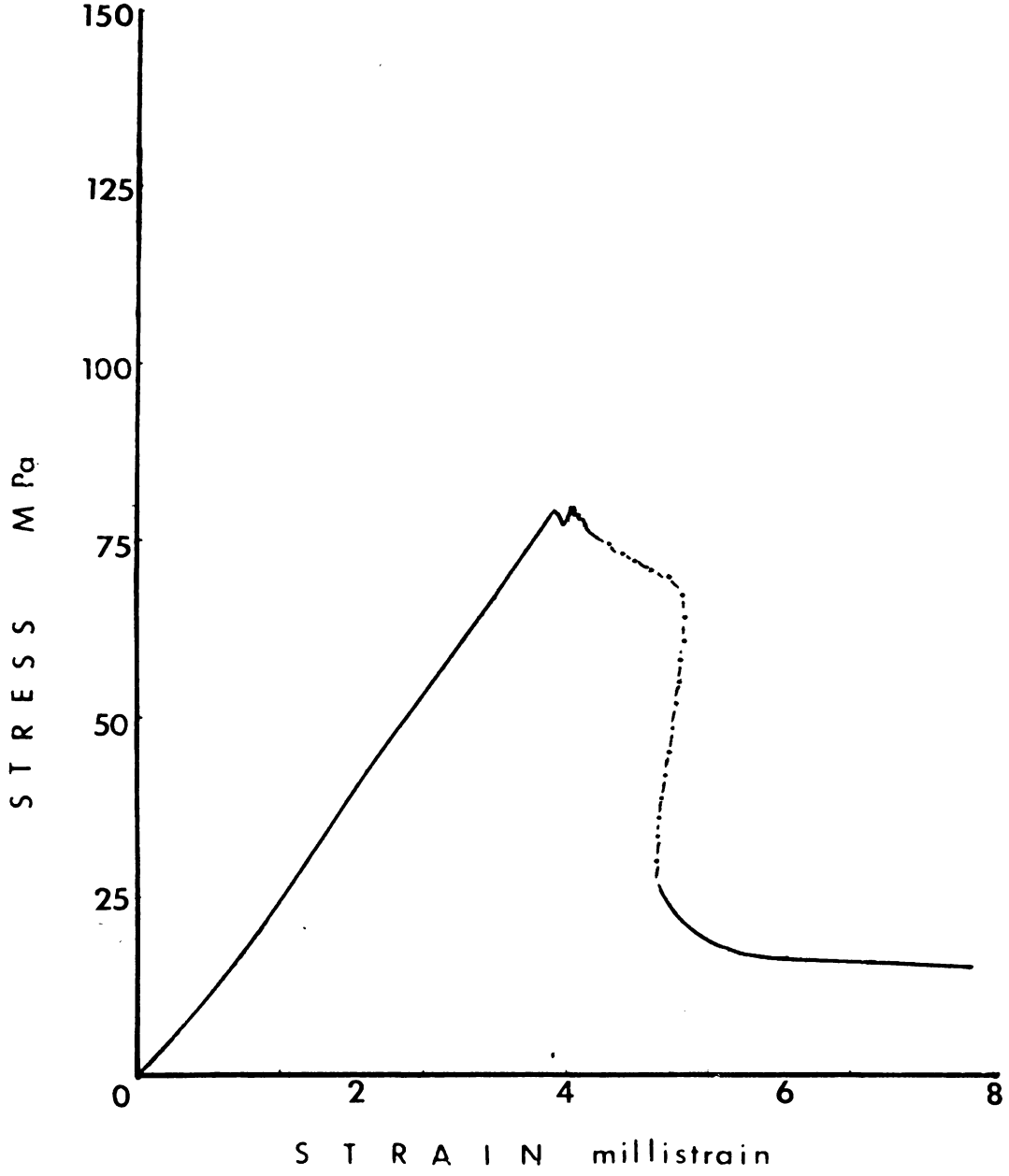

Fig.4.7 Stress-strain curve for S1.1

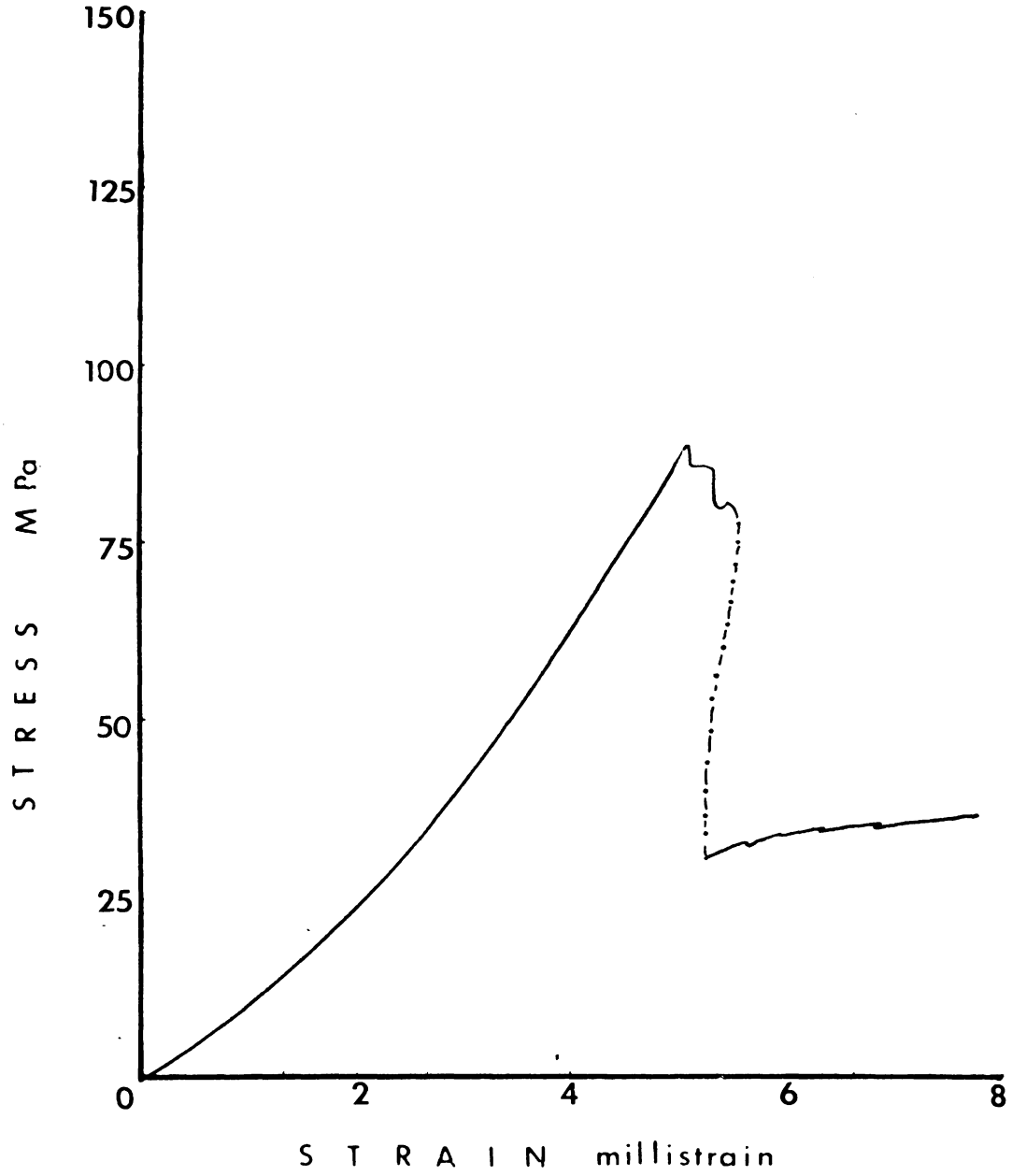

Fig.4.8 Stress-strain curve for S1.2

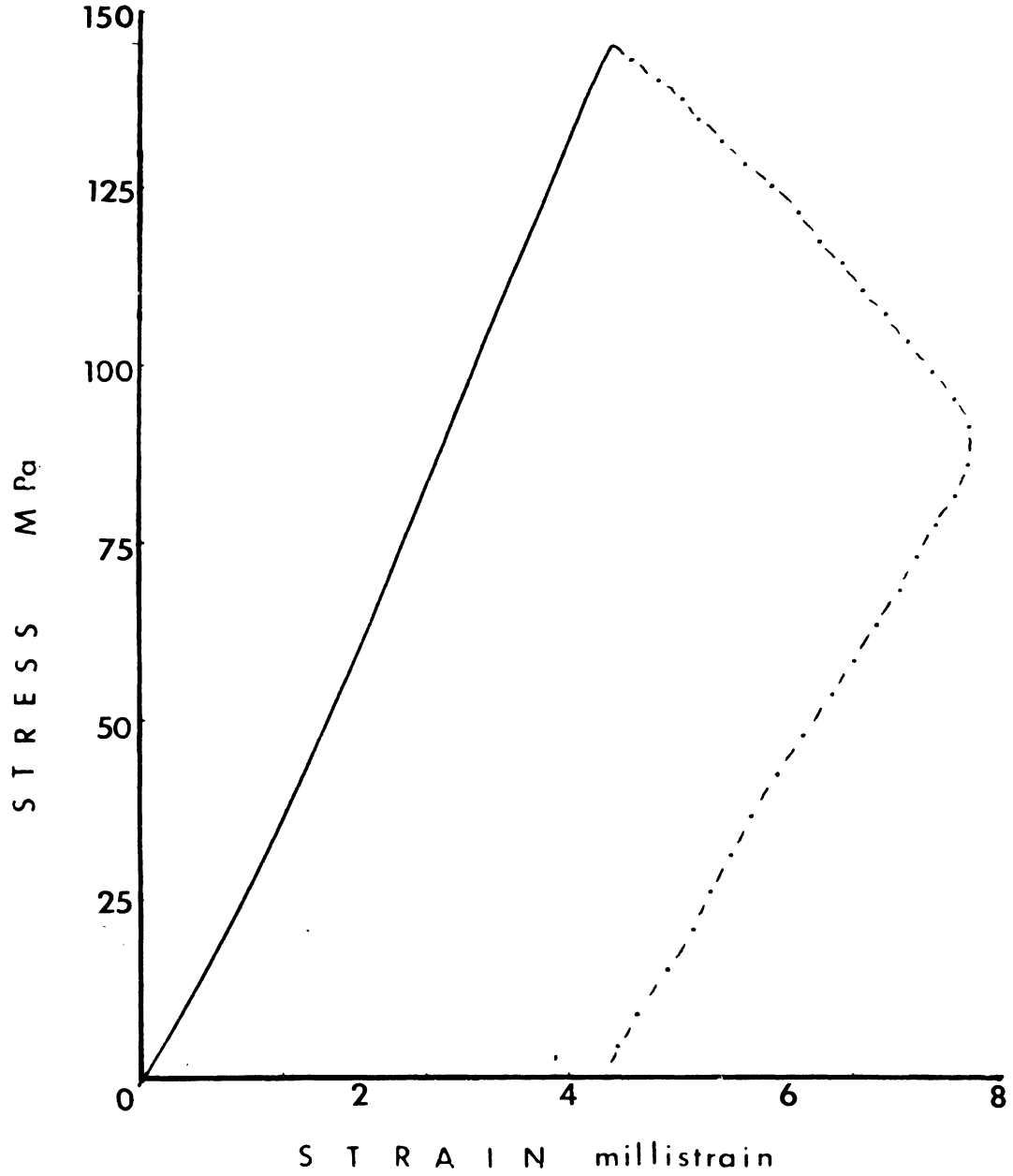

Fig.4.9 Stress-strain curve for S1.3.

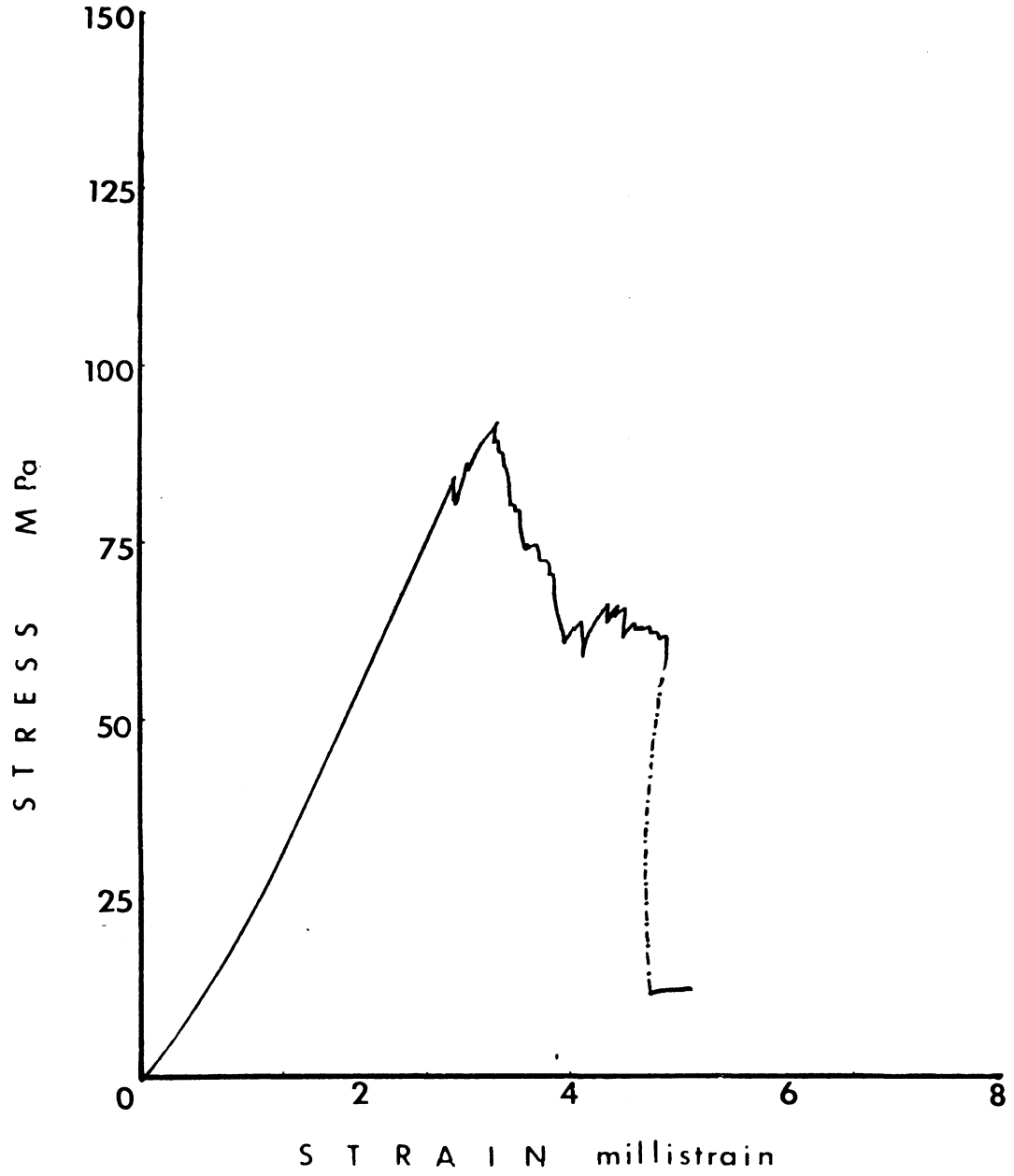

Fig.4.10 Stress-strain curve for S1.4.

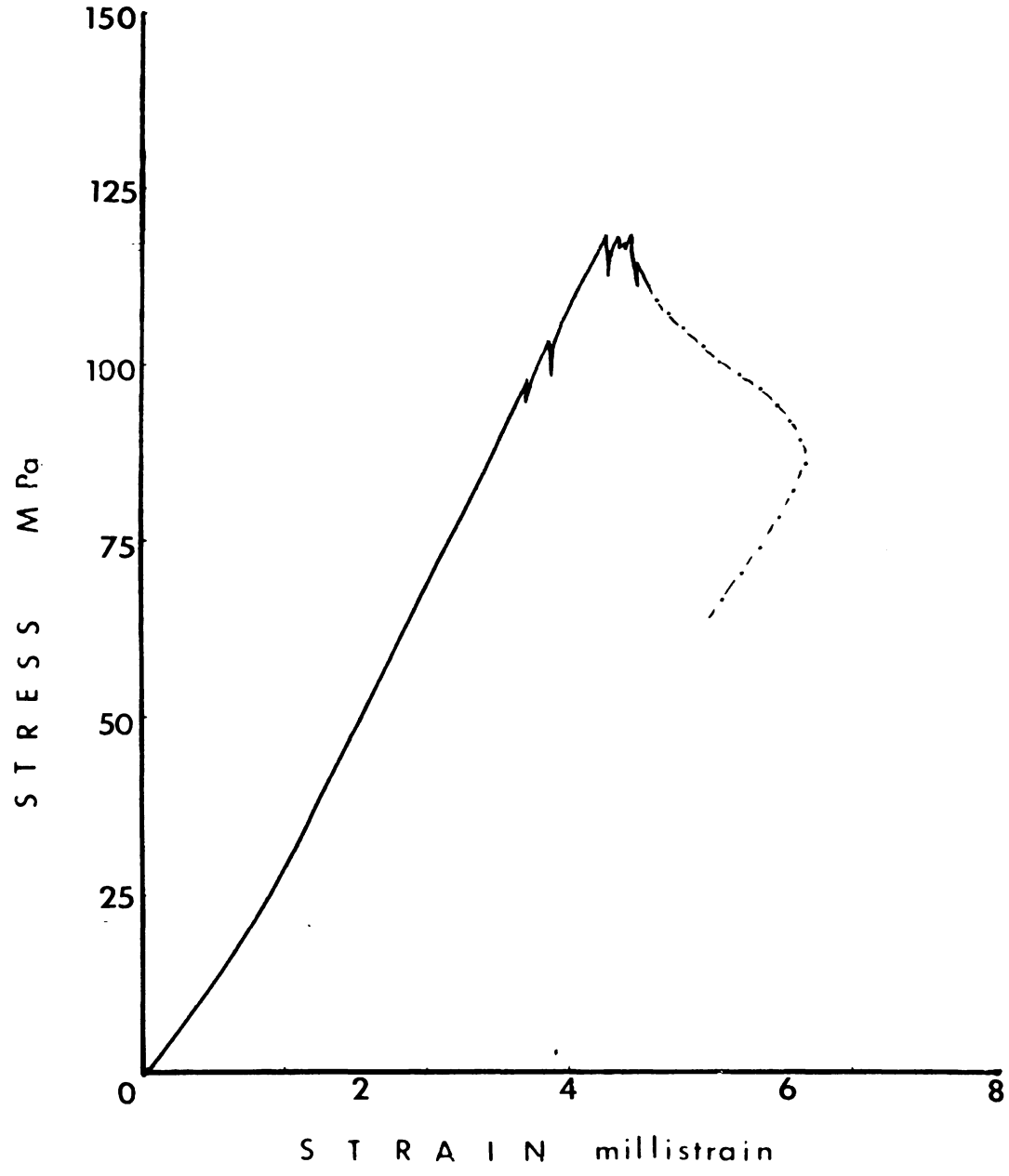

Fig.4.11 ;; Stress-strain curve for S1.5.

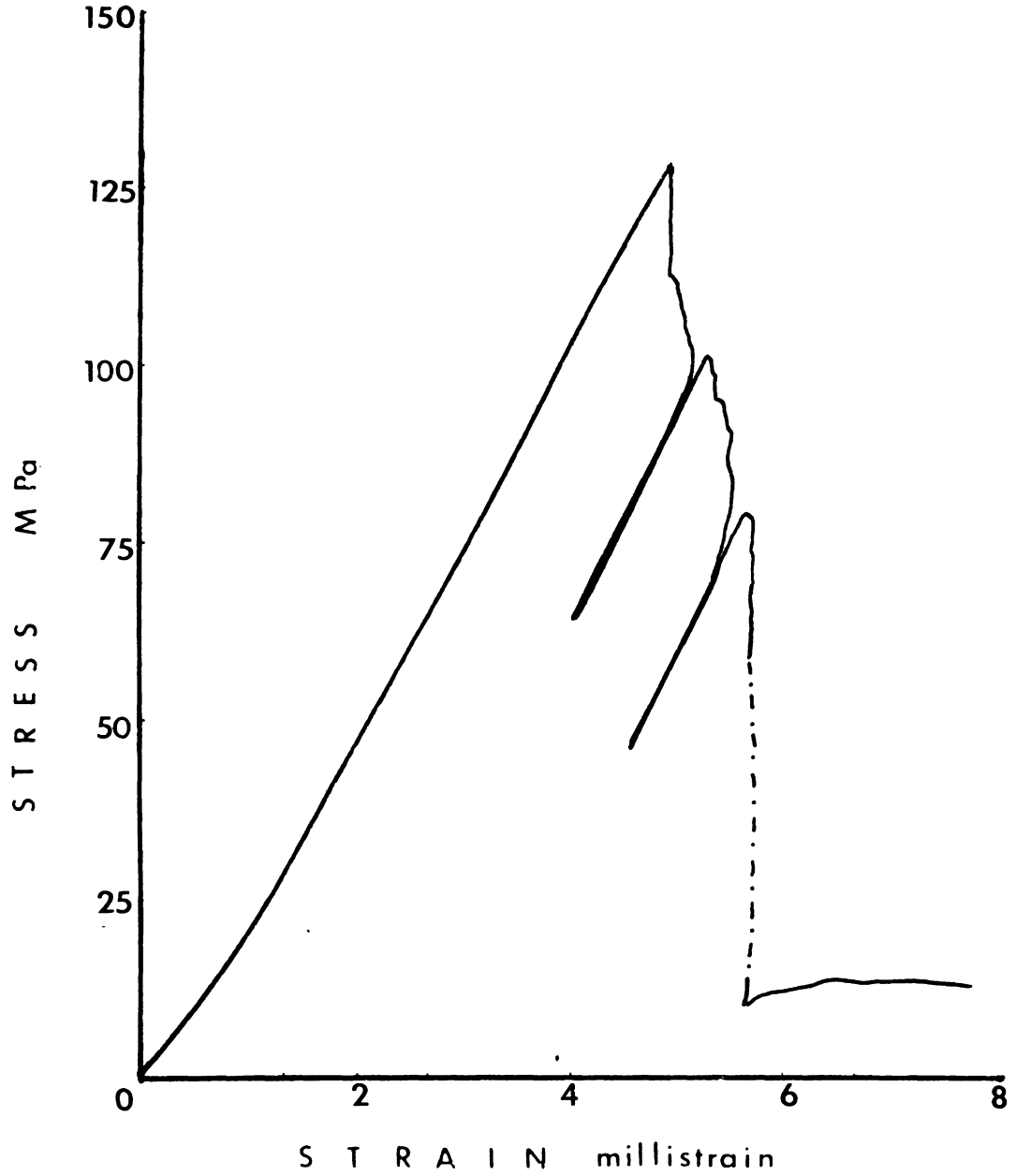

Fig.4.12: Stress-strain curve for S2.1 .

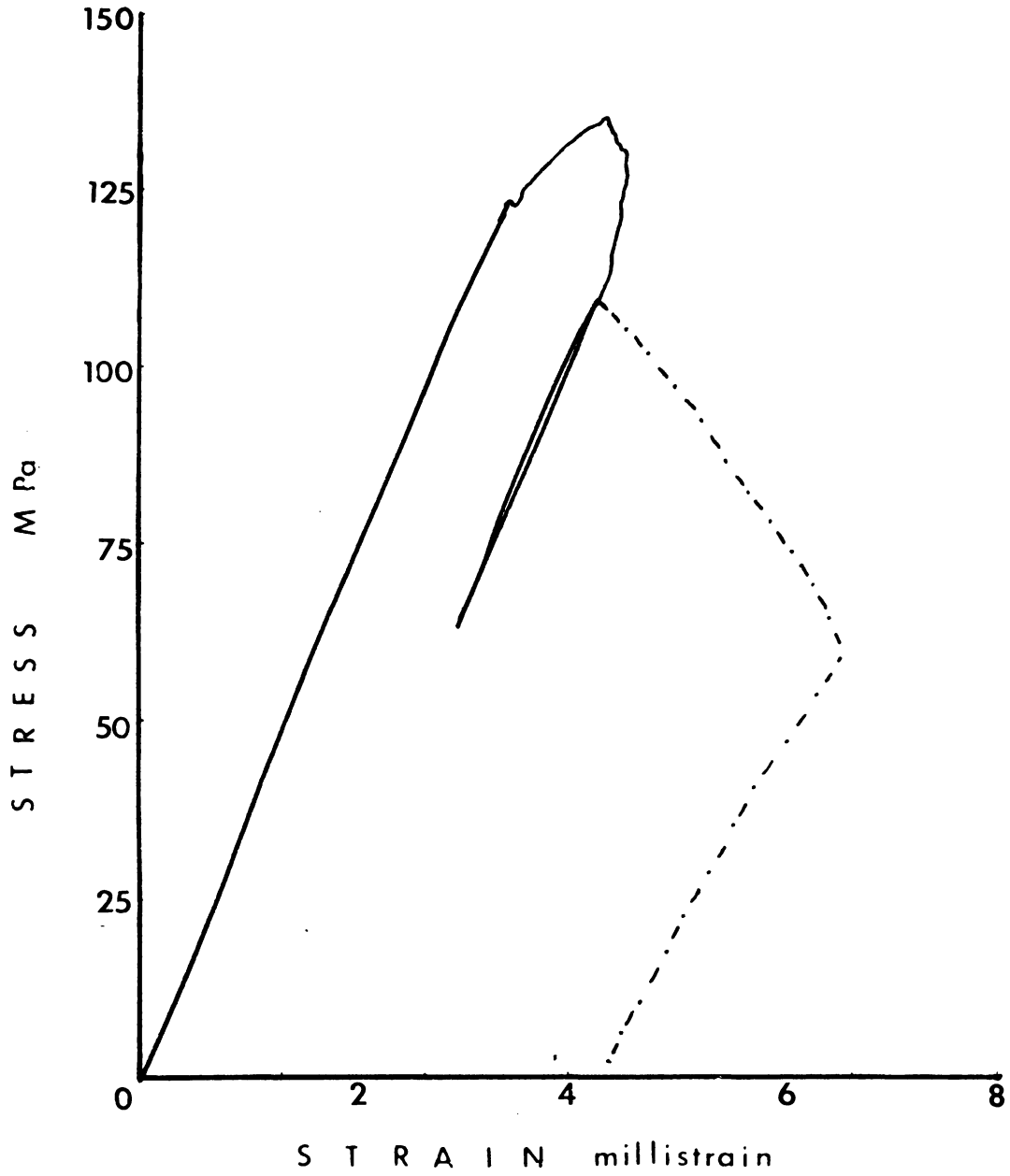

Fig.4.13. Stress-strain curve for S2.2.

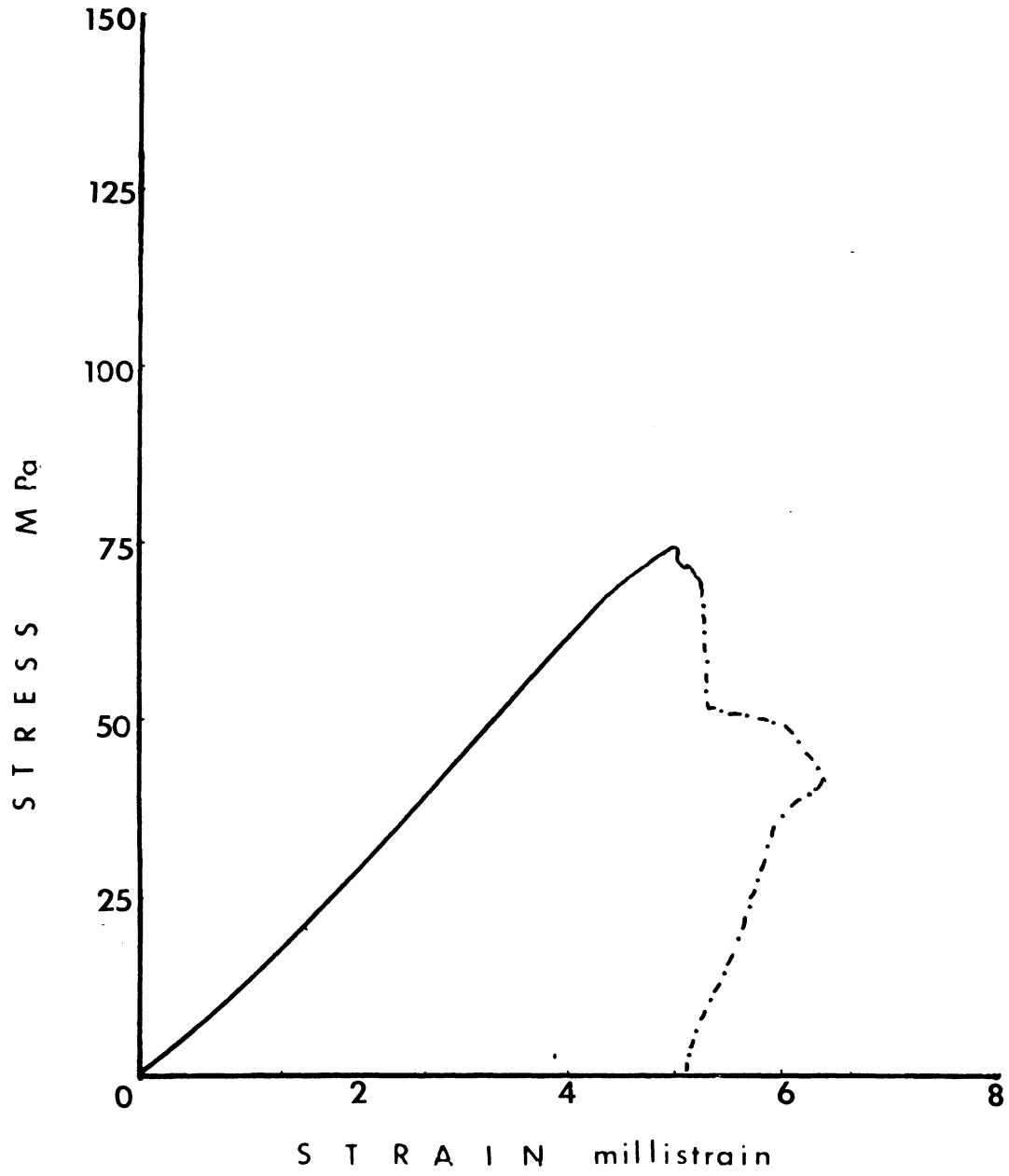

Fig.4.14. Stress-strain curve for S2.3.

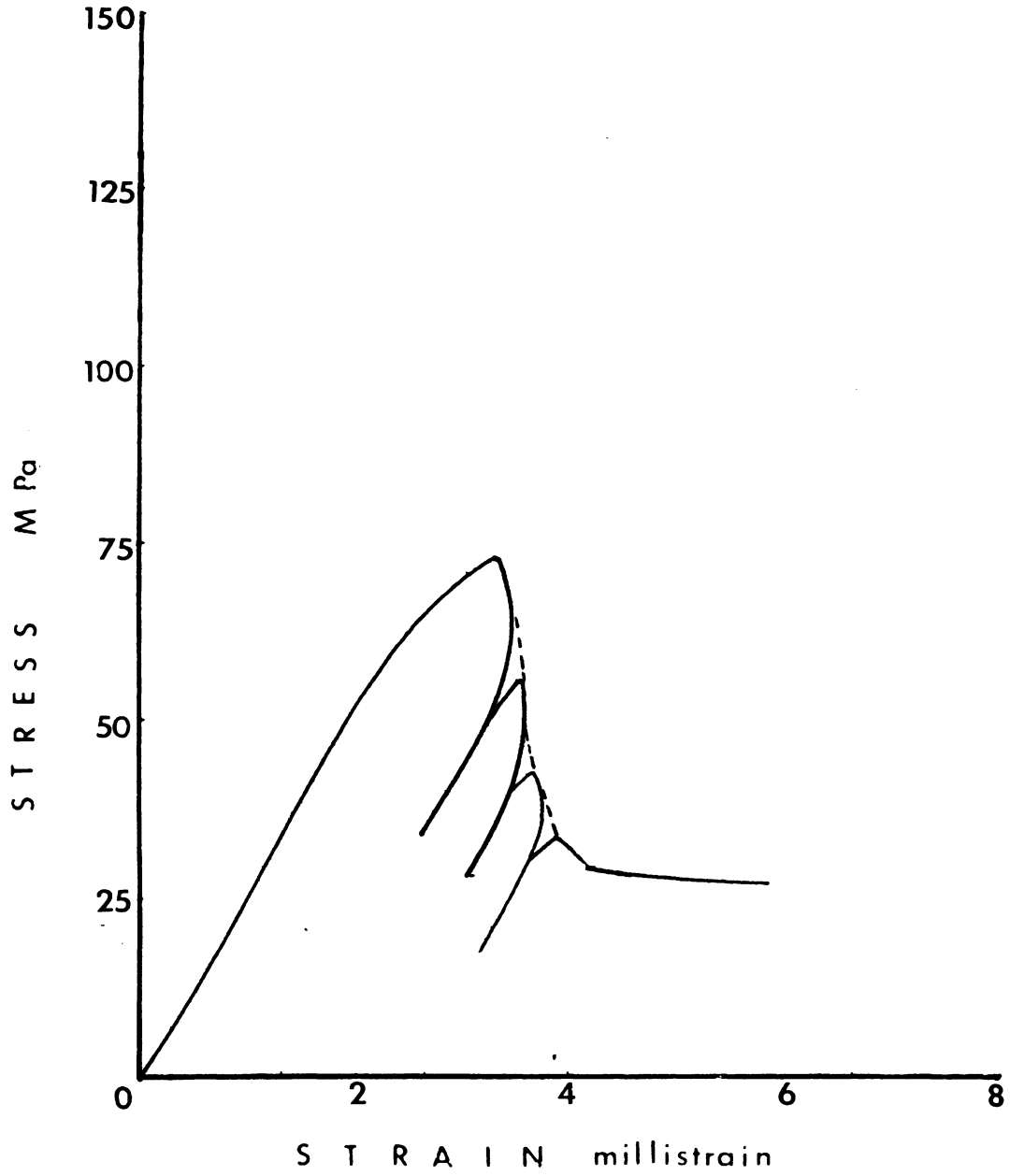

Fig.4.15. Stress-strain curve for S2.4.

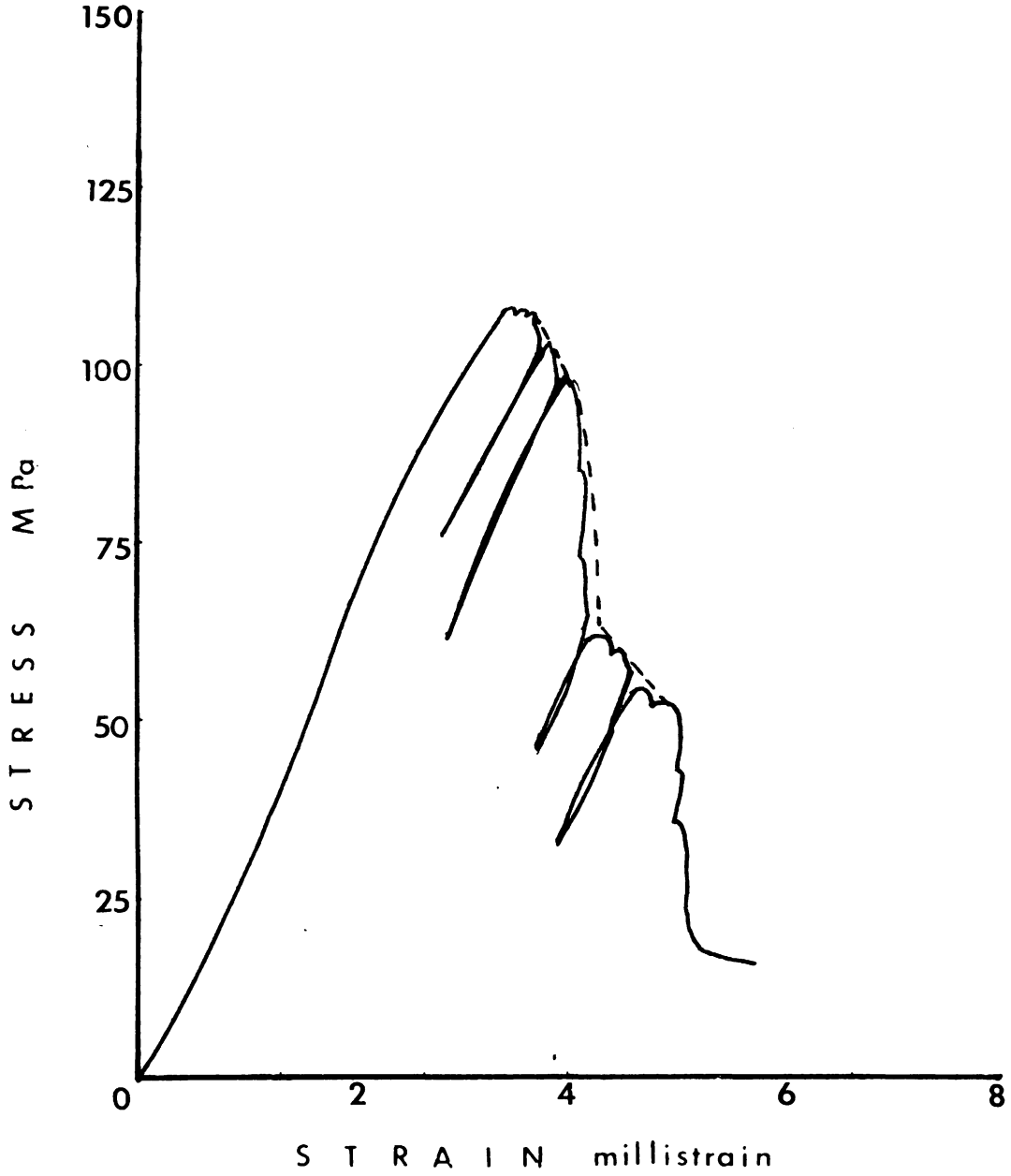

Fig. 4.16. Stress-strain curve for S2.5.

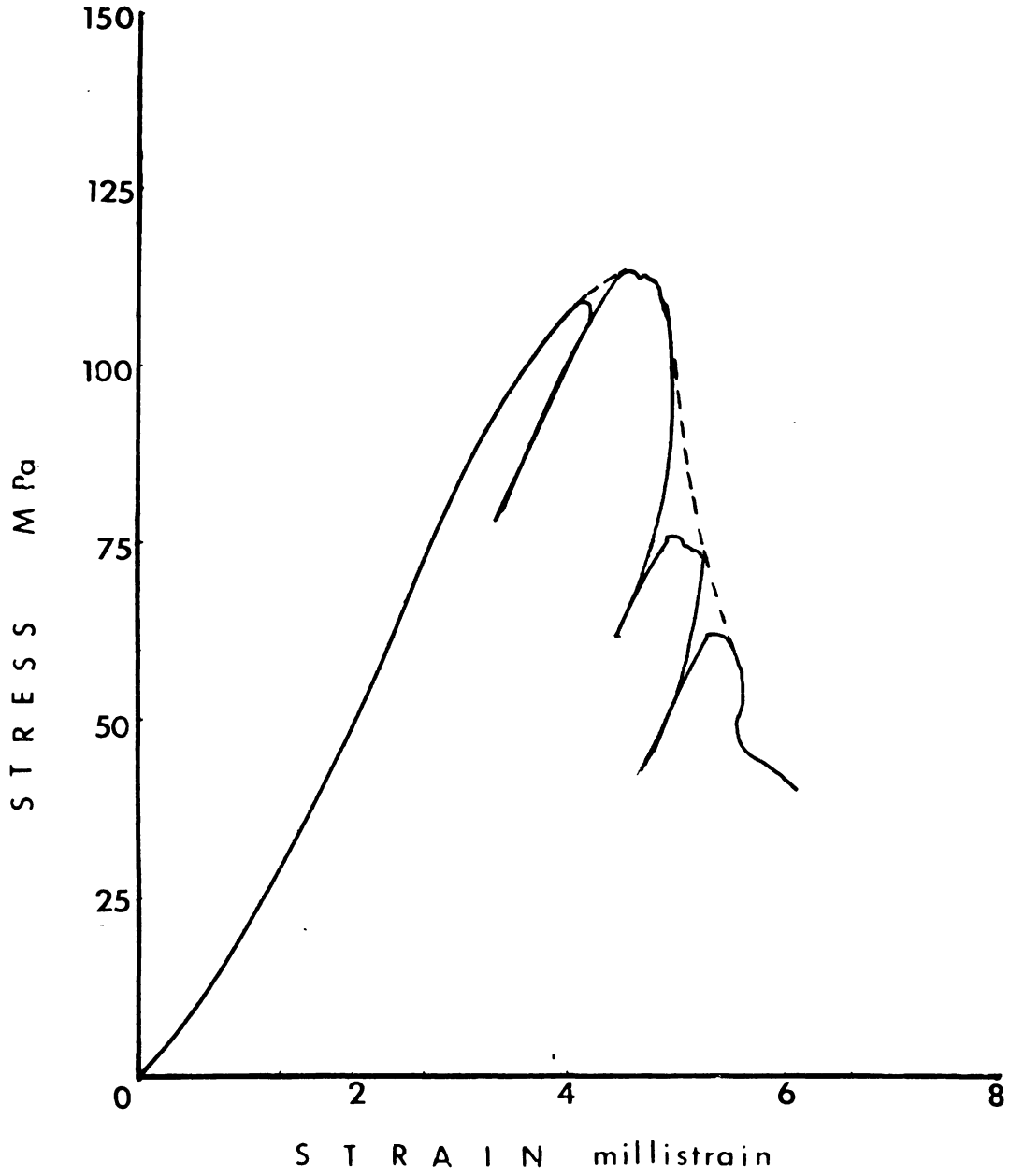

Fig.4.17. Stress-strain curve for S2.6.

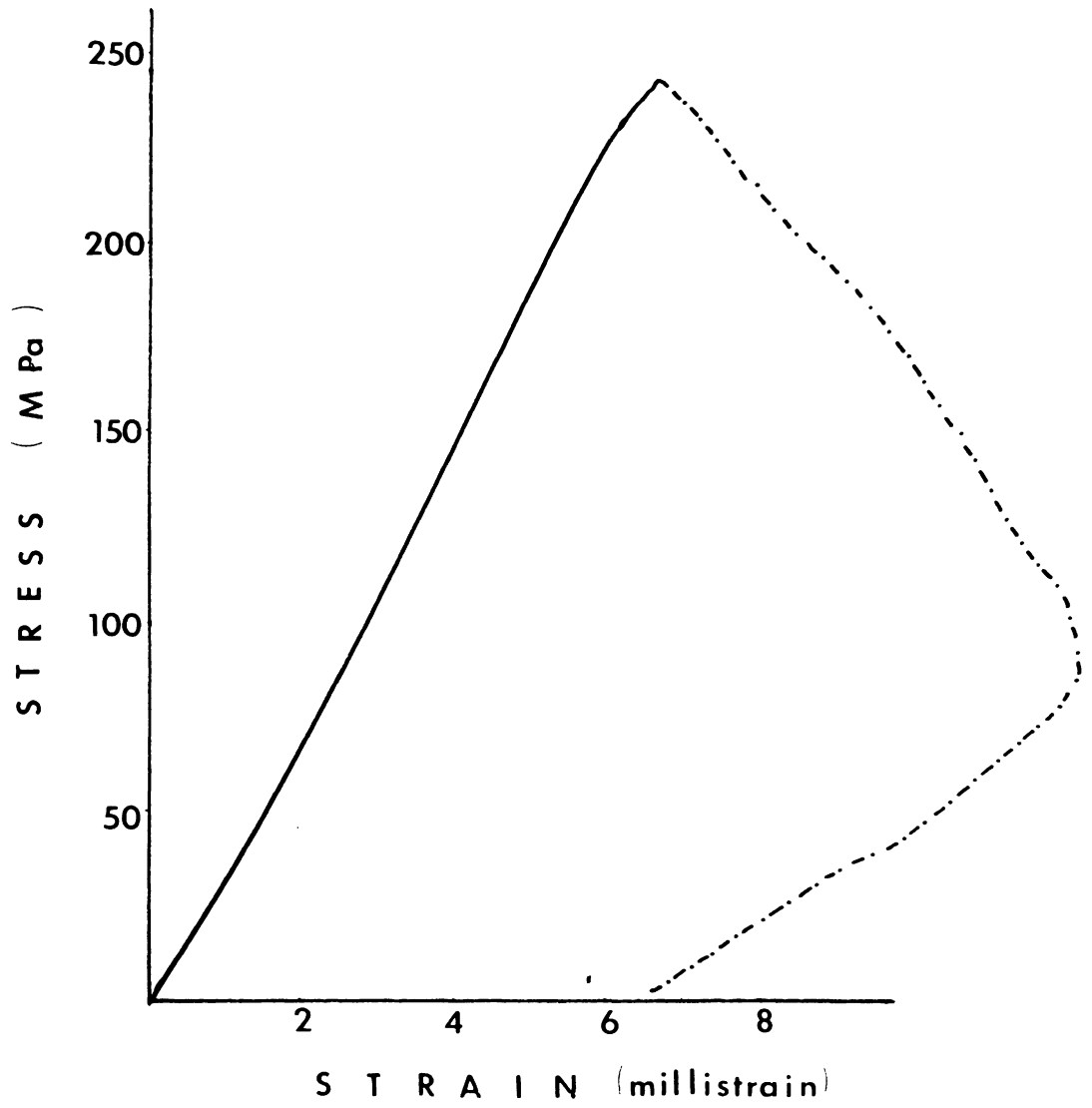

Fig.4.18. Stress-strain curve for S2.7.

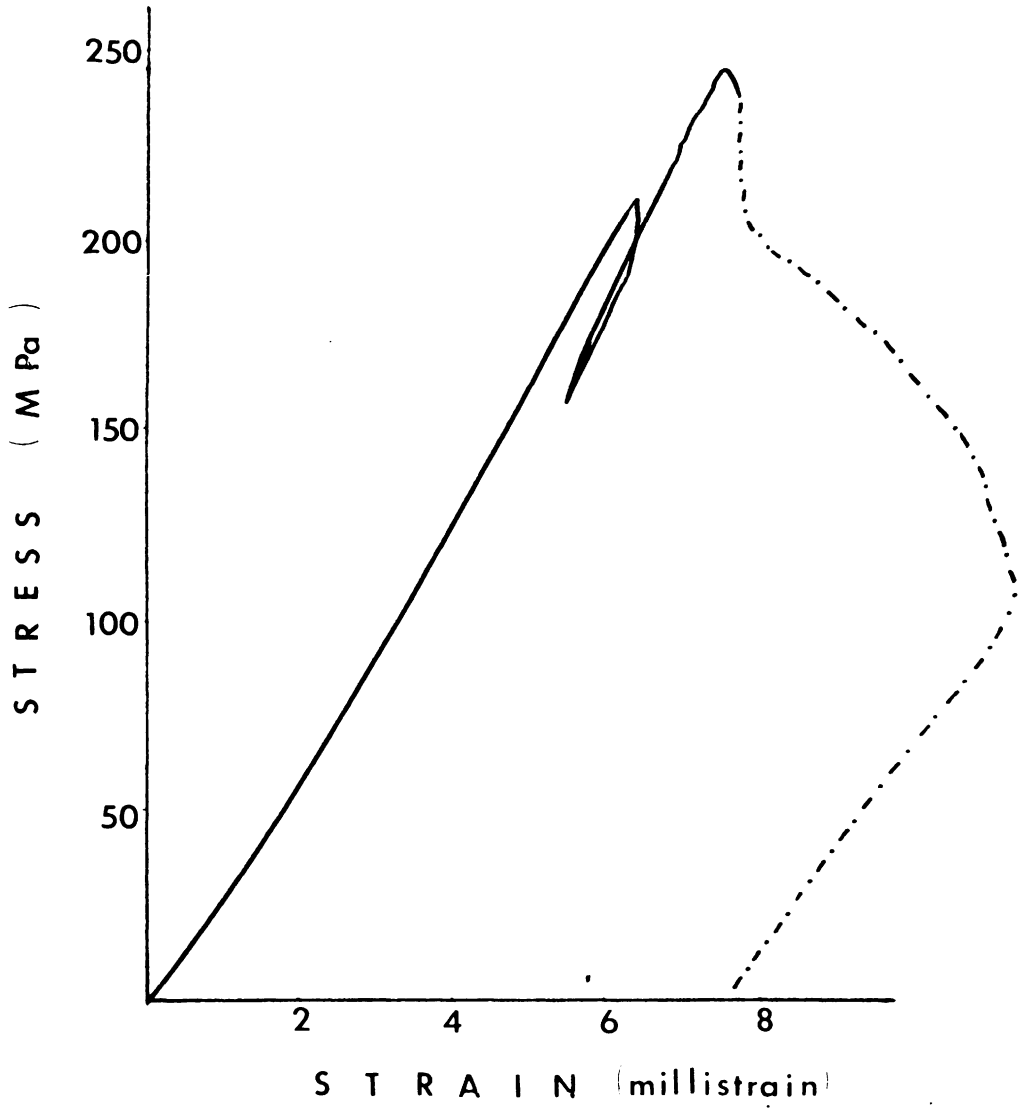

Fig.4.19. Stress-strain curve for S2.9.

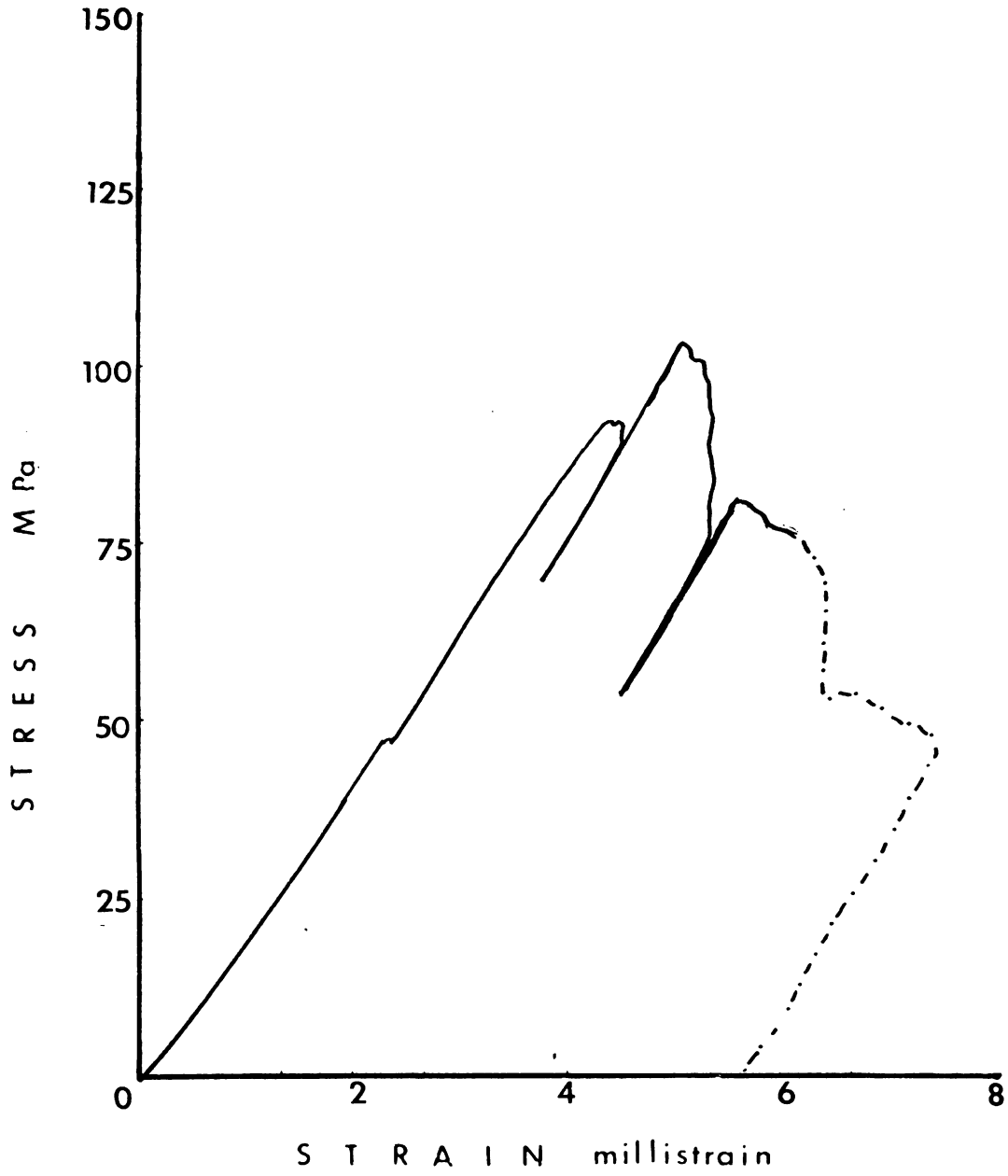

Fig.4.20. Stress-strain curve for S2.10.

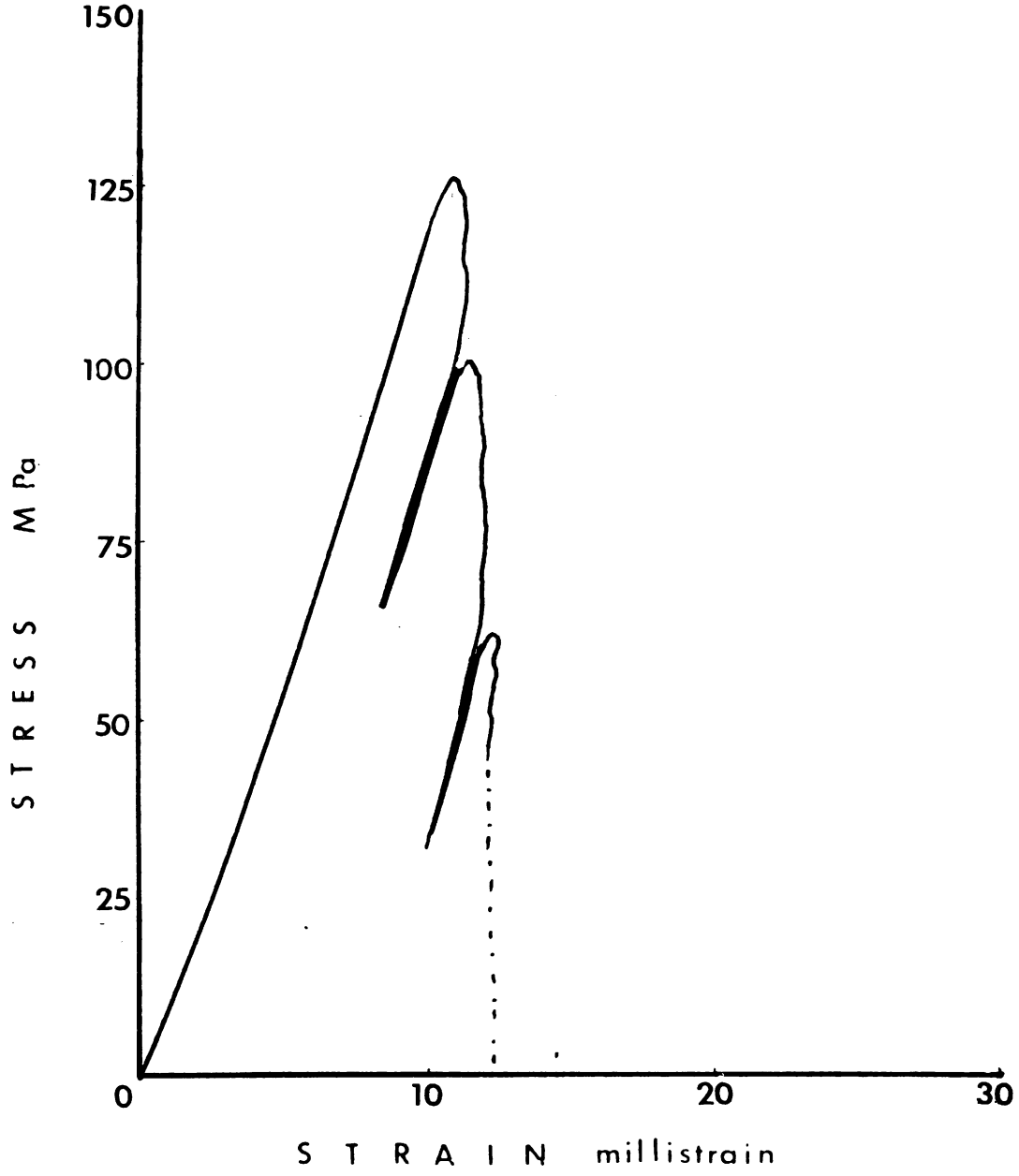

Fig.4.21. Stress-strain curve for S3.1.

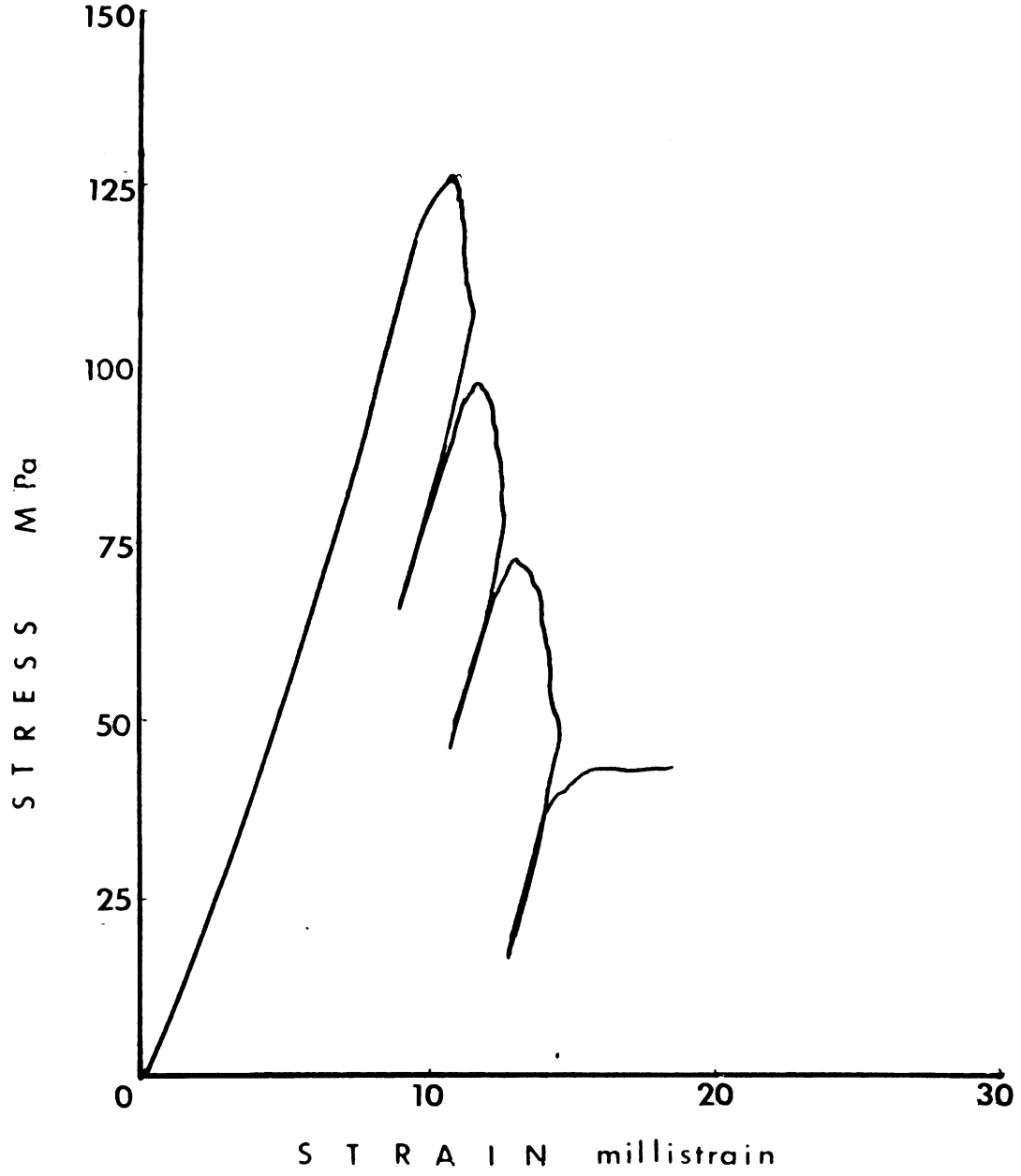

Fig.4.22. Stress-strain curve for S3.2.

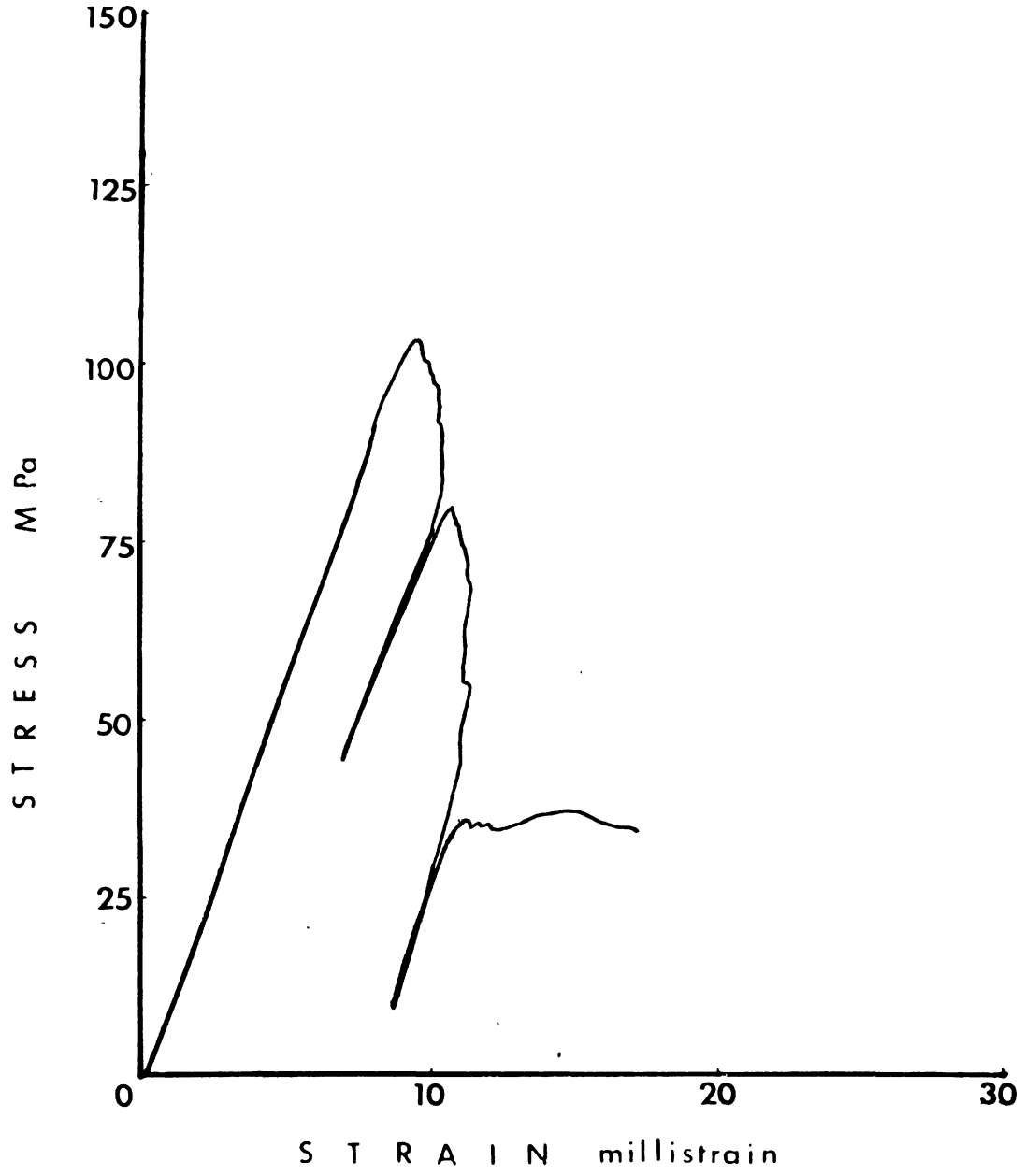

Fig.4.23. Stress-strain curve for S3.3.

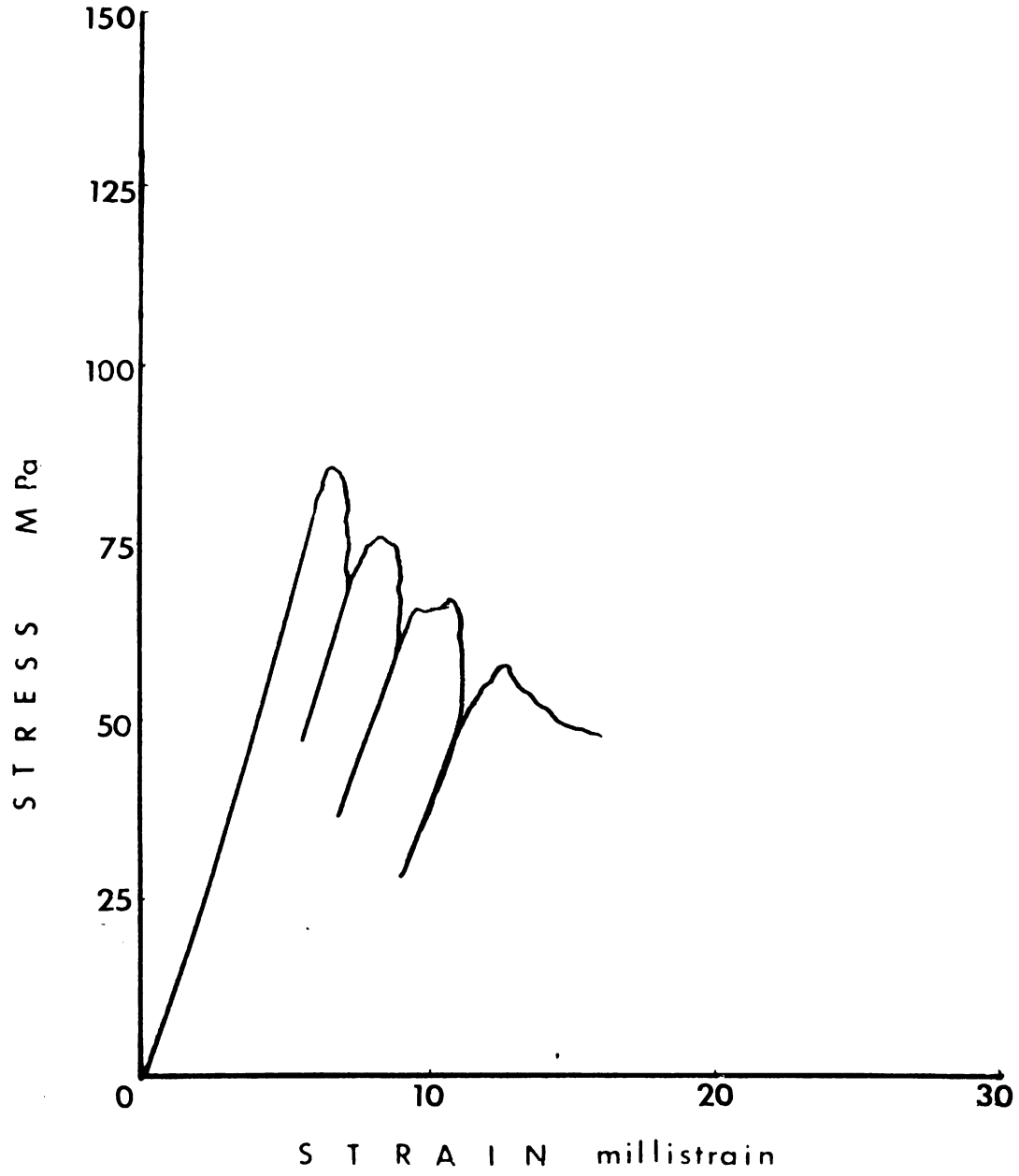

Fig.4.24. Stress-strain curve for S3.4.

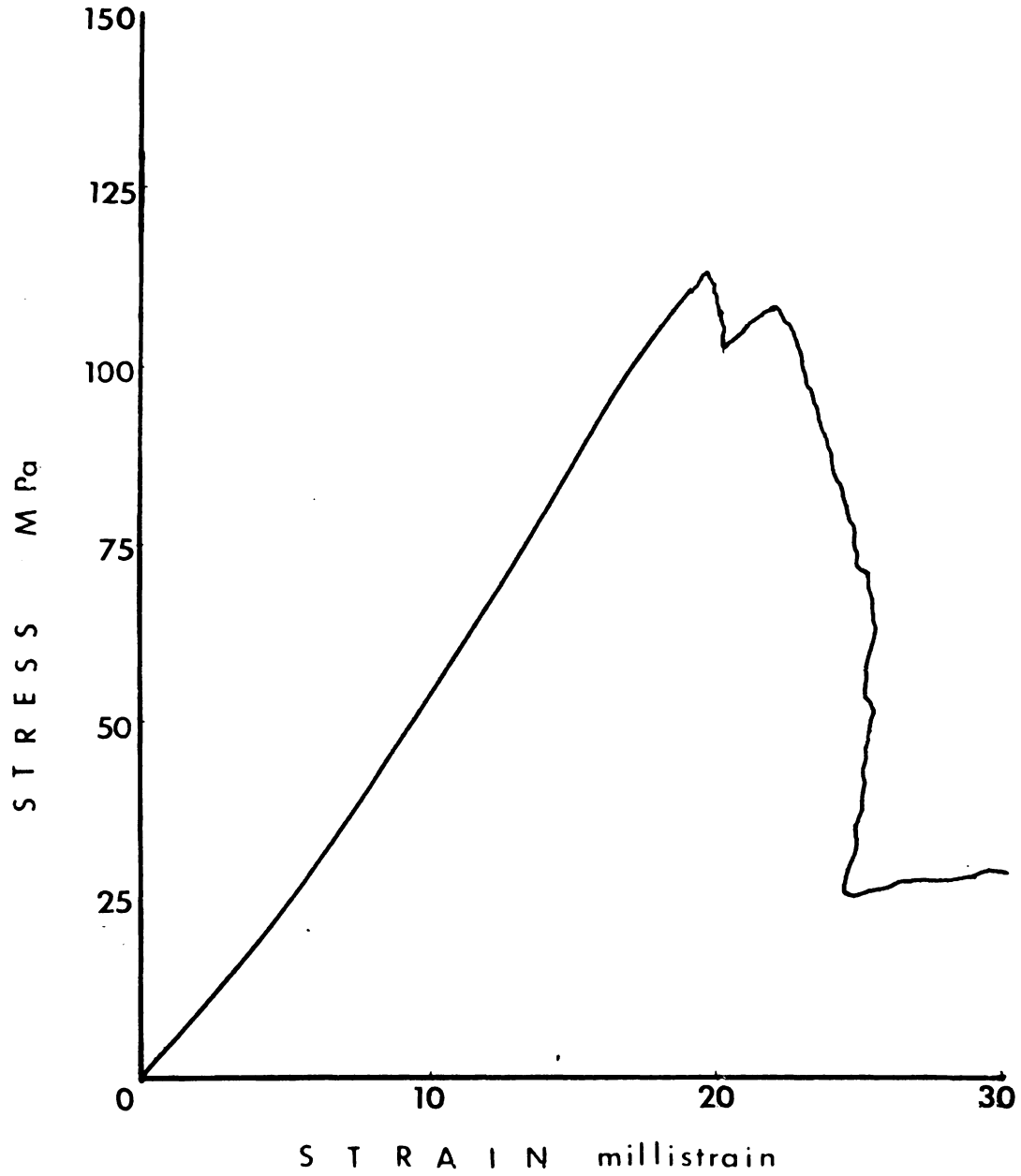

Fig.4.25. Stress-strain curve for S4.1.

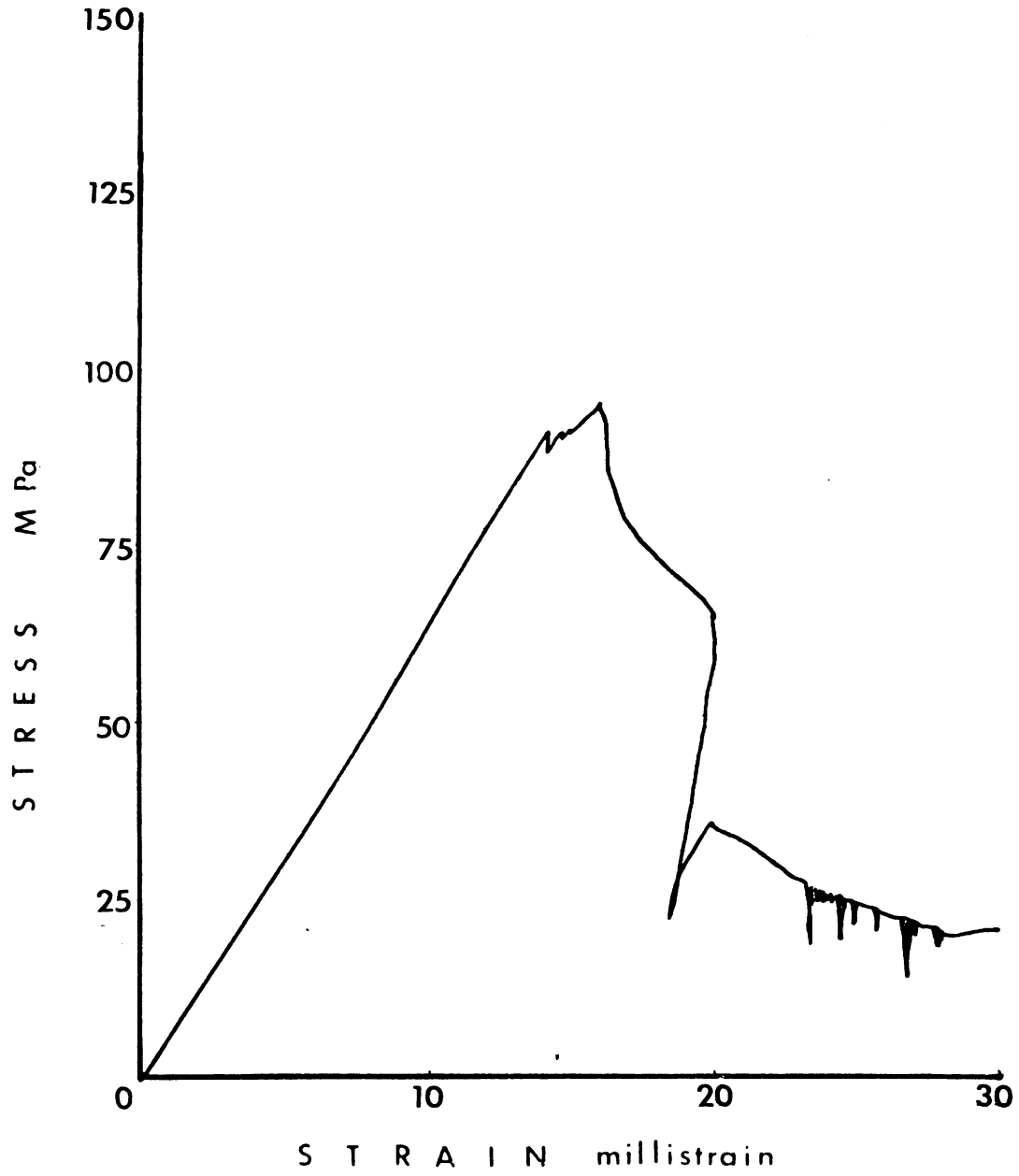

Fig.4.26. Stress-strain curve for S4.4.

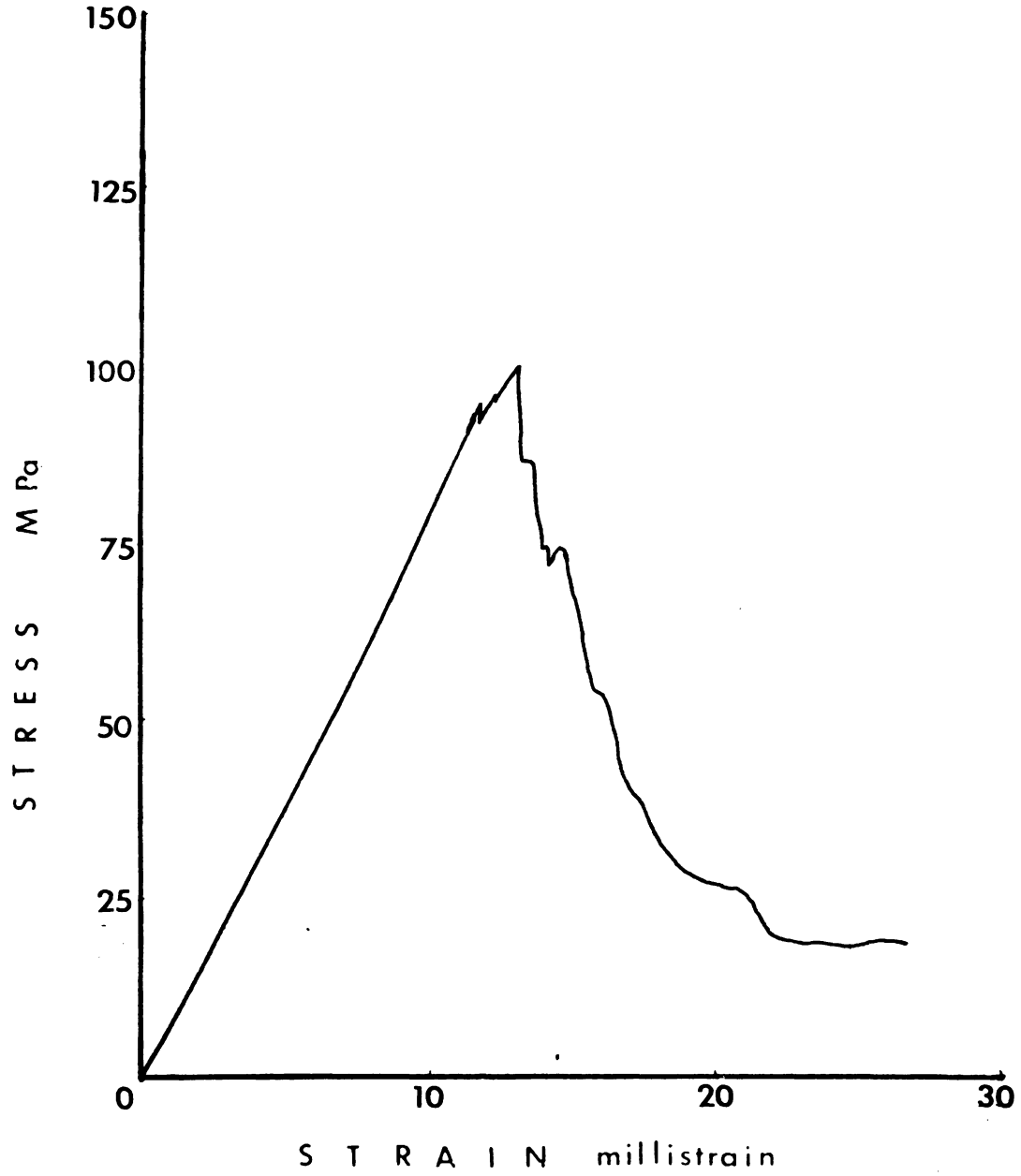

Fig.4.27. Stress-strain curve for S4.5.

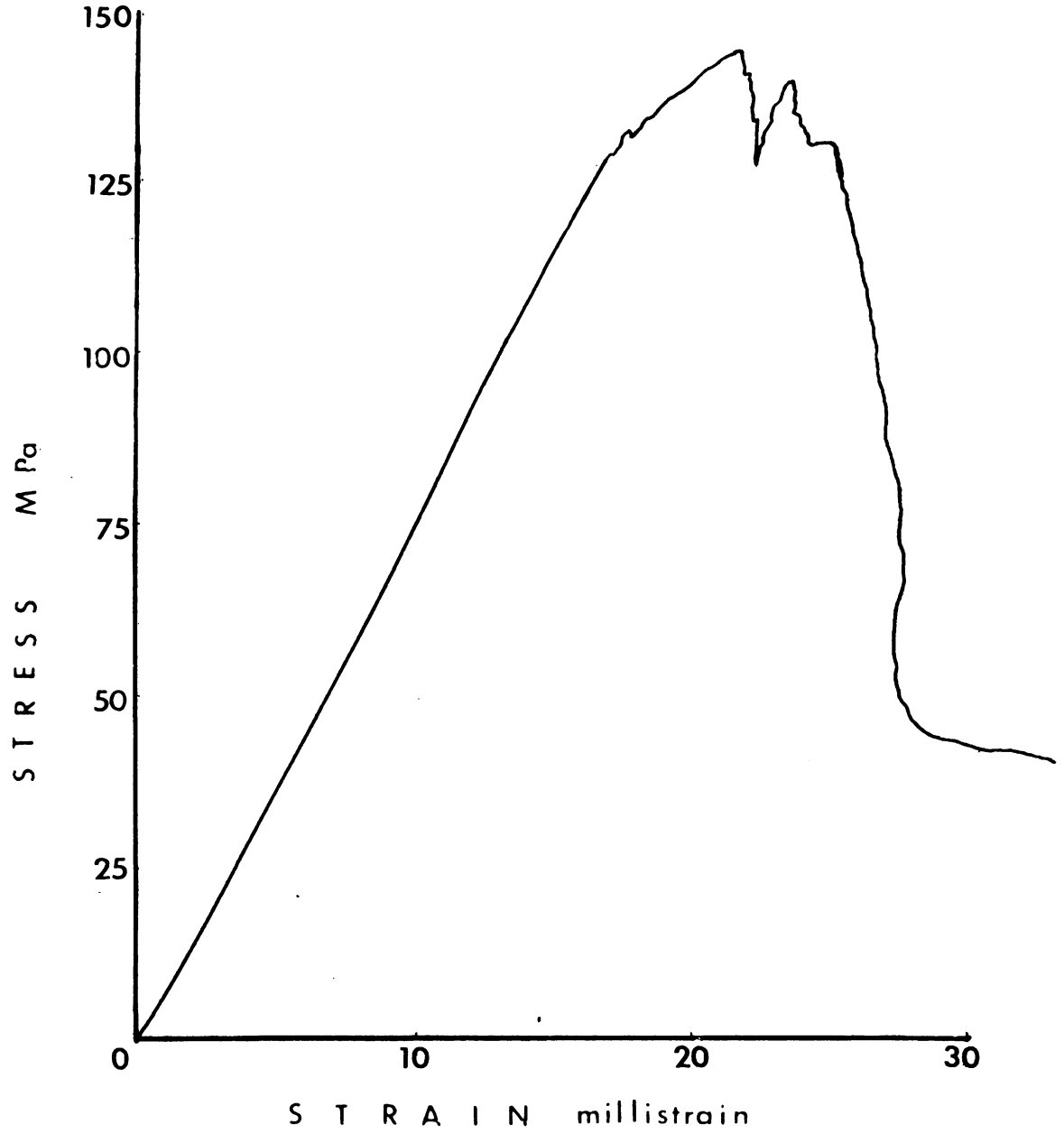

Fig.4.28. Stress-strain curve for S4.6.

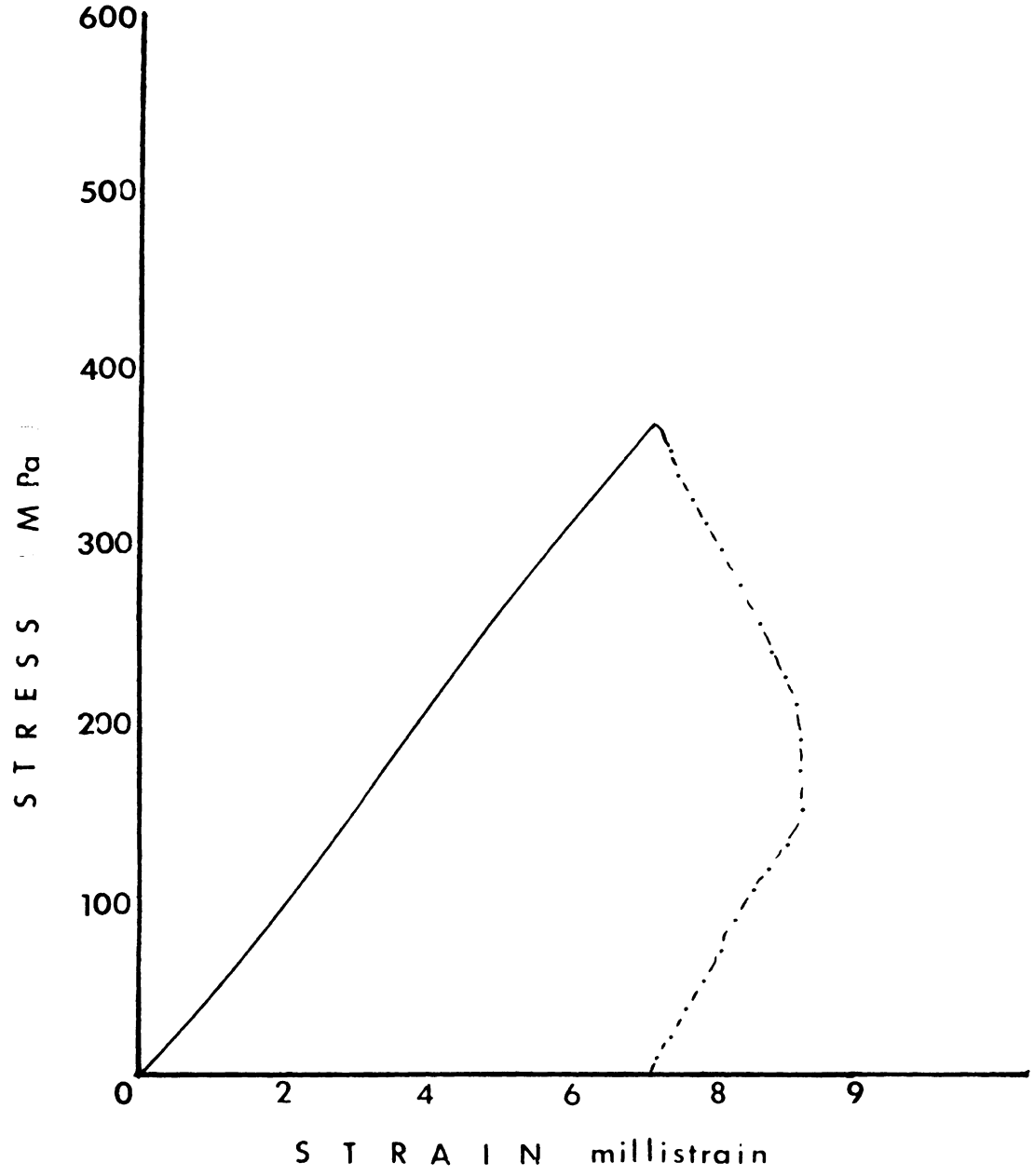

Fig.4.29. Stress-strain curve for P1.1.

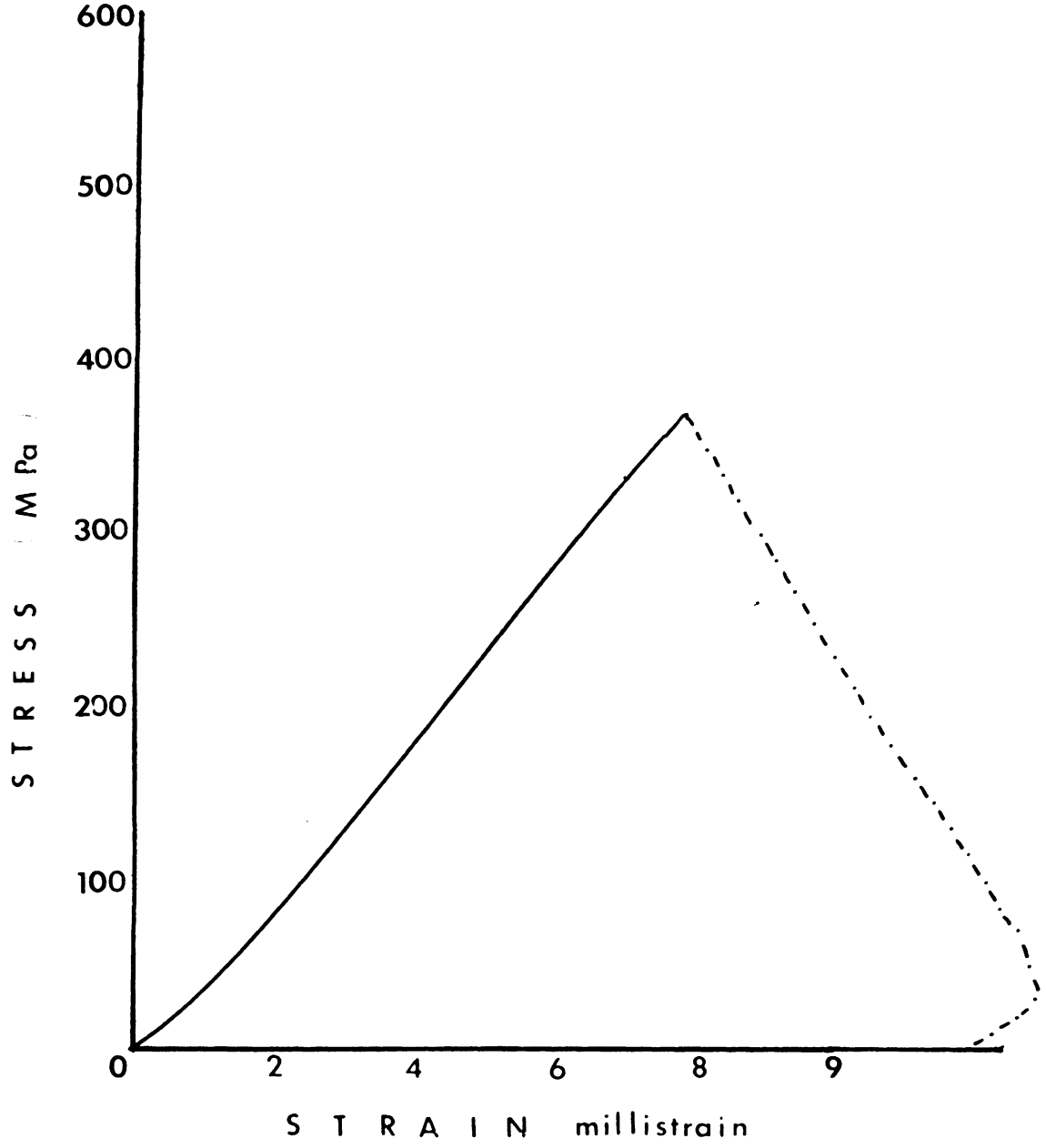

Fig.4.30. Stress-strain curve for P1.2.

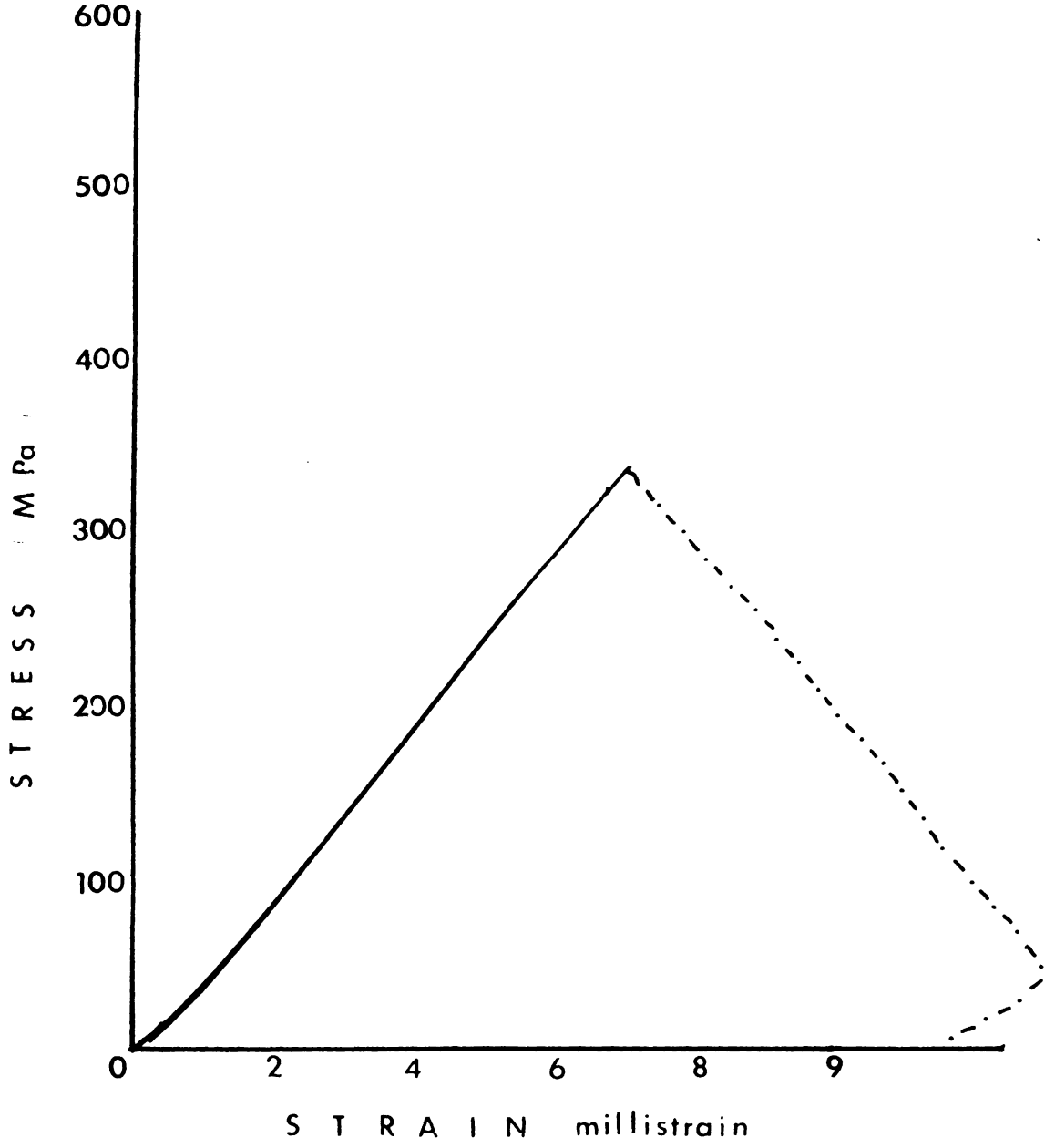

Fig.4.31. Stress-strain curve for P1.3.

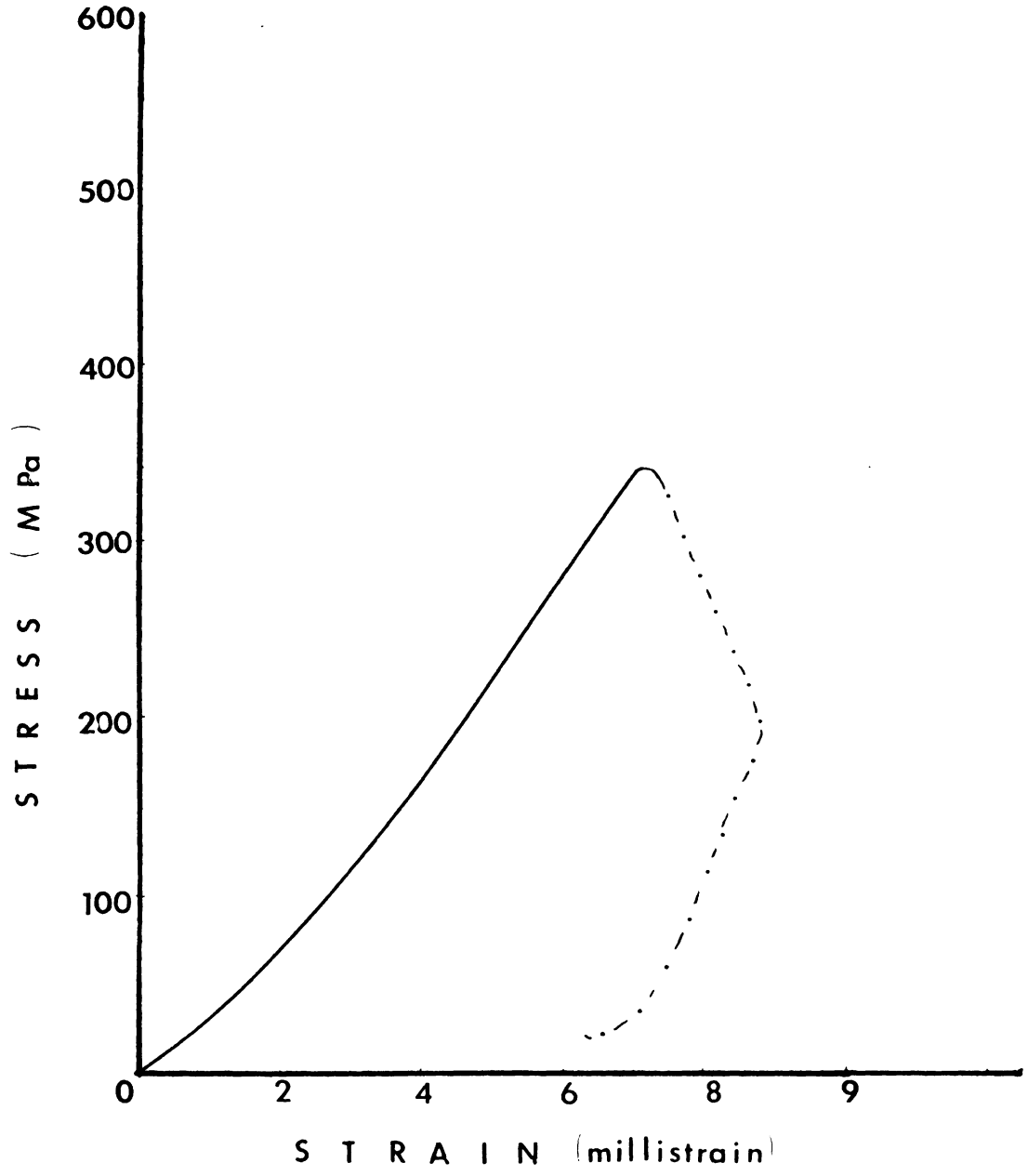

Fig.4.32. Stress-strain curve for P1.4.

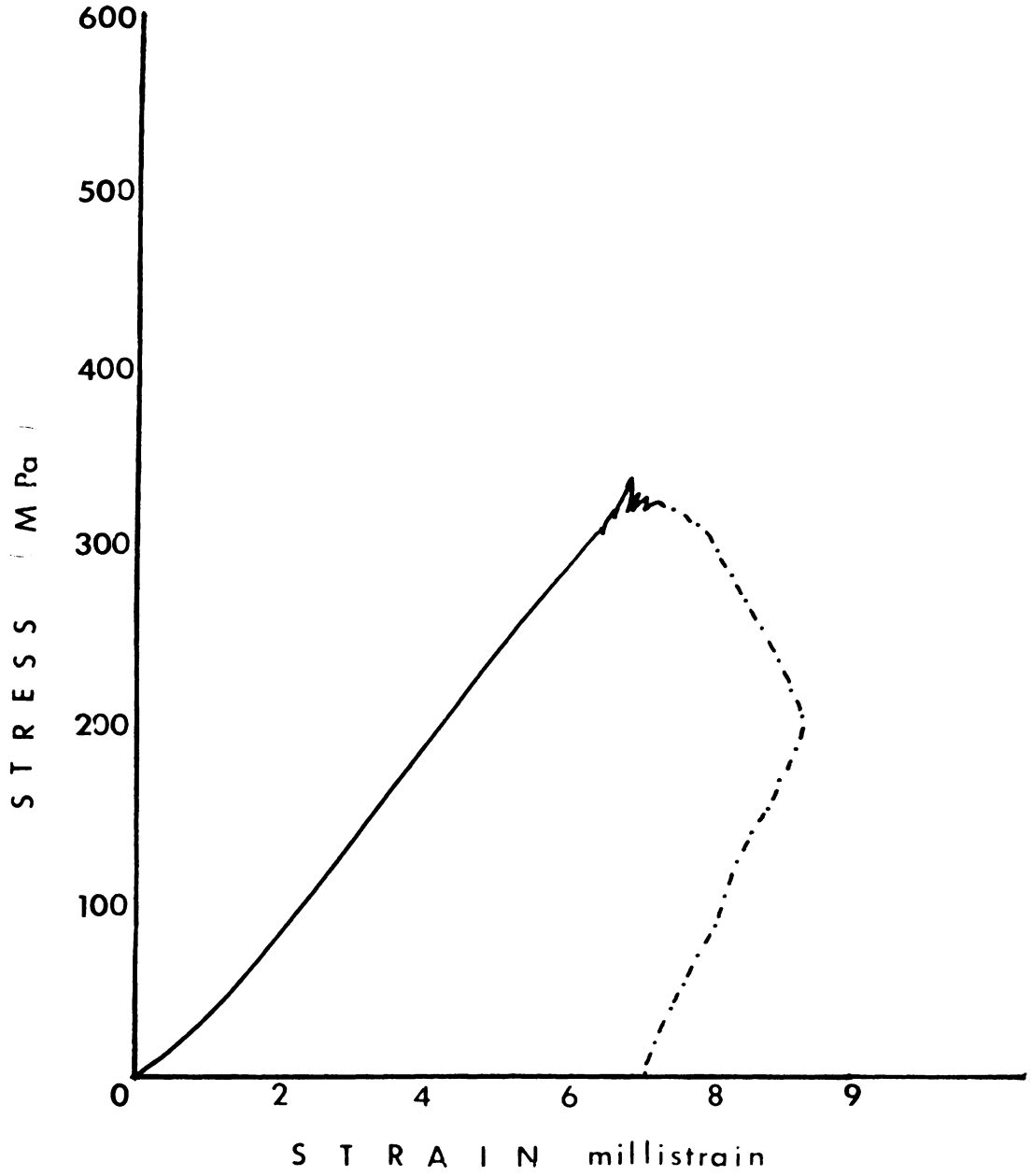

Fig.4.33. Stress-strain curve for P1.5.

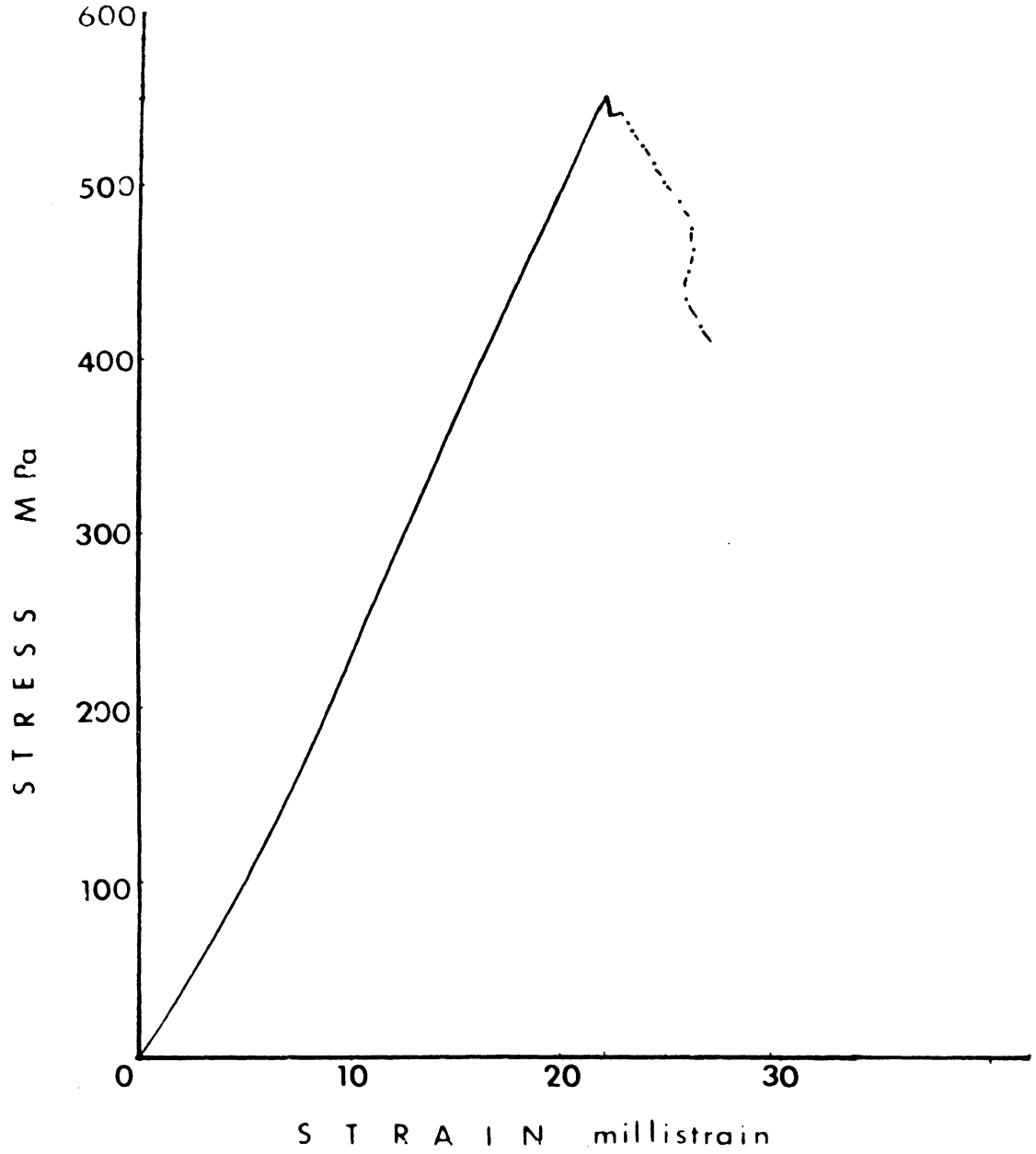

Fig.4.34. Stress-strain curve for P2.1.

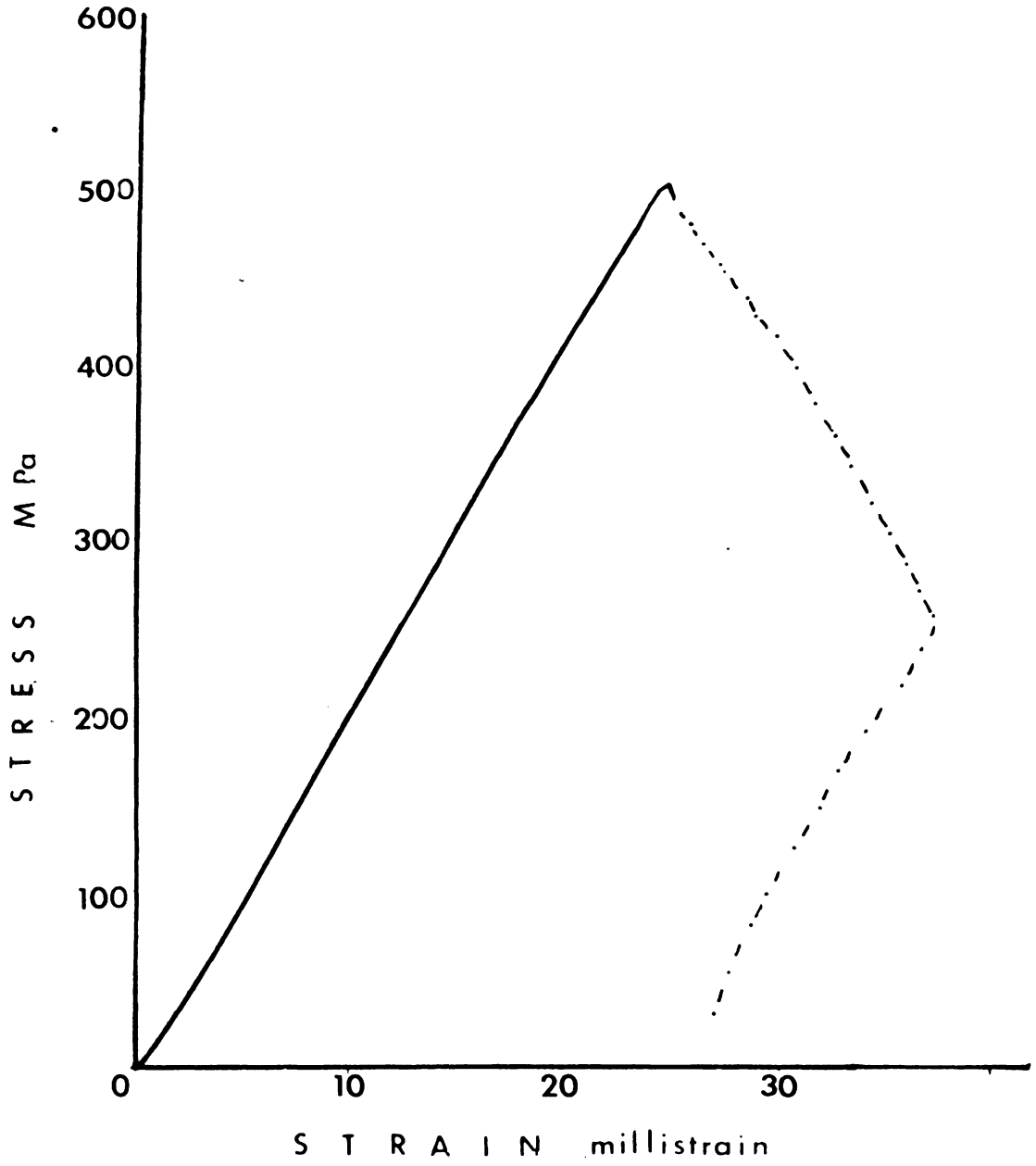

Fig.4.35. Stress-strain curve for P2.2.

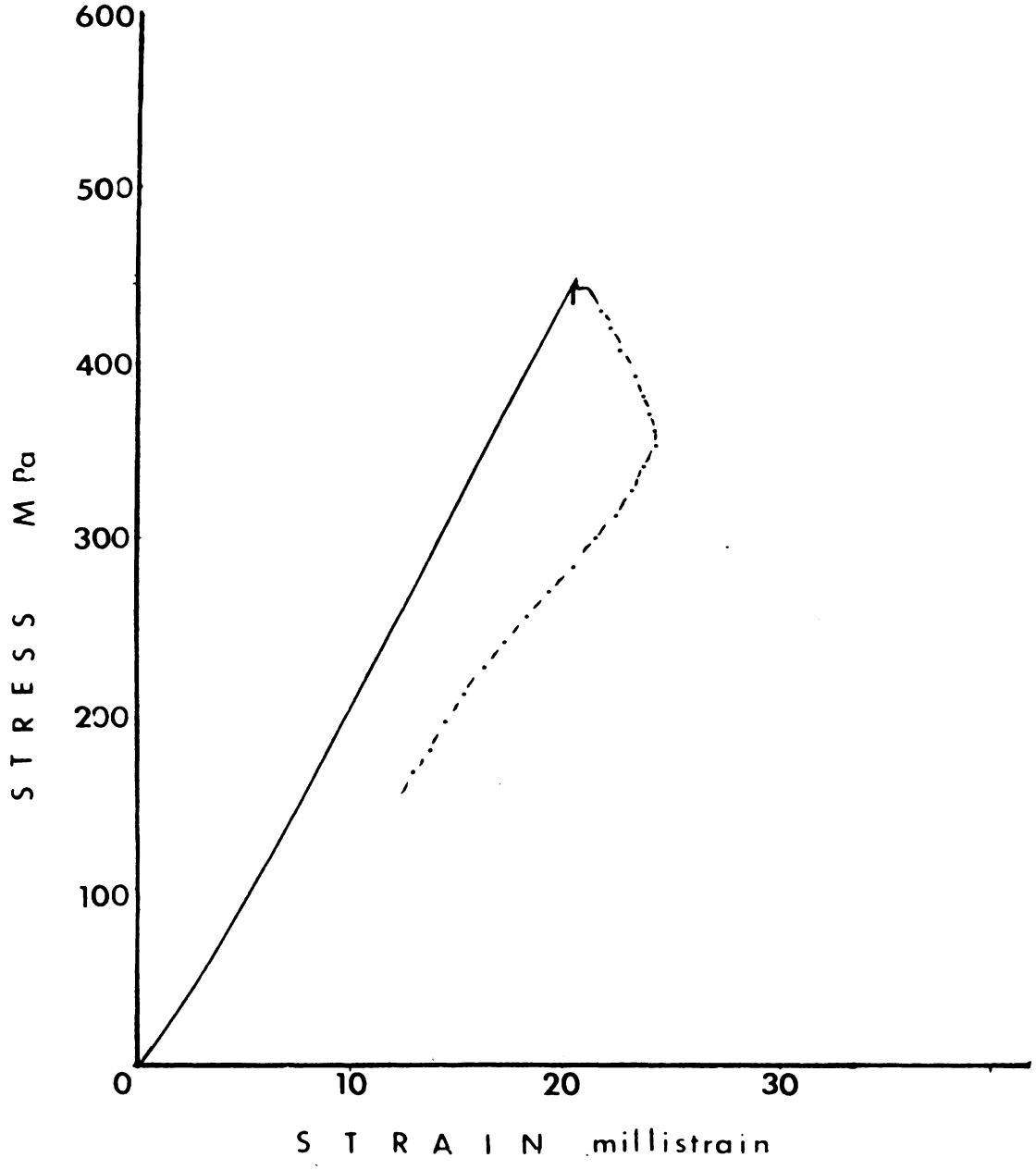

Fig.4.36. Stress-strain curve for P2.3.

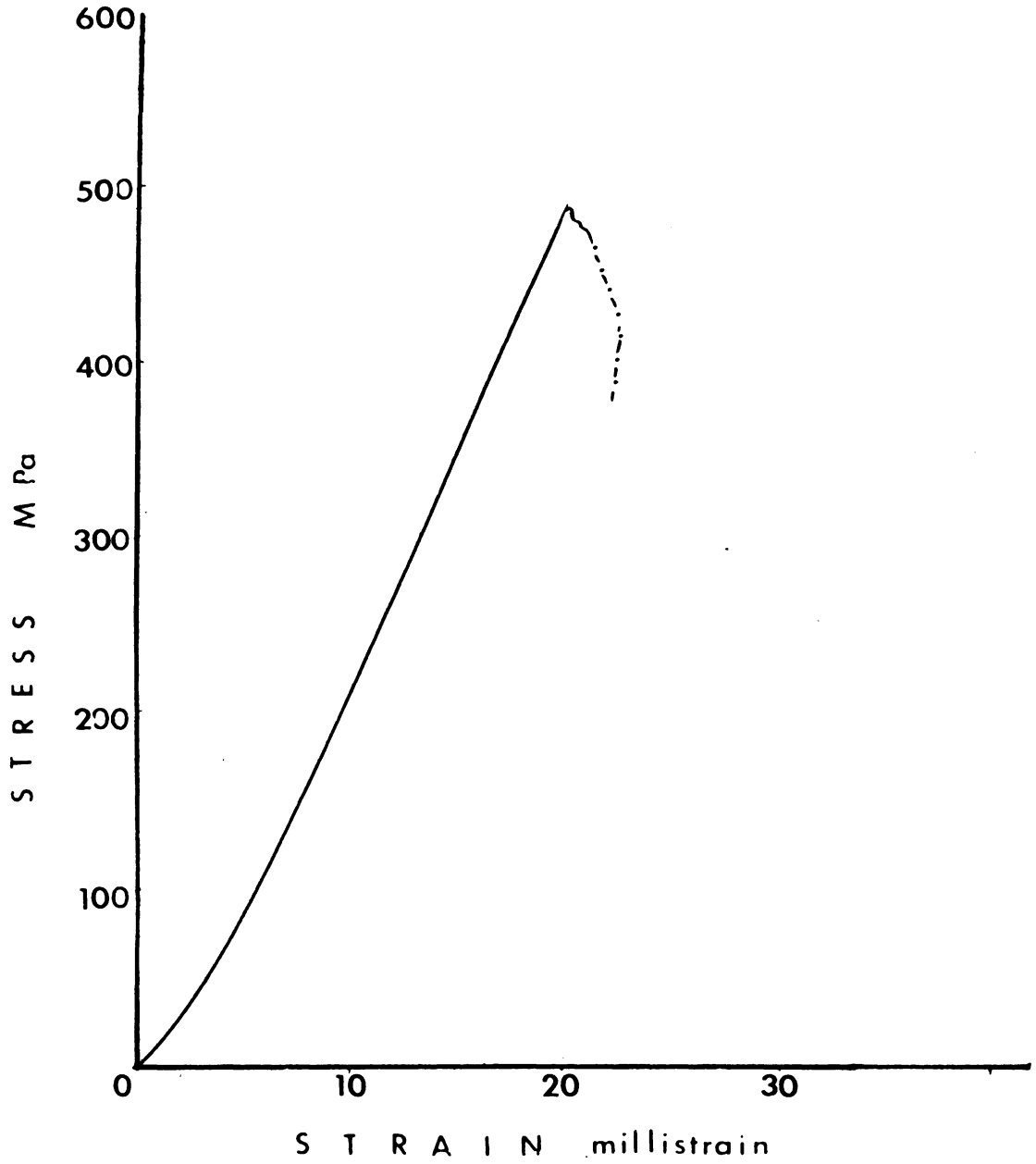

Fig.4.37. Stress-strain curve for P2.4.

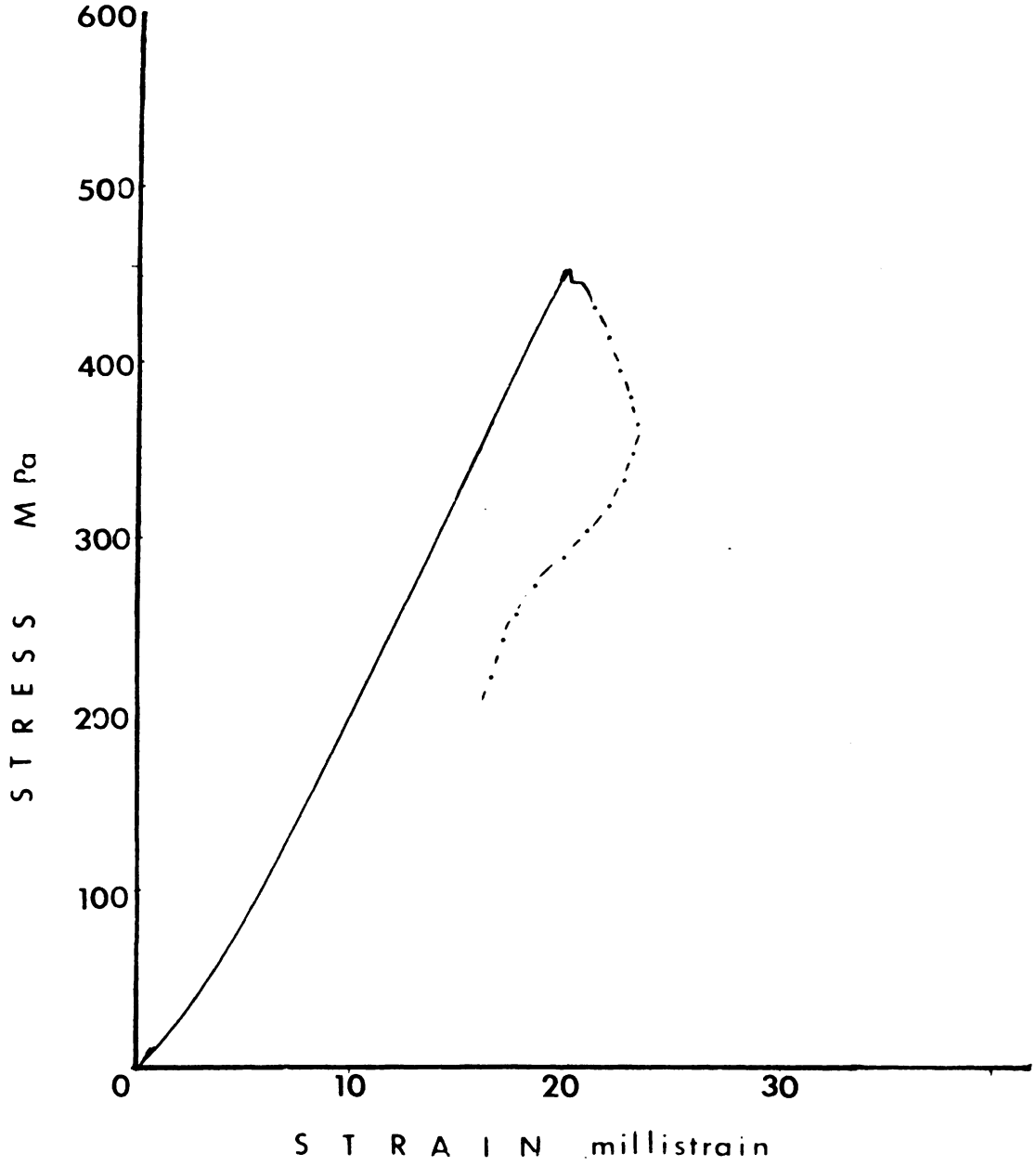

Fig.4.38. Stress-strain curve for P2.5.